Detection and biochemical investigation of

RNA BASE MODIFICATIONS

DISSERTATION

Zur Erlangung des Doktorgrades der Naturwissenschaften (Dr. rer. nat.)
der Fakultät für Biologie und Vorklinische Medizin
der Universität Regensburg

vorgelegt von Franziska Saller, geb. Weichmann

aus Weißenburg in Bayern

im Jahr 2019

Das Promotionsgesuch wurde eingereicht am
25.09.2019

Die Arbeit wurde angeleitet von
Prof. Dr. Gunter Meister

Unterschrift

_____
Franziska Saller

Willst du dich am Ganzen erquicken,
so mußt du das Ganze im Kleinen erblicken.

Johann Wolfgang von Goethe

"It is a rare mind indeed that can render the hitherto non-existent blindingly obvious.
The cry 'I could have thought of that' is a very popular and misleading one,
for the fact is that they didn't, and a very significant and revealing fact it is too."

Dirk Gently
(Invented by the ingenious Douglas Adams)

Content

ABSTRACT

Modifications of RNA bases are various and occur in almost all classes of RNA. Despite their abundance, most questions concerning RNA base modifications like the functions within the cell, remain elusive. To develop tools that can detect these modified bases is therefore an important step for helping to find answers to these questions. Especially issues concerning modification of the mRNA - the transcriptome - are of high interest. Following the epigenetics, the new field of "epitranscriptomics" has evolved. Next generation sequencing has made the research in this direction a lot faster and easier. However, there are several caveats to this quick generation of vast amounts of sequencing data. Several groups already performed transcriptome-wide sequencing experiments using – among other methods – antibodies against modified RNA bases. For some of these analyses, the results vary immensely among different groups. This could be partly due to different behaviours of the used tools, besides the disparate data evaluation methods. Thus, the set goal was, to generate more sensitive and specific antibodies, than the available ones. For the generation, ovalbumin-coupled nucleosides were used as antigens. After testing in various assays and optimisation of RNA-IP protocols, several antibodies can now be used to enrich for certain modifications. In this thesis, functional antibodies against the RNA base-modifications m^5C, m^6A, Ψ and m_2^6A are being presented and characterised. Different applications like immune fluorescence assays, and miCLIP (m^6A individual-nucleotide-resolution cross-linking and immunoprecipitation) experiments are conceivable methods to apply the newly generated tools. Data from possible RIP-Seq (RNA-Immunoprecipitation and Sequencing) experiments could hint to consensus sequences in which the modifications mainly occur. These sequences could be one way to find proteins that bind to the modifications and eventually lead to the holistic function behind the different modified RNA bases. To discover some unknown specific binding proteins of modified bases, or "reader" proteins, was yet another task to accomplish in this thesis. For that, a pulldown technique, developed by colleagues in the laboratory was amended and optimised for these purposes. RNA hairpins containing the modified base of interest were used to precipitate the proteins, which were then identified via mass spectrometry.

ZUSAMMENFASSUNG

RNA Basenmodifikationen sind vielseitig und können in nahezu allen RNA-Arten auftreten. Trotz ihrer Häufigkeit sind viele Fragestellungen rund um die Modifikationen, wie zum Beispiel ihre Funktionen in der Zelle, noch nicht beantwortet. Ein Werkzeug zu entwickeln, mit dem man diese modifizierten RNA-Basen detektieren kann, ist daher wichtig, um dazu beizutragen, diesen Fragen auf den Grund zu gehen. Besonders interessant sind dabei natürlich die Modifizierungen der mRNA-Basen, also des Transkriptomes. Nach der Epigenetik hat sich nun auch das neue Themengebiet der "Epitranskriptomik" entwickelt. Die neuen Sequenziermethoden haben die Forschung in diesem Gebiet wesentlich schneller und einfacher gemacht. Allerdings gibt es mehrere Nachteile dieser schnellen Erzeugung von großen Mengen an Sequenzierdaten. Verschiedene Arbeitsgruppen haben bereits transkriptomweite Sequenzierexperimente durchgeführt, bei denen sie, unter anderem, Antikörper gegen RNA Basenmodifikationen verwendet haben. Die Ergebnisse dieser Analysen weichen teilweise sehr stark voneinander ab. Neben den verschiedenartigen Daten-Auswertungsmethoden, könnte der Grund dafür auch an den unterschiedlichen Verhaltensweisen der verwendeten Antikörper liegen. Ziel war es daher, Antikörper zu generieren, die sensibler und spezifischer als die kommerziell erhältlichen arbeiten. Als Antigene für die Erzeugung der Antikörper wurden Nukleosid-Ovalbumin-Konjugate verwendet. Nach diversen Tests und Optimierungsschritten der RNA-Immunopräzipitations-Experimente, können einige Antikörper nun zur Anreicherung bestimmter Modifikationen verwendet werden. In dieser Arbeit werden Antikörper gegen die RNA Basenmodifikationen m^5C, m^6A, Ψ und m_2^6A präsentiert und charakterisiert. Verschiedene Anwendungen wie Immunfluoreszenz Tests und miCLIP (m^6A Einzelnukleotid „cross-linking and immunoprecipitation") Experimente sind denkbare Methoden, die neu generierten Antikörper zu verwenden. Die Daten von möglichen RIP-Seq Analysen (RNA-Immunopräzipitation und RNA-Sequenzierung) könnten auf Konsensus-Motive hinweisen, in welchen die Modifikationen hauptsächlich vorkommen. Derartige Sequenzen wären eine Möglichkeit, Proteine zu finden, die an Modifizierungen binden und letztendlich zu den holistischen Funktionen der verschiedenen modifizierten RNA-Basen führen. Solche unbekannten Basenmodifizierungs-bindende Proteine, oder kurz "Lese" Proteine zu entdecken war ein weiteres Ziel dieser Arbeit. Dafür wurde eine, von Kollegen entwickelte Pulldown-Methode abgeändert und für diese Zwecke optimiert. RNA-Haarnadelstrukturen, die eine modifizierte Base enthalten, wurden verwendet, um Proteine zu präzipitieren und herauszuziehen. Diese wurden anschließend mittels Massenspektrometrie identifiziert.

1.   INTRODUCTION

1.1   Posttranscriptional Modifications

The investigation of RNA bases and their modifications have their roots far in the past. From the 1950s, several labs already studied the complex world of the modified transcriptome in various species[1-6]. They analysed RNA modifications already to a great extent although methods were rather limiting compared to today's possibilities. The revolution of RNA analysis came with next generation sequencing. This had a tremendous impact on the field of "epitranscriptomics" – a new name for a quickly developing field of RNA research[7].

1.1.1   The discovery of modified bases in non-coding and coding RNA

Already in 1925, Johnson and Coghill were able to separate, crystalize and identify 5-methyl-cytosine from nucleic acids of the tubercle bacillus via microscopic comparison[8]. This was the first hint of an additional base besides adenine, cytosine, guanine and uracil/thymine in nucleic acid[8]. At that time however – after all 28 years before the discovery of the DNA structure by Watson, Crick[9], Wilkins[10] and Franklin[11] - the existence of two different nucleic acid species was not yet discovered. First thoughts to "yeast/pentose nucleic acid" being a second type of nucleic acid, namely RNA, were not mentioned until 1939[12]. Wyatt proved the existence of 5-methylcytosine (m^5C) in nucleic acids in 1950, using more biochemical methods[13]. In 1955, a "new base X" was found to be "6-methyl-aminopurine" (nowadays called N^6-methyladenosine or m^6A), however in deoxyribonucleic acid[14]. In 1956, Davis and Allen found uridylic acid to be the fifth abundant nucleotide in yeast ribonucleic acids (RNA)[5]. 5-Ribosyl-uracil (known as pseudouridine as proposed by Dr. A. Michelson[15]) was the first "new, unknown nucleotide" explicitly found in total ribonucleic acid (RNA) in 1956[5,16]. Two years later, thymine, 2-Methyladenine, 6-Methylaminopurine and 6-Dimethylaminopurine could be identified in total RNA of different bacterial strains, yeast and rat liver[17].

The first insights of modification of a certain ribonucleic acid species were achieved in tRNA (transfer RNA), at that time – the late 1950s - still known as soluble RNA or S-RNA[18,19]. In the beginning, the techniques used for detecting ribonucleic bases in RNA were rather simple. Paper chromatography, paper electrophoresis and UV absorption spectroscopy with hydrolysed RNA was used to analyse the components of RNA[17,20]. Using these methods, the groups of Dunn, Anders and Matthews could find several hydroxylated and methylated adenine, guanine and hypoxanthine bases[18-20] in tRNA. When Cohn investigated the salt-soluble RNA in more detail, he could find approximately 1 % of pseudouridine (Ψ) in this

fraction[16], which fits to the nowadays known composition of all tRNAs[21]. In the first attempt of solving the primary and secondary structure of a transfer RNA (alanine), Holley and colleagues proposed – among other schematic conformations - a clover leaf structure, comprising nine different "unusual" nucleotides, including inosine, pseudouridine, methylated and dihydroxylated residues[22,23]. Several similar analyses of specific tRNAs have shortly thereafter been carried out, leading to the discovery of more and more unknown nucleotides[24–27]. The group of Miyazaki, for example, also found nine different bases besides the abundant ones in isoleucine tRNA, i. a. N-(purin-6-ylcabamoyl)-threonine, a comparatively large ribonucleotide[28].

Methylation of other RNA species was initially thought to be contaminants of tRNA[29]. Using sucrose gradients and 2-dimensional chromatography, Starr and Fefferman could prove the existence of methylated adenines and guanines in purified ribosomal RNA (rRNA) of *E. coli* in 1964[29]. With the development of fractionating HeLa cell lysates into cytoplasmic, nucleoplasmic and nucleolar fractions in 1966[30,31], rRNA could be similarly analysed to a greater extend and in more detail in mammalian cells[3,4,32]. Brown and Attardi found hints, indicating rRNA-modification consists mainly of 2'-O-methylations and to a minor portion of methylated adenine and guanine bases with 6-dimethylaminopurine (m_2^6A) solely in the 18S fraction[3]. Greenberg and Penman did several experiments and found methylation to be mainly in the 45 S rRNA, which is the precursor of the 18S rRNA[4]. In another early study, Iwanami and Brown did a broader study regarding the identity of the specific RNA modifications. They could assign several modifications (e.g. 2'-O-Methylcytidine, 2'-O-Methyluridine, N4-Methylcytidine (m^4C), 3-Methylcytidine (m^3C), 3-Methyluridine (m^3U), 1-Methyladenine (m^1A), N6-Methyladenine (m^6A), N6-Dimethyladenine (m_2^6A), N2-Dimethylguanine (m_2^2G) and 1-Methylguanine(m^1G)) to the different fractions of the rRNA[32].

For a long time, the common thought was that methylated nucleotides solely appear in tRNA and rRNA and that mRNA is a "natural methyl-free species", as discussed in several reviews[33,34]. The lack of ability to detect methylation in mRNA was mainly due to insufficient methods that were applied. Fortunately, not everyone blindly believed in the common "knowledge". The first discoveries of methylated bases in coding RNA were made in rat[6], mouse[35], hamster[36] and HeLa[37] cells in the 1970s. The groups of F. Rottman, D.E. Kelley, R.H. Taylor and A. J. Shatkin did poly-A selection of ^3H-methyl Methionine and $^{32}P_i$/^{14}C-Uridine-treated cells and found the methylated bases by analysing the RNA via density gradient sedimentation and electrophoretic methods[6,35–37]. These groups all measured m^6A to be present at least once and on average 4 to 5 times per mRNA molecule[6,35–37]. Additionally to m^6A, Desrosiers et al. found 2'-O-methylnucleosides and small amounts of m^1A and m_2^6A[6]. In 1975, the m^7G-triphosphate-cap was discovered to be at the 5'-end of mRNA and firstly

2

designated as "bizarre 5'-termini"[38]. The same group also detected m6A, four ribose-methylated nucleosides and small traces of another two unidentified bases in mRNA of mouse myeloma[38]. In the 1980s, initial genome-wide studies of the composition of mRNA of Rous Sarcoma Virus[39] and bovine prolactin[40] have been made by hybridizing the mRNA to a cDNA library, digesting the RNA, m6A-immuno precipitation (IP)/labelling and thin layer chromatographic (TLC) analysis[39,40]. Kane et al. thereby could determine a consensus sequence (PuGm6ACU)[39] in mRNA, which has emerged earlier in several organisms as well[41–43]. For centuries, the biological relevance of the unusual RNA-components however was not apparent and could not be determined with the limited methods available.

1.1.2   Developments in the field of epitranscriptomics

In the early 2000s, different approaches have been made to elucidate the transcribed regions of the genome, like various variations of genome array assays[44–46]. With the development of RNA-Seq (mapping and quantification of transcriptomes by deep sequencing) in 2008, the global analysis of RNA became much more accessible[47–51]. For the epitranscriptomics-research, this innovation turned out to be the reboot. In 2012, the group of Gideon Rechavi did the first genome-wide m6A RNA sequencing in human cells[52]. In the same year and the two following years, the sequencing and transcriptome-wide detection of m6A and other modifications like m5C and Ψ went on[53–58]. In chapter 1.4, the different methods for detecting RNA base modification are summarized. Nowadays, a database of RNA modifications - "Modomics" - lists 171 different RNA modifications[21,59] and it is not sure, if this list is complete. In the last few years, the field of research has slightly moved from the detection of the modified RNA bases to the functional implications and this has exploded. The next chapters (1.2 and 1.3) deal with a lot of these functional findings, but the research is still actively going on, leaving a lot of questions open for now.

1.2   RNA modifications in different RNA species

The roles and effects of modified RNA are very widespread and are most probably not at all discovered to its final extend. Especially in mRNA, a lot more is to be elucidated and scrutinised until all pathways are fully explained. A short overview of the diverse functions of certain, most investigated RNA modifications found to date in different RNA species is shown in Figure 1.
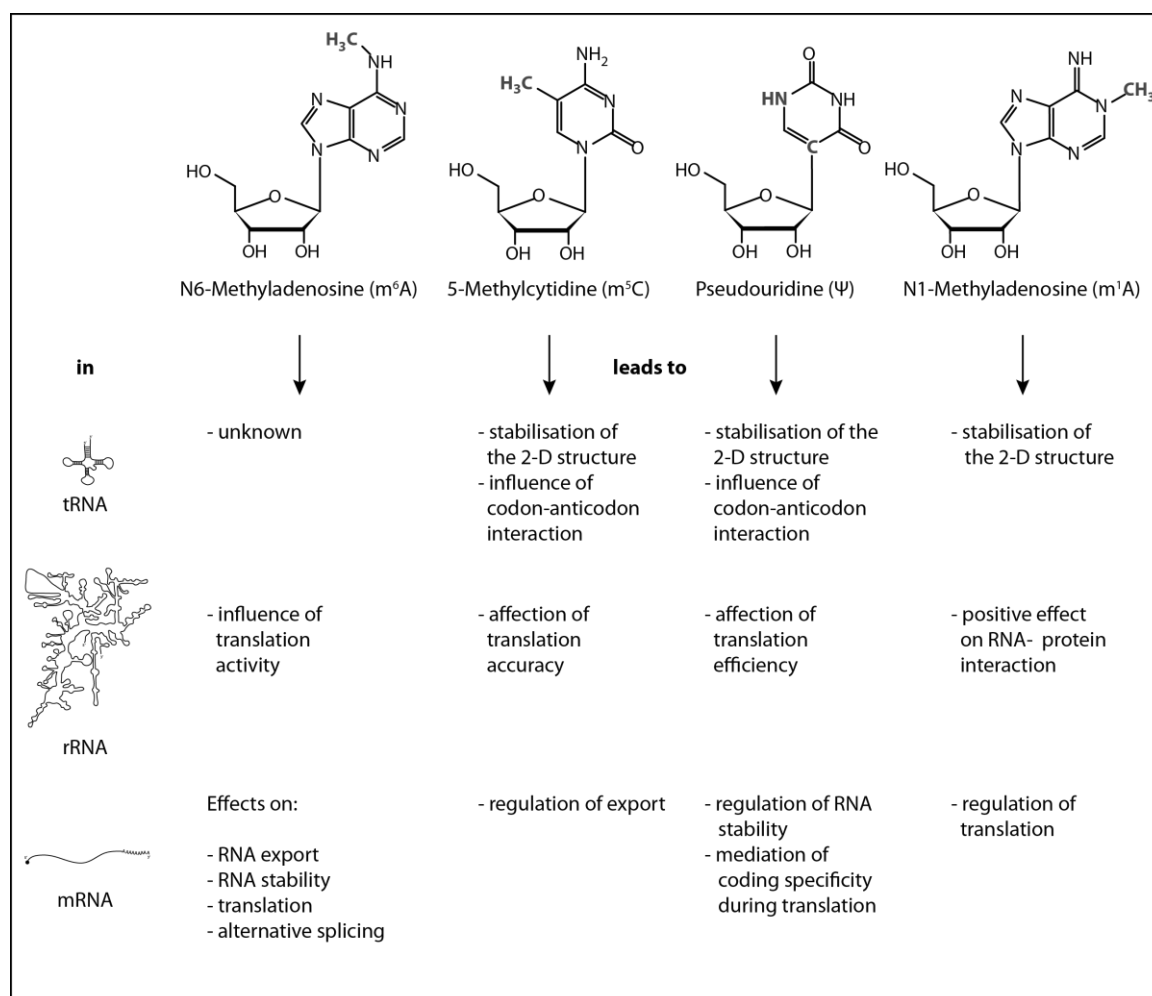
Figure 1: Overview of the effects of four modified nucleotides in different RNA species. The structures of m6A, m5C, Ψ and m1A are shown. The table shows different functions and effects of these nucleotides, observed in three classes of RNA (tRNA, rRNA and mRNA). These implications are, among others, further discussed in this chapter.

1.2.1 tRNA modifications and their functions

tRNA is the most abundantly modified RNA species overall. Almost one hundred different RNA base modifications have been detected in tRNA[21,60] (see Figure 3). These modifications serve various different structural and functional purposes[61,62]. One example is the stabilisation of the tRNA-2D-structure by forming additional hydrogen bonds with other bases (Ψ), base stacking improvement (Ψ, m5s2U, m5C), flexibility changes (2'O-methylations, dihydrouridine), building water bridges to other molecules (m5C and Ψ) or by allowing to bind additional metal ions (m5C)[61,62]. The m5C-methylation at position 40 in yeast, for example, has been shown to have an important role in magnesium ion binding[63]. Another m5C site is proposed to have base stacking and hydrophobicity enhancing functions[64]. 2'O-methylations have the ability to protect tRNA from endonucleolytic degradation[62]. M1A and m22G prevent misfolding of the tRNA, by helping to avoid potential undesirable interactions[62]. Another

function of modified bases in tRNA is the influence on the acetylation by aminoacyl-tRNA synthetases[65]. Lysidine (k^{2}C), t^{6}A and m^{1}G have negative effects on the recognition of the tRNA by the aminoacyl-synthetase enzyme[66,67]. A third example for the purposes of tRNA base modifications is that the codon-anticodon interaction can be influenced by some bases's tendency to enhance base stacking (e.g. m^{5}C, s^{2}C or Ψ) when they are present in the stem or the immediate neighbourhood of the anticodon[62]. Similar to that, bases at the position 37, such as m^{1}I, i^{6}A, t^{6}A or m^{1}G are not able to base-pair in a Watson-Crick fashion and thus prevent frameshifting, since this position is adjacent to the anticodon[62]. Therefore, modified nucleosides can modulate codon recognition and are important for the maintenance of the correct reading frame during translation[62]. Another function can be found in bacteria, where s^{4}U can protect the tRNA from photo-induced damages[68,69]. Phosphoribosyl-Purines (Arp and Grp) can prevent the tRNA from binding to certain elongation factors in several fungal and plant species[70]. Mutations in the tRNA modification pathway have shown to have serious effects, leading to neurological and metabolical disorders in many organisms, like Alzheimer's disease, ALS, epilepsy, intellectual disability, X-linked mental retardation and many more[71–73]. The effects described above are just examples of the variety of possibilities, modifications of RNA bases can open up in tRNA function.

1.2.2   Impact of modified RNA bases on ribosomal function

rRNA is heavily modified. However, compared to the highly diverse set of modifications that occur in nature, rRNA only comprises a limited number of (in the human 80S ribosome for example) 14 different post transcriptional modifications[74,75] (Figure 3). Until now, around 100 Ψ and 2'O-methylation sites each have been found in human rRNA and several sites of only 15 different other modifications (m^{1}acp^{3}Ψ, ac^{4}C, m^{1}A, m^{5}C, m^{7}G, m$_2^6$A, m^{3}U, m^{6}A, m^{3}C, m^{4}C, m^{1}G, m^{2}G, m$_2^2$G, m^{1}Ψ and cm^{5}U) in eukaryotes[75–80]. Like in tRNA, the functions of modified RNA bases include effects on the structure of the ribosomal RNA[61,81]. M$_2^6$A, m^{2}G and Um (2'O-methylated uridine) have been shown to affect the rRNA structure and stabilisation of the secondary folding[82–84]. M^{3}U, in contrast to m$_2^6$A promotes hairpin structure formation[85,86]. For m^{7}G and m^{1}A, a positive effect on RNA-protein interactions was observed[87]. Most modified RNA nucleotides cluster around functionally important regions, like the peptidyl-transferase centre or the decoding and tRNA binding sites, suggesting a role in translational fidelity and efficiency[88,89]. Certain m^{2}G, Um, m^{1}acp^{3}Ψ and m^{5}C sites were found to be in direct contact to tRNAs or close to the P-site of the ribosome, affecting translation accuracy[90]. Ψ and 2'O-methylated sites near the A-site were shown to be involved in maintaining efficient translation[91].

In bacteria, ribosomes are very often a target for antibiotics. Methylation of the rRNA can change the affinity of these kind of drugs to the ribosome, thus pointing out a way for antibiotic resistance in bacteria[92,93]. The methyltransferases, which are responsible for the resistances against kasugamycin, erythromycin and avilamycin have been identified and investigated[94–97].

1.2.3 Modifications found in other non-coding RNA species

The most prominent RNA base modification in small RNAs, observed in the recent past is the m6A-methylation of the snRNA (small nuclear RNA) U6[98,99]. Warda et al. found several other non-coding RNAs to be m6A-methylated as well[98]. The function of these new m6A sites however is not yet clarified, but the position of the methylation in U6 snRNA suggests to be connected to splicing regulation[98]. Other snRNAs have been identified as new classes of m6A containing non-coding RNAs[100,101]. Several snRNAs contain Ψ and 2'O-methylations as well[100,101]. The U2 snRNA for example comprises several 2'OMe and Ψ sites at the 5' end, which all seem to be required for the assembly of the spliceosome[102]. But also other small RNAs can be affected by modifying enzymes, such as microRNAs (miRNAs)[103,104]. The m6A mark was found on primary miRNAs (pri-miRNAs) for example. Also 2'O-methylation was detected in plant miRNAs[105]. This modification is located at the 3' terminal nucleotide and most likely protects the miRNAs from 3'-uridylation and subsequent decay[105]. Furthermore, pri-miRNAs, as well as mature miRNAs have been shown to be targets of A-to-I editing by ADAR (adenosine deaminase acting on RNA), whereby an adenine is modified to an inosine[106–110]. Editing of miRNAs can have impacts on their biogenesis and can further affect asymmetric strand selection[111].

1.2.4 Implications of the epitranscriptome on messenger RNA

In mRNA, only a limited number of different RNA modifications is described (Figure 3). The most prominent modification is the 5' cap, which is, together with the 3' poly(A)-tail, crucial for mRNA stability, nuclear export and translational efficiency[112,113]. In eukaryotes, the best known 5'cap comprises a m7G(5')ppp(5')N structure (Figure 2A) ,which is very stable and can only be de-capped by specific enzymes, such as the decapping enzyme Dcp2, allowing for subsequent degradation by the exonuclease Xrn1[37,114–116]. In addition to the m7G modification and the 5'-to-5'-triphosphate bridge, N6,2'-O-dimethylation on the first adenosine and 2'-O-methylation on the second adenosine (m7Gpppm6AmAm) have been observed in vertebrates [117,118119] (Figure 2A).
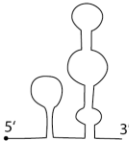
Just recently, a new cap structure has been described in several species, the NAD-cap[120–124] (Figure 2B). In these cases, a Nicotinamide adenine dinucleotide (NAD) is attached to the 5'

end of certain mRNAs, via the 3'OH of the adenine ribose of the molecule. In bacteria, where it was assumed that mRNA is not capped, this NAD-cap was shown to protect the RNA from 5'-processing by the RNA-pyrophosphohydrolase RppH and endonucleolytic restriction by ribonuclease RNaseE[122]. As a decapping enzyme, NudC was identified, which triggers RNase E mediated decay[122]. In mammals however, the NAD-cap promotes mRNA decay by the "deNADding" enzymes DXO/Rai1, other than the translation-promoting m7G-cap[120,125]. After a mass spectrometric approach, further cap structures like FAD, UDP-Glc and UDP-GlcNAc were detected[126].
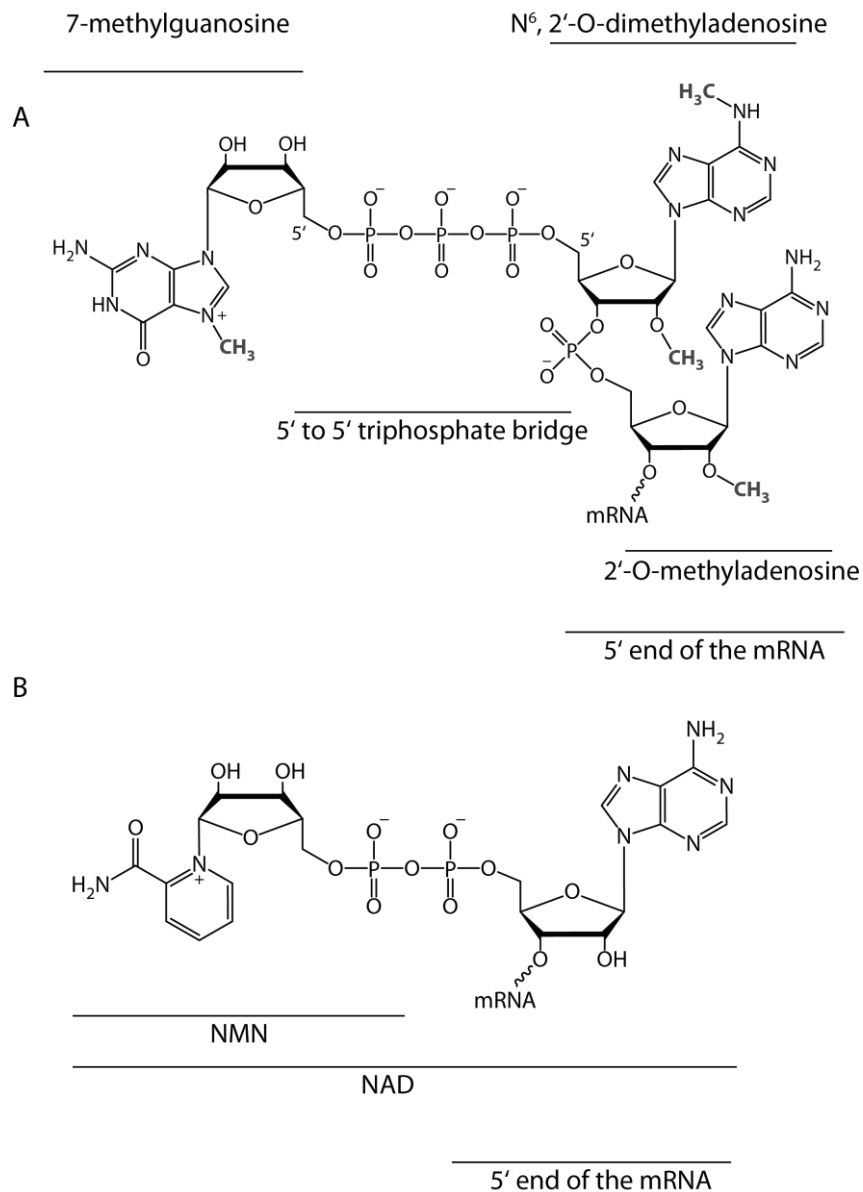
Figure 2: Cap structures found in mRNA. (A) The canonical 5' cap structure comprising an m7G modification, a 5'-to-5'-triphosphate bridge, N6,2'-O-dimethylation on the first adenosine and very often a 2'-O-methylation on the second adenosine (m7Gpppm6AmAm), how it appears in vertebrate mRNA. (B) The NAD structure is shown. It appears to be the 5'cap of mRNAs of various species.

The "internal" modifications, found in mRNA are m^6A, Ψ, 2'O-methylations, inosine, hm^5C, m^5C and m^1A[127,128] (Figure 3). The first, very extensive research on internal mRNA modifications was done on m^6A[52,53]. Up until now, it is the most investigated modification in mRNAs and research is continuously evolving for a complete understanding[129]. The effects, already found for the m^6A-mark in mRNA are very widespread and reach from nuclear export and alternative splicing effects[130–132], over mRNA-decay[133,134] to the regulation of translation[135] (see chapter 1.3.2). The destabilizing role of m^6A has an important function regarding stem cell differentiation by regulation of pluripotency factors[136–139]. Also m^6A demethylases have been found, making this epitranscriptomics mark very dynamically regulated[140,141]. There are hints for a role of this demethylation in splicing[142]. However, that much functional investigation has not been accomplished for all of the mRNA modifications. The group of Sammy Jaffrey described a m^6Am (2'O-methylated m^6A) demethylase[143–145]. The authors presented this new mRNA modification m^6Am to be part of an alternative 5'cap and having a positive impact on mRNA stability[143,146]. Another RNA modification - m^5C - was found mainly in certain untranslated regions, suggesting a role in mRNA silencing[54]. Another group found hints that point to a role of m^5C in mRNA export[147]. For the m^1A modification, even less information was revealed yet. The group of Schraga Schwartz found implications, that m^1A methylation in mRNA leads to translational repression due to its disruptive impact on base pairing[148,149]. The group of Chengqi Yi demonstrated that m^1A in mitochondrial mRNA interferes with translation[150,151]. Merely 5 years ago, Ψ was found to be another modified base present in mRNA[55,57,152]. Using different sequencing techniques, three independent groups found several hundred Ψ-sites on mRNA[55,57,152]. Functionally, Ψ is assumed to stabilise the secondary structure of RNA, since this modified base is known to affect the structure in tRNA likewisely[127,153]. Another interesting finding was that Ψ in stop codons leads to efficient read-through and incorporation of specific amino acids in yeast[154,155]. In this study, it was further observed that Ψ, m^6A, m^5C and 2'O-methylation sites in specific codon contexts can reduce the protein production, m^5C even was observed to change the coding from a proline to a leucine in *E. coli*[156]. Still a lot has to be elucidated in this field and future work will surely explain a multitude of biological processes. For an overview of all the RNA modifications found so far in the different RNA species, see Figure 3.

Figure 3 (schematic structures of tRNA, rRNA, snRNA and mRNA with lists of modifications):

tRNA

m^1Am	inm^5Um	m^2G
m^1Gm	inm^5s^2U	m^4_2Cm
m^1Im	inm^5U	ac^4Cm
m^1A	nm^5s^2U	ac^4C
m^1G	ncm^5Um	io^6A
m^1I	ncm^5U	ac^6A
$m^1\Psi$	$cmnm^5Um$	g^6A
Am	$cmnm^5s^2U$	hn^6A
Cm	$cmnm^5U$	i^6A
Gm	f^5Cm	m^6t^6A
Ψm	f^5C	m^6A
Um	ho^5U	t^6A
$Ar(p)$	mcm^5Um	C^+
$Gr(p)$	mcm^5s^2U	G^+
m^2A	mcm^5U	D
ms^2io^6A	mo^5U	oQ
ms^2hn^6A	m^5s^2U	$galQ$
ms^2i^6A	mnm^5se^2U	$OHyW$
ms^2m^6A	mnm^5s^2U	I
ms^2t^6A	mnm^5U	$imG2$
s^2Um	m^5C	k^2C
s^2C	m^5U	$manQ$
s^2U	tm^5s^2U	$mimG$
acp^3U	tm^5U	o_2yW
m^3C	$preQ1$	Ψ
imG-14	$preQ0$	Q
s^4U	m^7G	$OHyW^*$
m^5Cm	m^2Gm	cmo^5U
m^5Um	$m^{2,7}Gm$	$mcmo^5U$
chm^5U	m_2^2Gm	yW
$mchm^5U$	m_2^2G	imG

rRNA

m^1acp^3Y
m^1A
m^1G
$m^1\Psi$
Am
Cm
Gm
Im
Ψm
Um
m^2A
acp^3U
m^3C
$m^3\Psi$
m^3U
cm^5U
hm^5C
m^5C
m^5U
m^7G
m^8A
m_2^2G
m^2G
m^4Cm
ac^4Cm
ac^4C
m^4C
m_2^6A
m^6A
D
Ψ

snRNA

Am
Cm
Gm
Ψm
Um
$m^{2,2,7}G$
m^2G
m^6Am
m^6A
D
Ψ

mRNA

Am
Cm
Gm
Um
m^3Um
m^5C
m^7G
$m^{2,7}G$
$m^{2,2,7}G$
m^6Am
m_2^6Am
m^6A
m^1A
I
Ψ

Figure 3: Summary of RNA modifications in different RNA species. The upper part shows schematic structures of tRNA, rRNA, snRNA and mRNA. Underneath, lists of the abbreviations of modifications are shown, which are described to be found in the different RNA species of all phylogenetic classes (archaea, bacteria and eukarya). 2'O-methylations are marked with a terminal "m" after the base. For more information and full names of the modification symbols, see https://mods.rna.albany.edu/mods/[60,80].

1.3   Proteins involved in the pathway of modified RNA bases

RNAs are not modified during transcription by incorporating modified nucleosides by RNA polymerases. Instead, RNA modifications are generated by proteins that modify the nucleotide post-transcriptionally. These proteins have been termed "writers". The de-modifying enzymes that have been described, have (analogous to the writers) been named "erasers". For resulting in direct functions of the RNA modifications, RNA binding proteins – the "reader" proteins – are of particular importance. Those enzymes are by far not found and

described for all RNA modifications. The proteins, responsible for m⁶A, m⁵C, Ψ and m¹A-modification in RNA and for their subsequent function are discussed in this chapter. In Figure 4, a summary of the proteins, described in the literature that interact with the epitranscriptome is shown.
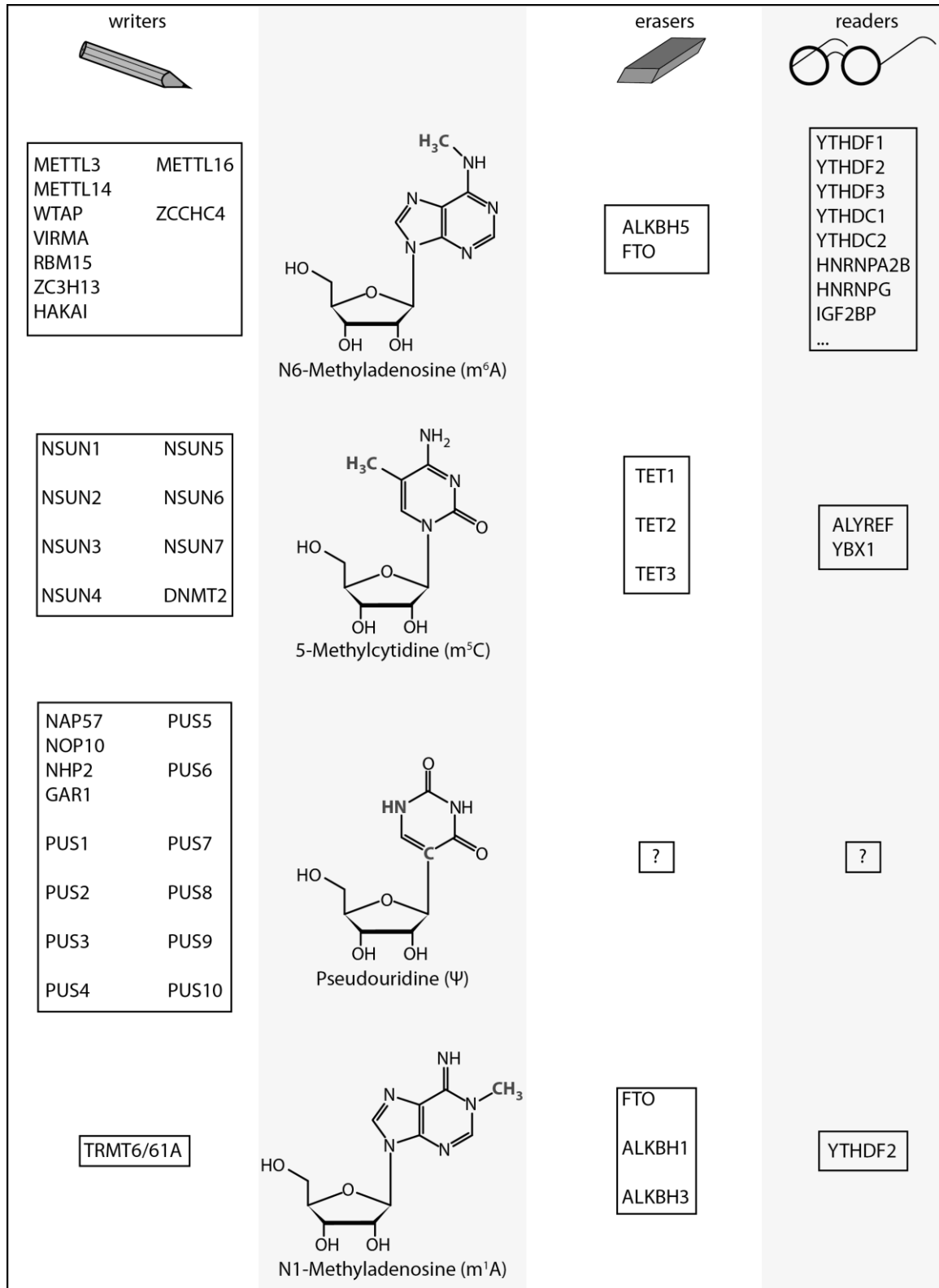
Figure 4: Suggested RNA modification interacting proteins for m⁶A, m⁵C, Ψ and m¹A. In the left row, the modifying enzymes ("writers") that are described in the literature are listed. The next row shows the structures of the nucleotides. In the third row, "erasers" and in the fourth row, "readers" are summed up, as suggested by several groups for the different nucleotides. The depicted proteins are discussed in this chapter.

1.3.1   RNA-modifying enzymes

1.3.1.1   Catalysing m⁶A-methylation and demethylation in RNA

Over 20 years ago, Methyltransferase Like 3 (METTL3), a subunit of the m⁶A-writer complex was described for the first time[157,158]. Subsequently, more and more parts of this large enzyme complex were identified. METTL14[159–161], WTAP (Wilm's Tumor 1 Associated Protein)[162,163], KIAA1429 or VIRMA (*Vir* in *Drosophila*[130,164])[161,165], RBM15/15B[166], ZC3H13 (Zinc finger CCCH domain-containing protein 13, *Flacc* in *Drosophila*)[167–169] and HAKAI were all found to contribute to m⁶A-methylation in mammals (Figure 5). METTL3 is the catalytic subunit, generating a methylation at an adenosine base within the RR**A**CH motif (with R = G or A, H = A, C or U) of mRNAs with the help of the cofactor S-Adenosyl methionine (SAM)[170,171]. This protein was found to be able to interact with the translation initiation factor eIF3H, thus enhancing translation[172]. METTL14 comprises RGG repeats at its C-terminal end, with which it brings the RNA target into place and stabilizes the binding, probably by binding to a secondary RNA structure[170,171,173]. Recent research has shown that METTL14 binds specifically to the histone H3 trimethylation at Lys36 (H3K36me3), guiding the whole complex to the m⁶A sites co-transcriptionally[174]. The specific RNA signal has further been suggested to be recruited by RBM15[166]. WTAP has a nuclear localisation signal, targeting the complex into nuclear speckles[162,173]. VIRMA (KIAA1429) has shown to be required for functional m⁶A-methylation[161] and to guide the modification at the specific site[165]. ZC3H13 was just recently found to serve as a bridge between RBM15/15B and WTAP in *Drosophila* and may also have localisation duties[167,168]. The function of HAKAI remains elusive to date, but several studies found this protein to interact with other components of this methylation complex[165,167,168,175].
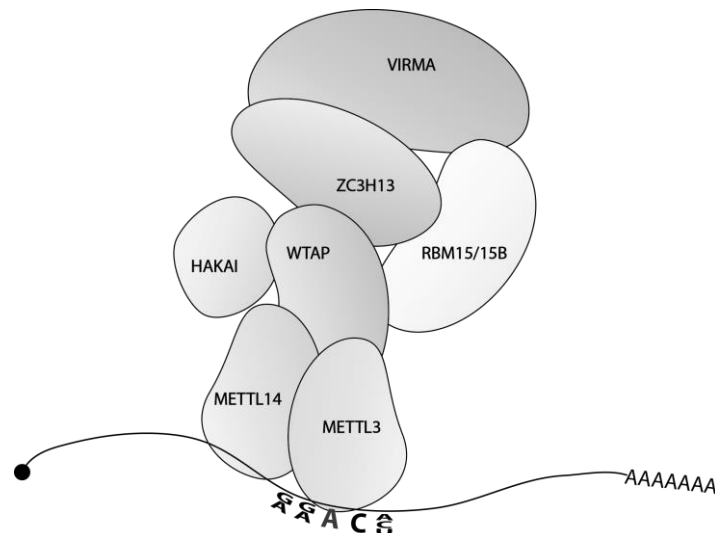
Figure 5: Schematic depiction of the METTL3-METTL14 complex. The methyltransferase complex, responsible for the catalysis of the reaction from an adenosine (A) to m[6]A in the context of a RRACH motif (R=G/A, H=A/C/U). The methylating complex consists of METTL3, METTL14, WTAP, RBM15/15B, ZC3H13, VIRMA and HAKAI.

Another m[6]A methylating enzyme, independent from the METTL3-METTL14 complex was found to act on mRNA as well: the m[6]A modification of the N6,2'-O-dimethylation (m[6]Am) on the first adenosine after the m[7]G cap. This modification was found to be generated by the RNA polymerase II-associated methyltransferase PCIF1, renamed as CAPAM (cap-specific adenosine methyltransferase)[118].

Recently, another methyltransferase, METTL16, has been found to catalyse m[6]A modification in RNA, more specifically in the U6 snRNA and different other non-coding RNAs (ncRNAs) and pre-mRNAs[98,99]. ZCCHC4 is a very recently added member of the m[6]A methyltransferases that acts on ribosomal RNA[79].

The "eraser" proteins FTO[140] and ALKBH5[141] have been discovered to demethylate m[6]A in mRNA, thus adding another layer of regulation to this epitranscriptomic mark.

1.3.1.2 Generation of m[5]C in RNA

RNA m[5]C methyltransferases (RCMTs) can be sub-classed in two clades, DNMT2 and the NOL1/NOP2/sun (NSUN) proteins, which all belong to the superfamily of Rossman fold-containing enzymes, using SAM as their methyl-donor[176]. In mammals, the NSUN family consists of seven proteins, namely NSUN1 - 7[177]. NSUN1 and NSUN5 and their yeast homologues Nop2p and Rcm1p have been identified as being rRNA methylating enzymes[178,179]. NSUN4 acts as a RCMT on mitochondrial rRNA, forming a stoichiometric complex with MTERF4, which recruits NSUN4 to the ribosome[180,181]. Transfer RNAs also harbour m[5]C-methylations. DNMT2 is one of the tRNA-RCMTs[182,183], targeting tRNA[Asp], tRNA[Gly] and tRNA[Val] in the consensus motif CACGCG[184–186]. NSUN3 is another tRNA m[5]C methyltransferase, which methylates tRNA[Met] in

mitochondria[187–189]. The tRNA affecting m5C-methyltransferase NSUN6, introduces m5C in tRNA[Thr] and tRNA[Cys] in humans[190]. NSUN2 methylates several specific tRNAs in the variable loop region[185,191,192]. This enzyme was also found to be responsible for the m5C-methylation in several other ncRNAs[193,194]. A third RNA species that NSUN2 specifically targets, are mRNAs[54,147,193,195–197]. The function of NSUN7 is not completely clear yet. However, there are hints that it might be specifically methylating enhancer RNAs (eRNAs), a class of short non-coding RNAs, transcribed from DNA-enhancer regions[198]. In DNA, TET enzymes are known to demethylate m5C[199], but the enzymes TET1-3 have also been shown to act on RNA as erasers[200].

1.3.1.3 Pseudouridylation in RNA

Pseudouridine (Ψ) can be installed via two different pathways: through "stand-alone" enzymes or via small RNAs-dependent enzymes. For the first class of enzymatically pseudouridylated RNAs, ten different PUS (<u>P</u>seudo<u>u</u>ridine <u>s</u>ynthase) proteins are responsible (PUS 1-10 in eukaryotes)[201]. They differ in localisation (nucleus, cytoplasm or mitochondria) and domain composition, but share a common catalytic domain[201]. These enzymes convert the N-C glycosidic bond between N1 of the uracil ring and the ribose sugar into a C-C bond, thereby enabling an RNA structure stabilisation[201]. Various U-sites in tRNAs are affected by PUS 1, 2, 3, 4, 7 and 8[201,202]. The only known consensus sequence however is UG<u>U</u>AR (with R = G or A), which is recognised only by PUS7[203]. Also mRNA is affected by several PUS enzymes at various sites[55,57]. PUS5 on the other hand modifies mitochondrial rRNA at one position[204]. Ribosomal RNA is otherwise pseudouridylated by a protein called dyskerin or NAP57 in humans, which is also a pseudouridine synthase, but is incorporated into a snoRNA guiding complex[205]. There are three further core proteins, important for this enzymatic functionality. NOP10 stabilises the complex and serves as a binding surface for NHP2, which has RNA-binding properties[206–208]. GAR1 is the fourth core protein, which has binding ability to the catalytic domain of NAP57 and is required for substrate turnover during the enzymatic reaction[209,210]. Apart from the proteins, mentioned, small so-called snoRNAs (small nucleolar RNA) are relevant for the generation of the modification. There are two classes of snoRNAs (small nucleolar RNA) that guide chemical modifications to RNAs: The C/D box snoRNAs, which are responsible for 2'-O-methylations and H/ACA box snoRNAs, which are associated with pseudouridylation of other RNAs[211]. These snoRNAs direct the protein complex to the target RNA, where certain hairpin structures lead to a perfect positioning of the RNA to be modified[212–215].

1.3.1.4 m^{1}A-modification in RNA

Not much is investigated yet about the methylation process of adenosine at position N1 The group of Schraga Schwartz found m^{1}A methylation to be catalysed by TRMT6/61A[148,149]. Also demethylases have been suggested, namely ALKBH1 and ALKBH3, which have been described to demethylate m^{1}A in tRNA[216,217].

1.3.2 RNA modification reader and effector proteins

The modification of RNA bases and the associated change of properties can directly affect stability, base-pairing, charges or secondary structures, thus leading directly to modulation of localisation, translation or processing[218]. Reader proteins are a way of indirectly affecting properties of RNAs. The best investigated readers are the m^{6}A recognising proteins. The YTH protein family was found to bind specifically to m^{6}A in mRNA contexts[52,219,220]. There are five different proteins in the YTH (YT521-B Homology) family, YTHDF1, -DF2, -DF3, YTHDC1 and – DC2[221,222]. They are all cytoplasmic, except YTHDC1 (YTH domain-containing protein 1), which is found in the nucleus and is involved in several nuclear functions[223]. After binding to m^{6}A in an RNA, YTHDC1 directly binds to SRSF3, a serine/arginine-rich splicing and mRNA export factor and thus contributes to alternative splicing[130,131,219]. Through the interaction with SRSF3, YTHDC1 is also involved in the regulation of the polyadenylation process of m^{6}A-containing pre-mRNAs[224]. YTHDC1 was further found to enhance the export of m^{6}A-methylated mRNA, also via interaction with SRSF3[131,132]. Another function of YTHDC1 is to assist in transcriptional repression of X-chromosome genes by binding to the long non-coding RNA XIST (X-inactive specific transcript)[166]. YTHDC2 has several functions in the cytoplasm[223]. Among others, the protein has 3'-5' RNA helicase activity[225,226], plays a role in the proliferation of cancer cells[227,228] and binds to the 40S ribosomal subunit near the mRNA entry/exit site[229], thereby pursuing opposing duties: it enhances translation efficiency by recruiting meiosis-specific m^{6}A-mRNAs to the ribosome[230,231] but also decreases mitotic mRNA stability by recruiting exonucleases [225,229–232]. YTHDF2 has further been shown to regulate the decay of m^{6}A-containing mRNA via interaction with the CCR4/NOT complex, the major deadenylase in eukaryotic cells[133,134]. This role of YTHDF2 seems to be conserved in evolution, since in *S. cerevisiae*, the YTH protein Pho92 also interacts with a component of the CCR4-NOT complex[233]. Interacting with RNaseP/MRP via the adaptor protein HRSP12, YTHDF2 was shown to be involved in endoribonucleolytic cleavage of m^{6}A containing RNAs[234]. In contrast, YTHDF1 is facilitating the translation initiation, thus enhancing translation efficiency of certain RNAs, which are m^{6}A-methylated in the 3'UTR[135]. YTHDF1 can recruit and interact with ribosomal subunits, namely the 40S subunit and the eIF3 complex, forming a loop between the methylated 3'UTR

and the translation start site[135]. Independently of YTHDF1, eIF3 also has the ability to bind directly to the 5'UTR of m6A-containing RNA under stress conditions, promoting cap-independent translation[146]. YTHDF3 is able to act synergistically in a cooperative way together with YTHDF1 and 2, being able to enhance translation (with YTHDF1) or degradation (with YTHDF2)[235,236]. Oxidative stress leads to re-localisation of only YTHDF3 to stress granules, selecting and sorting out specific affected mRNAs[237]. The three YTH proteins have also been found to act together in decreasing different m6A-containing viral RNA reverse transcription rates or inhibit viral replication[238–242]. It has been specifically looked into the Hepatitis C virus, Zika virus and HIV, however, the findings have to be further investigated for a complete elucidation[238–241].

With all these different specific functions of the YTH proteins, the YTH domain seems to have specifically evolved as an m6A binding domain. Figure 6 shows the perfect fitting of the m6A RNA oligo in the YTH domain with m6A buried in the hydrophobic binding pocket.
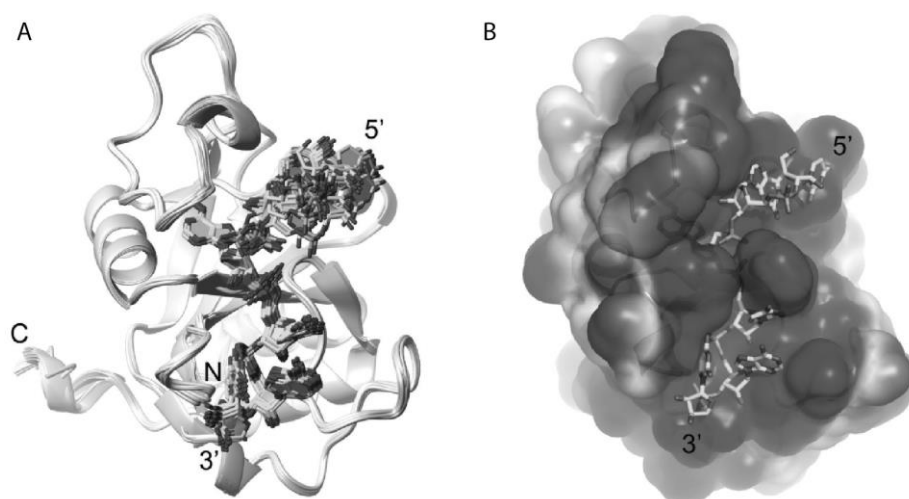
Figure 6: Structure of the YTH domain in complex with an RNA oligo (5'-UG*m6A*CAC-3'). (A) The YTH domain is shown in ribbons, the RNA is displayed in stick representation. The figure shows an ensemble of 20 selected structures. (B) Electrostatic potential of the surface of the YTH domain structure. The RNA oligo fits perfectly in the YTH domain and m6A is buried in the hydrophobic core, which serves as the m6A binding pocket. Figure from Theler et al., 2014[220].

In addition to the YTH proteins, several other specific m6A reader proteins were identified in different screens[52,243–245]. HNRNPA2B and HNRNPG were found to bind m6A, thereby affecting and regulating alternative splicing and, in case of HNRNPA2B1 also mediating primary miRNA processing via interaction with the micro-processor complex protein DGCR8[103,244,245]. HNRNPC has also a binding affinity to m6A, however only when the base is in a certain secondary structure[246]. M6A has the ability to alter the secondary structure in RNA[246]. This so-called "m6A-switch" facilitates the binding of HNRNPC, thus affecting alternative splicing[246]. Another

protein family, IGF2BP 1, 2 and 3, were found to recognise m6A in RNA to enhance stability and translation of mRNAs[247]. The group of Michiel Vermeulen did a large SILAC-based screening, where they found specific binders and repellents of m6A[243]. As novel reader proteins, they found CPSF6, ZCCHC8, SF3B4, RBBP6, FMR1 and FXR1&2 among others[243]. Already in 2012, ELAVL1, DBN1, DHX36 and also HNRNP proteins were found to bind to m6A in a study of Dominissini et al.[52]. However, all these factors are found in large-scale screening approaches and need to be further validated. The function of these proteins in biological pathways have still to be clarified.

Not only for m6A, but also for m5C, RNA-reader proteins have been described, one of them is the mRNA export factor ALYREF (and ALY1 in *Arabidopsis thaliana*)[147,248]. Both in animals and plants, it was thus suggested that m5C acts as a regulator of mRNA export[147,248]. Not much has been investigated in this direction and further research is needed to understand the effects of potential m5C methylation in mRNA. Another new specific reader protein for m5C has recently been described which is a well-known RNA binding protein - YBX1[249,250]. Two independent studies found this protein to preferentially bind to m5C methylated mRNA with its cold shock domain (CSD), thus influencing the stability of mRNA and early embryogenesis[250,251]. For m1A, one reader protein was described to have specific binding properties. Pre-published data suggests a potential binding of YTHDF2 to m1A[252].

The described proteins are most probably not all the interactors and readers of modified RNA bases that exist. The finding of more of these proteins will help elucidate the importance and function of the base modifications in RNA.

1.3.3   Discussion and debate about certain modifications in mRNA

For a few modifications, the suggested sites and also proteins, involved are not fully accepted by all researchers in the field. In fact, the mere existence of m5C[54,253] and m1A[148–151] in mRNA is still highly debated, since for both, several independent groups have found contradictory results in their sequencing approaches. Several groups found various m5C modification sites within untranslated regions and in the coding sequences of the mRNA[54,147]. The groups of Frank Lyko and Mark Helm however, claim that the m5C marks found in mRNA are artefacts of the bisulfite treatment, necessary for sequencing[253]. Using a "statistically robust" computational approach they doubt m5C to be present in mRNA at all[253]. For the potential m1A sites in mRNA it is similar. Two groups are having a lively discussion, whether or not this modification is highly abundant in human mRNA[148,150]. Using more or less the same method with different approaches of analysing the data, the group of Schraga Schwartz only found m1A methylation to be present very sparsely in mRNA at nine specific sites and , as mentioned before, to be catalysed by TRMT6/61A[148,149]. The group of Chengqi Yi however, detected more

than 450 sites and claimed them most likely not to be installed by TRMT6/61A[150,151]. With both groups having reanalysed the data and still having divergent views, it shows how still today the investigation of RNA is not trivial[148,150]. Furthermore, concerning m6A, recent research found contrary results, suggesting no m6A-demethylation via ALKBH5 occuring on mature mRNA[254]. In this article, the authors also claim that m6A is not involved in ALKBH5-dependent splicing events[254,255]. Chuan He's group also investigated the matter of demethylation in more detail and claimed recently that FTO demethylates m6A as well as m6Am and even affects m1A in tRNA[256]. One last matter of debate are the exact Ψ-sites, which are also not finally clarified, since also here, the sites differ a lot between the different sequencing data sets[55,57,58]. Using pseudoU-Seq, one group found over 200 sites, another described over 300 sites and the slightly different method CeU-seq identified over 2000 Ψ-sites[55,57,58]. With all this uncertainty and no common ground in the field of RNA modification research, it seems very important to generate tools and methods for clarification, as they are urgently needed to shed some light in the jungle of RNA modifications.

1.4   Detection strategies of RNA modifications

There are several methods to detect modified RNA bases, some of them developed in very early times (see chapter 1.1.1). Thin layer chromatography, paper chromatography, UV absorption and even microscopy belonged to the first detection methods[8,13,17,20]. The application of different RNases helped to analyse and partially understand the RNA composition[22–24]. Using the isotopes ^{14}C and ^{3}H, several groups endeavoured chase experiments of the modified bases[4,6,32,35–37]. As the methodical range grew broader, also the work with RNA and its different modified bases was becoming easier. With electrophoresis methods[257], northern blotting[258] and mass spectrometry[259,260], a much wider scale of RNA science could be conducted. Using mass spectrometry, the group of James McCloskey could for example detect and find the structure of 93 different modified nucleosides in RNA in 1994[261]. Another important finding was that some modified bases leave specific reverse transcriptase (RT) signatures in the cDNA from which the modified base can be deduced. The RT mis-incorporates certain bases, like a cytosine instead of a thymine at the site of inosine[262,263] or characteristic mismatch rates for m1A[264,265]. Some modifications, like m1G, m3U and also m1A can cause the RT to stop and thereby block any extension of the cDNA or change its fidelity[266–268]. A method to detect m1A was developed, taking advantage of the Dimroth rearrangement of m1A to m6A under basic conditions, thus avoiding the RT to stop and to gain clearer signals[149,269,270]. To make the signal of the modified bases more obvious or to enhance their signatures, RNA can be treated with different compounds[271,272]. Using the chemical CMC-

T (*N*-Cyclohexyl-*N'*-(2-morpholinoethyl) carbodiimid-methyl-*p*-toluolsulfonat) for example, pseudouridine sites can be uncovered by an induced RT arrest[55,57,58,273]. Bisulfite is known to deaminate unmethylated cytosines (which are then reverse transcribed to thymine) but doesn't affect 5-methylcytosine (m5C)[54,56,274]. The m5C sites are reverse transcribed into cytosines and can thus be determined[54,56,274]. Inosine can be N-alkylated using Acrylonitrile, leading to RT arrest (ICE-seq method)[275]. There are much more examples for reagents that specifically bind to certain RNA base modifications, having an impact on the reverse transcription[272].

The RNA can subsequently be analysed with the perhaps most important development in RNA research, the RNA next generation sequencing methods[47–51]. For an analysis like that, the RNA base modifications have to be enriched. Several methods were developed to achieve that[272,276]. There is a strategy, where a mutated modifying enzyme is trapped on the target site, which then covalently crosslinks to the RNA. Primer extension and sequencing then give rise to the modified position[181,188,193]. A second enrichment method is the use of biotinylated clickable chemicals, which can be specifically linked to a certain modification on a fragmented RNA via the "Click" reaction. Through the biotin tag, the fragment can then be pulled out using streptavidin and prepared for sequencing[122,152,277]. Very commonly in use are antibodies against modified RNA bases for enriching those. Either the simple methylated RNA immunoprecipitation (MeRIP)[52,53] can be applied, where fragmented RNA is subjected to an antibody selection, followed by isolation of the RNA fragments via stringent washing steps and finally library preparation. Other applications of antibodies are combinations of MeRIP and iCLIP (individual nucleotide resolution crosslinking (UV 254 nm) and immunoprecipitation), called miCLIP[278] or MeRIP and PAR-CLIP (photoactivatable ribonucleoside-enhanced crosslinking (*in vivo* s4U-incorporation and UV 365 nm) and immunoprecipitation), called PA-m6A-seq[279].

From the first generation of an antibody against an RNA base in the 1970s on, these very helpful and convenient tools made them be irreplaceable for studies with modified bases. Their potentially high specificity and sensitivity make antibodies such precious tools.

1.5   Detection of RNA modifications by specific antibodies

1.5.1   Short history of antibodies

The roots of immunology lay far back with the works of Dr. Edward Jenner, who discovered in 1796 that variolia vaccinia (or cow-pox) could induce protection against smallpox in humans and called the method vaccination[280,281]. Dr. Emil Behring, an assistant of Robert Koch,

made a great progress in the field of vaccinations in the 1890s[282]. He observed a developing immunity against diphtheria and tetanus in mice and rabbits when treated with cell-free blood fluid. Shortly thereafter, he was the first scientist to treat humans with a purified antitoxin (against diphtheria) in a larger scale, industrially produced by Farbwerke Hoechst in 1894[283]. For this, he was awarded the very first Nobel Prize for Physiology/Medicine in 1901[284]. The analysis of antibodies went on, until Behring and colleagues found the antitoxic substance to be in the protein fraction, more specifically a member of the globulin family and called it paralbumin (today called gamma-globulin)[283]. Antibody research, or immunochemistry was in the subsequent years on the one hand moving in the clinical direction, but also biochemical applications were investigated. Nowadays, antibodies are regularly used for clinical and research applications.

1.5.2   Functional and structural depiction of immunoglobulins

The immune system is a very complex, potent and vast network of cells, molecules, organs and tissues that spread throughout the body to protect an organism from pathogens like bacteria, viruses, fungi or toxins[285]. Its task is to recognize and destroy antigens and to ultimately extinguish the source of their production[285]. There are two types of immune responses, the innate immune response and the adaptive response, where antibodies play an important role[285]. Antibodies are proteins acting in the immune system and are also called immunoglobulins. They are secreted from specific B-lymphocytes, when a pathogen enters an organism[285]. The pathogen, in this case a virus, produces antigens (short for <u>anti</u>body <u>gen</u>erators), which are bound by dendritic cells (DCs)[285]. These cells are then activated, turning into APCs (antigen-presenting cells) and express MHCs (major histocompatibility complex I and II) with the viral peptides on their surface[286]. The antigen-binding MHC-II presents the antigen fragments to helper T-cells (CD4+ T-cells), activating them thereby[286]. The helper T-cells in turn activate specific B-lymphocytes that become antibody secreting plasma cells. There are several effector functions of the secreted antibodies[286]. They can attach to pathogens, blocking their binding to cell-surface receptors[286]. Another response of antibodies is the direct binding of soluble mediators, excreted by pathogens and blocking their toxic activity[286]. Antibodies can also trigger a part of the innate immune response, namely the complement system, which promotes inflammation and lysis of the pathogen[286]. Granulocytes can bind to the antibody-bound pathogen and induce inflammatory processes and phagocytosis[286]. The MHC-I also binds to antigens and is bound by natural killer and cytotoxic T-cells (CD8+ T-cells), which have been activated by cytokines, secreted by MHC-II to eventually lyse the infected cell[285]. To prevent a second attack by the pathogen, memory B-

cells are produced that can secrete the specific antibody, when necessary. An antibody can only bind specifically to a small region of an antigen, called epitope, for which it is produced[285]. Generally, antibodies consist of a constant and a variable region[287]. Within the molecule group of immunoglobulins, there are five different classes – IgM, IgD, IgG, IgA and IgE, which vary in their constant region[287]. As the class of IgG antibodies is the most abundant and also the most relevant for this work, they will be described in detail. The class of IgG antibodies, can be subdivided into several subclasses[285]. In humans, there are the subclasses IgG 1 to IgG 4 A, mice and rats show the subclasses IgG1, 2a, b and IgG3. The schematic view of an antibody is depicted in Figure 7.
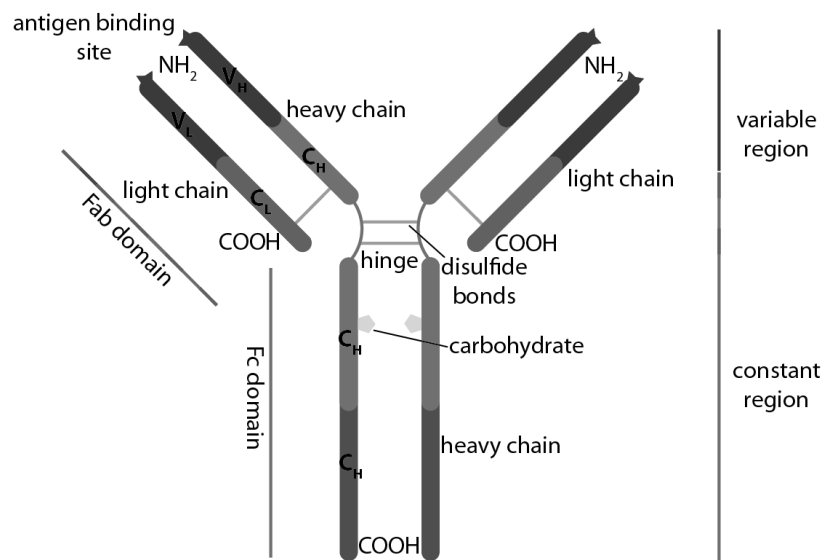
Figure 7: General structure of an antibody. Disulfide bonds connect the two light chains to the two heavy chains, and the two heavy chains at the hinge domain together. The very N-terminus of all four chains are variable in their amino acid sequence and bind the antigen. The C-terminal constant region has the purpose to bind to effector molecules and cells[287].

These molecules are Y-shaped and consist of three globular parts that are connected by the flexible hinge region and that are more or less same in size[287]. IgG antibodies are approximately 150 kDa in size and consist of four polypeptide chains[287]. The two identical heavy chains (around 50 kDa each) are connected via disulfide bond. Each heavy chain binds one of the two identical light chains (around 25 kDa each) also via disulfide bond[287]. There are carbohydrate side chains attached to the middle C_H-domain which are located between the heavy chains[287]. The amount of these side chains varies between the different classes of antibodies and determines the structure. The arms of the Y-shaped molecule are called Fragment antigen binding, or Fab-domain. The Y-stem could be crystallized easily and is therefore called Fragment crystallisable, or Fc-part[287]. Each region of 110 amino acids builds up a discrete immunoglobulin domain. The N-terminal variable domains of heavy and light chains differ between antibodies in the first 110 amino acids (variable region, V_H and V_L),

whereas the C-terminal domains of the heavy and light chains are constant within the same isotype (C_H and C_L)[287]. This property entails the N-terminal domain to bind the different antigens and the C-terminal domain to interact with effector cells and molecules of the host[287].

1.5.3 Generation of monoclonal antibodies

There are two types of antibodies: polyclonal and monoclonal. Polyclonal antibodies are secreted from different B cell lines within one organism[288]. They are a compilation of different antibodies, each recognising a different epitope, but altogether reacting to a specific antigen[288]. They can be harvested and purified from the blood serum of animals after immunisation[288]. In contrast, monoclonal antibodies come from a single B cell and are a homogenous mixture of mono-specific immunglobulines[288]. In 1975, Köhler and Milstein developed the technique of fusing spleen cells and myeloma cells to hybridoma cells for monoclonal antibody production[289]. The technique is schematically depicted in Figure 8.
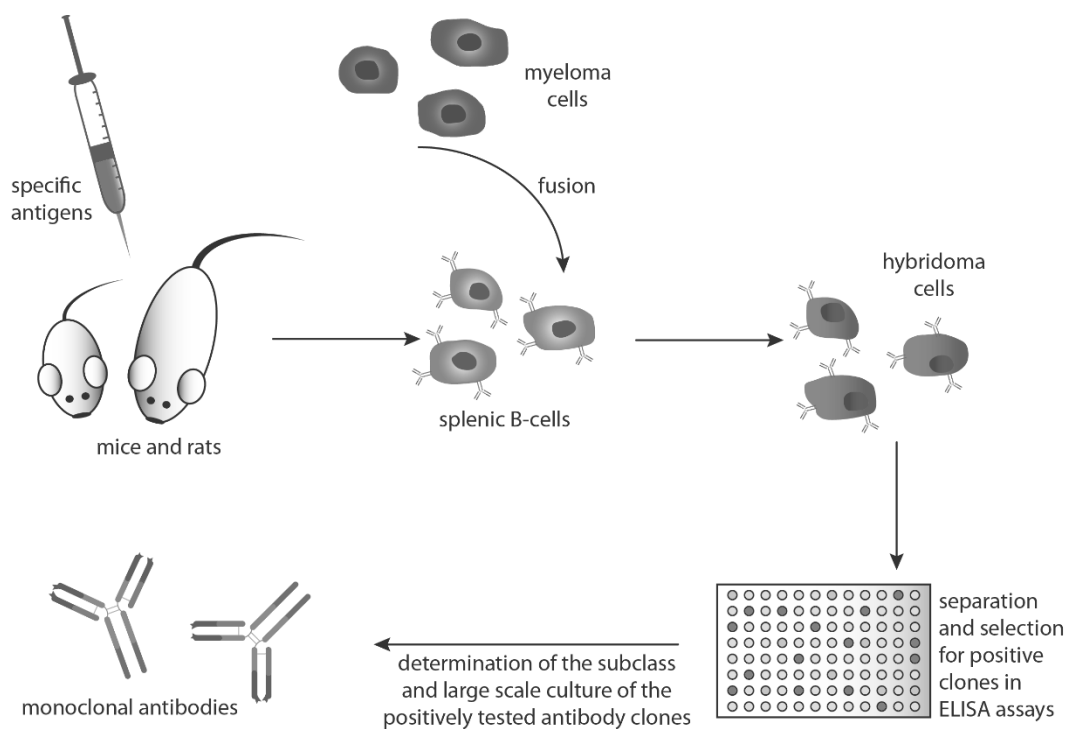
Figure 8: Schematic overview of the generation of monoclonal antibodies. Mice or rats are immunized with the specific antigen of interest. After a few weeks, the antibody producing B-cells from the spleen are fused with a myeloma cell line to gain hybridoma cells. The positive clones are then selected via Elisa assay, the subclass is determined and finally, the positive monoclonal antibody clone can be produced in a larger scale.

Laboratory animals, typically mice, rats or rabbits are immunized with the specific antigen[290]. After a few weeks, the B cells which are produced in the spleen of the animals are then fused with myeloma cells to gain immortal hybridoma cells[290]. These cells then have to be separated

and selected in HAT medium[290]. The first hybridoma screening is normally done via enzyme-linked immunosorbent assays (ELISA). The subclass of the antibody clones is determined using HRP-linked antibodies specific for the different IgG subclass. The cells are then cultivated for bulk antibody production[290]. For a better understanding and also for engineering the immunoglobulin, the antibodies can be isolated, sequenced and cloned into a vector for recombinant expression and purification[288].

1.5.4   Antibodies against modified nucleic bases

In 1964, Erlanger and Beiser developed a method to conjugate a riboside to a protein in order to achieve an antigen for immunisation[291] (Figure 9). This achievement was important to be able to create antibodies against nucleic bases.
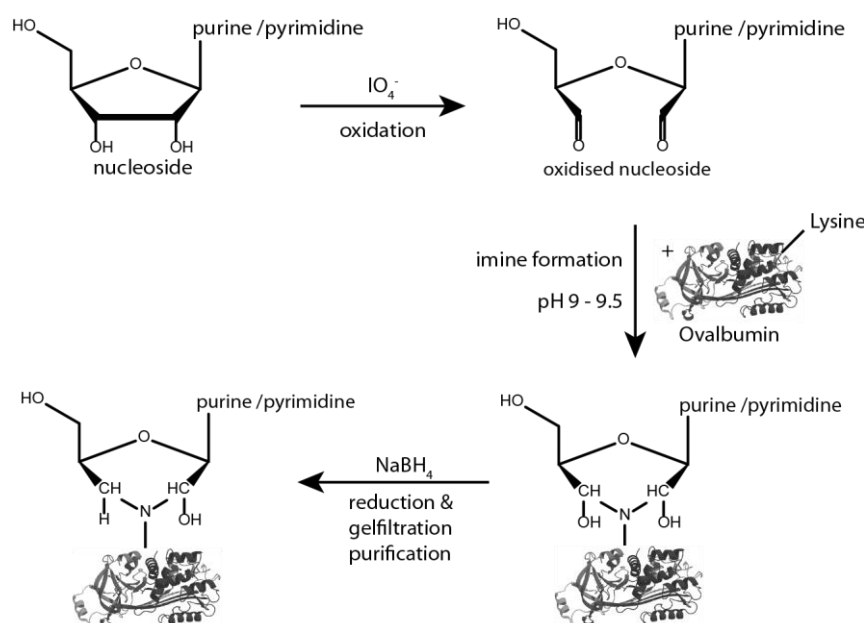
Figure 9: Coupling reaction of a riboside to ovalbumin. The RNA or DNA nucleoside is oxidised, using IO_4^-. To that, ovalbumin is added under basic condition to achieve an imine formation. This molecule then has to be reduced, using $NaBH_4$. After gel filtration and purification, the conjugate can be used as an immunogen. Figure adapted from Erlanger and Beiser, 1964[291].

In the figure shown above, ovalbumin is used as an immunogenic carrier protein. Ovalbumin has long since been used for this application since it has a great number of free and accessible amine groups[292]. BSA is also very commonly used as a carrier protein, as it is a basic protein, comprising several free NH_2-groups. The ribose ring of the nucleoside is oxidised with IO_4^-. Two aldehyde groups are formed, to which the carrier protein can bind under basic conditions, resulting in an imine. Reducing this molecule with $NaBH_4$ yields in the conjugate

that can be used for immunisation. The ribose ring is opened during the reaction and the protein is linked to the nucleoside via the 2' and the 3' position. This leads to the consequence that antibodies resulting from an immunisation with these antigens will not be able to discriminate between DNA and RNA as well as 2'-O-methylated and unmodified 2' and 3' OH-groups[278]. As of now, there are no published antibodies against nucleosides, generated differently from this coupling method[293].

The development of antibodies against modified nucleic bases was partly driven by the urge to detect DNA that was structurally modified by chemical carcinogens[294–296]. In the 1970s, several labs started to work on generating antibodies detecting RNA nucleosides. Munns *et al.* characterized antibodies against m6A and m7G, using BSA-nucleoside conjugates[297]. Sawicki *et al.* used the same technique to devise antibodies against 5-bromouracil, 5-iodouracil and 6-methyladenosine[298]. Some groups even developed antibodies against relatively large modifications, like N6-(Δ2-isopentenyl)-adenosine[299] or N-[9-(β-D-ribofuranosyl)purin-6-ylcarbamoyl]-L-threonine[300].

For several bigger analyses and studies, commercially available antibodies have been used. Among others, the most widely used were the polyclonal antibody against m6A from Synaptic Systems (no. 202-003)[52,103,160,270,278,301–303], the anti-m1A antibody from MBL (clone AMA-2)[149,151,270,304,305], the antibodies against m5C from MBL (clone FMC-9)[304] or Diagenode (clone 33D3)[56,306–308] and the anti-Ψ-antibody from MBL (clone APU-6)[304,309,310]. However widely used, several laboratories reported unsatisfying results regarding affinity and specificity for RNA molecules of certain antibodies[304]. Although there have been a few intentions to generate anti-m6A antibodies, until now, only the polyclonal antibody from Synaptic Systems met the high requirements of the scientists[278]. The urge for more rigorous and detailed characterisation of antibodies can be read in several publications[272,293,311].

1.6   Aim of this thesis

This thesis was pursued with the aim of generating and establishing highly specific and most sensitive monoclonal antibodies against a set of certain nucleic base modifications. We adapted and optimised a method for the synthesis of the antigen. Subsequently, the different antibody hybridoma clones had to be validated regarding specificity and sensitivity. To achieve that, the verifying experiments had to be designed and optimised. With the best performing antibodies, different applications, like immunofluorescence and miCLIP analysis have been carried out.

A second study deals with the search for unknown "reader" proteins – RNA binding proteins that bind specifically to modified bases of the RNA. For that, an established pulldown

experiment using RNA hairpin structures was redesigned. First, the hairpins had to be cloned, *in vitro* transcribed and ligated in an optimisation process. The precipitated proteins were then analysed via mass spectrometry and evaluated for positive binding to modified RNA.

2. <u>RESULTS</u>

2.1 Antibodies against modified nucleosides

To generate and validate highly sensitive and specific antibodies against a number of modified RNA bases was the aim in this chapter.

2.1.1 Synthesis of the antigens for immunisation

First, modified bases were selected, which were subsequently used for antigen generation. For that, the most common modifications m^6A, m^5C and Ψ were chosen. To have a broader spectra of antibodies later, also m_2^6A, m^1A, m^3C, m^1G, m^5U and m^3U nucleosides were elected to work with. The chemical structures of the selected RNA bases are depicted in Figure 10.
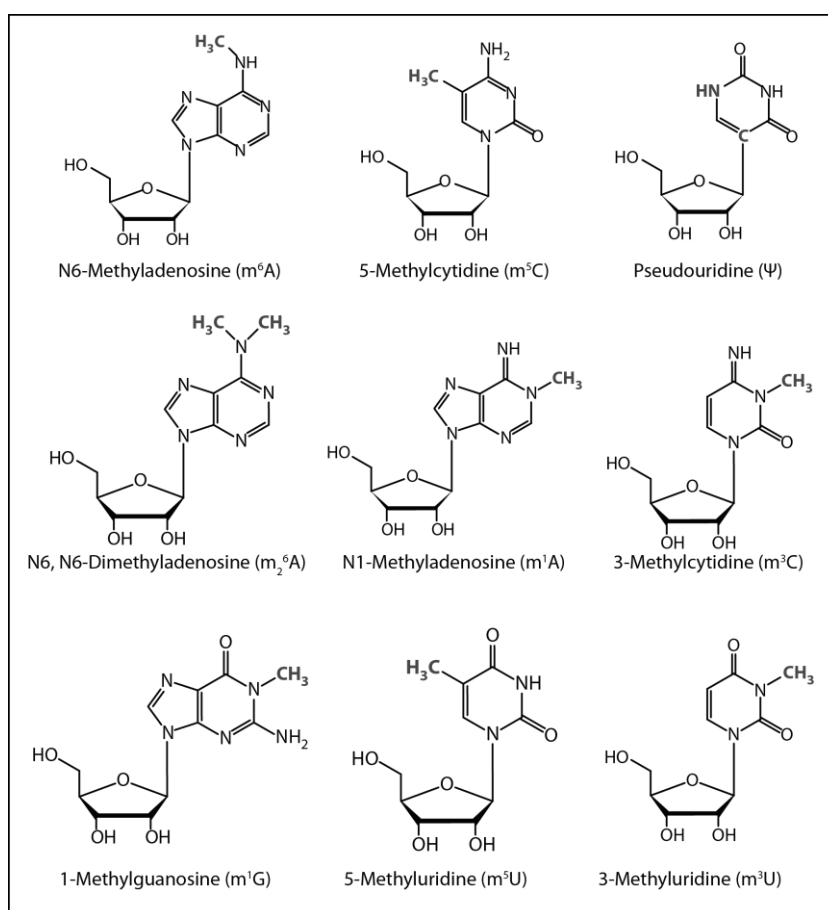
Figure 10: Selected modified RNA bases used for antigen synthesis and immunisation. The chemical structures of the nine selected RNA bases, which were used for antigen synthesis. The common names are written underneath each structure.

For immunizing mice and rats, a suitable antigen needed to be developed. Single nucleosides alone do not trigger an efficient immune reaction, so ovalbumin (OVA) was used as a carrier

protein, since OVA will lead to an immune response. In Figure 9 (chapter 1.5.4) and Figure 11A, an overview of the coupling of nucleoside to carrier protein using the Erlanger/Beiser method[291] is depicted. The same reaction was performed with BSA as carrier protein for subsequent analysis of the antibodies in ELISA experiments (Figure 13, right part). During the reaction, the ribose is converted, thus the nucleoside loses its RNA-specific properties. After the reaction, the coupling efficiency was tested using UV-photometric analysis. The absorbance of the conjugate was measured at 5 different wavelengths (250 nm, 260 nm, 270 nm, 280 nm and 290 nm). The measured data points were then fitted to the corresponding calculated absorption values. The best fit composition of nucleoside and carrier protein was determined using a grid search, which builds a model for every combination of the parameters and evaluates them. The grid search was performed with a resolution of 0.1 µg, using the sum of squares of the deviation between measured and calculated absorption values. For that, the conjugate-spectrum was assumed to be the sum of the spectra for nucleoside and ovalbumin (Figure 11B).
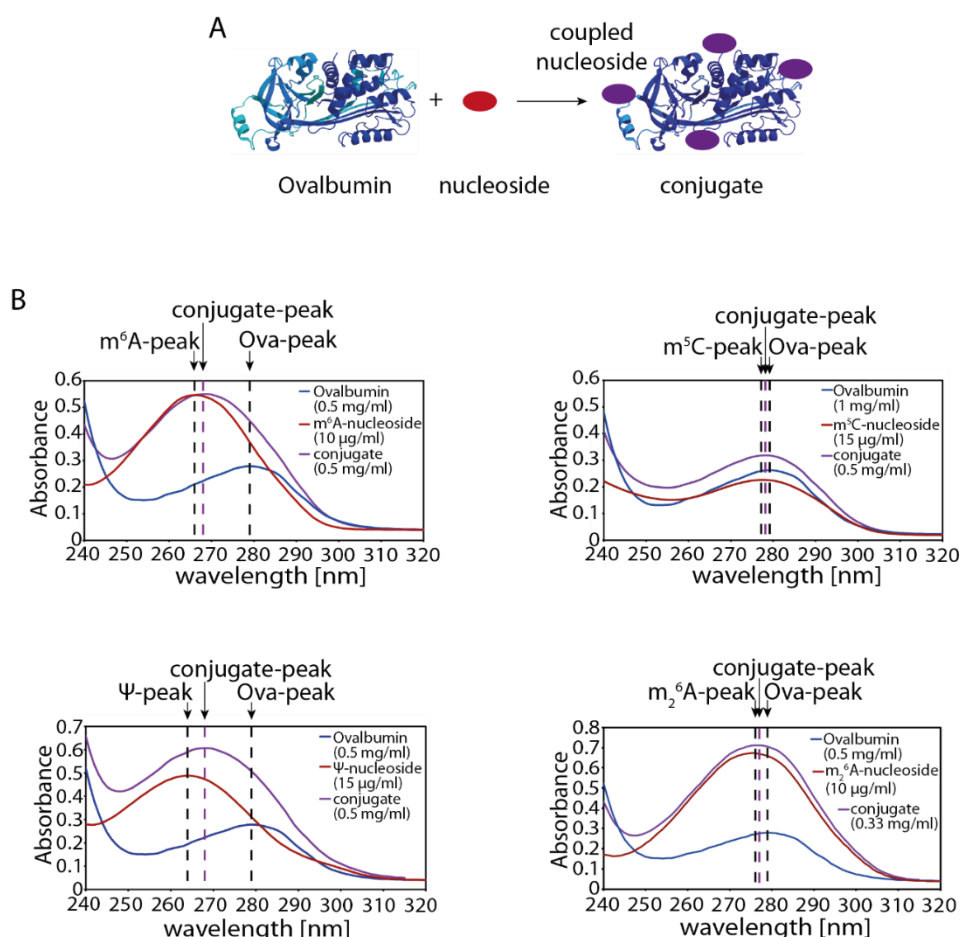
Figure 11: Absorption curves for ovalbumin, nucleosides and the resulting conjugates. (A) Schematic depiction of the reaction between ovalbumin (blue) and the nucleoside (red) to form the conjugate (purple). (B) Absorption curves of the members of the reaction with the same colour scheme as in (A). The spectra for m6A, m5C, Ψ and m2 6A are shown.

Here, the blue line depicts the ovalbumin curve, the red line shows nucleoside-absorption and the purple graph shows the best fit for the conjugate, as described above. Only the absorption curves for m^6A, m^5C, Ψ and m_2^6A are shown in Figure 11B. The same was executed with all modified nucleosides used for coupling (see Figure 10). From these absorption curves, the molar ratios of bound nucleosides per carrier protein and thus the efficiency of the reactions was estimated (Figure 12). From the 20 lysines in ovalbumin, there were on average 4 - 5 coupled to a nucleoside, which sums up to 20 to 25 %.
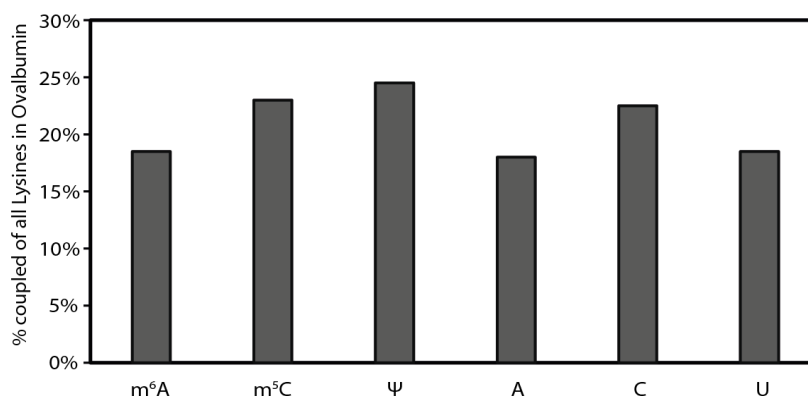
Figure 12: Estimated coupling efficiency of the nucleoside to ovalbumin conjugation reaction. Of the 20 lysines in Ovalbumin, on average 4 – 5 were coupled to a respective nucleoside. This was estimated using the values gathered in the absorption experiments (shown in Figure 11B).

The coupling reaction of nucleosides and OVA/BSA, as well as the validation of the data and estimation of the reaction efficiency was performed by Robert Hett in the lab.

After having synthesised the required conjugate antigens, immunisation and fusion of myeloma and splenic B cells of the immunised mice were done in the Helmholtz Center in Neuherberg by the group of Dr. Regina Feederle (chapters 1.5.3 and 4.2.3.2). Figure 13 (left part) gives a complete overview of the generation of monoclonal antibodies.
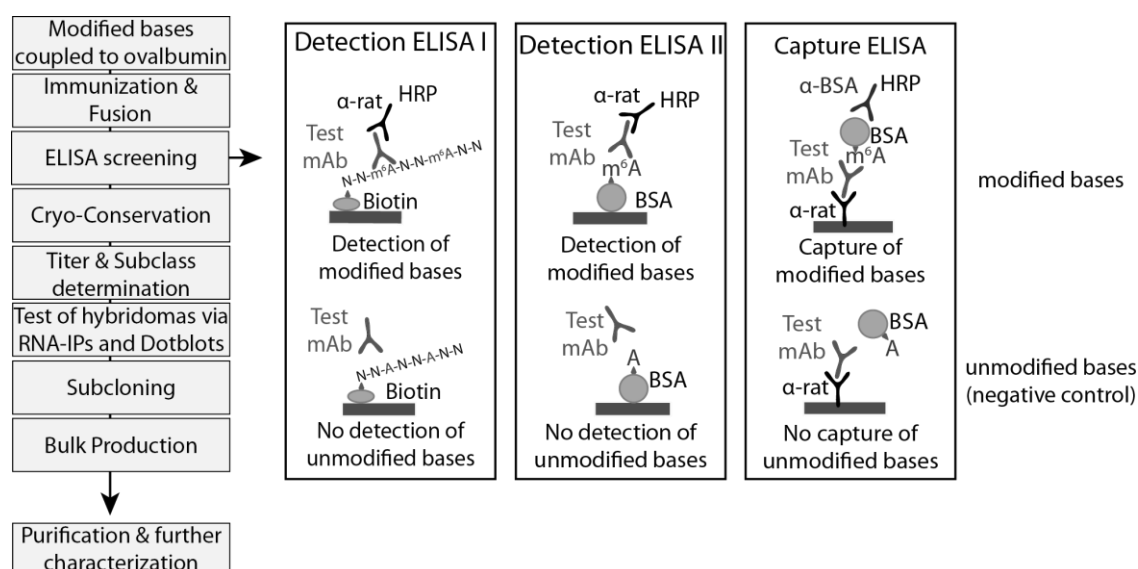
Figure 13: Workflow for the generation of monoclonal antibodies and schematic depiction of ELISA. The left section shows the workflow for generating the antibodies. The three boxes on the right are overviews of the detection ELISAs, which were done for first validation of the hybridoma clones.

The different ELISA screening methods that are shown on the right section of Figure 13 were also conducted in the laboratory of Dr. Feederle. In the first detection ELISA assay, the plates were coated with biotinylated DNA oligos (modified and unmodified), the second detection ELISA was performed with BSA-coupled modified nucleosides. For the capture ELISA, the antibodies were coupled to the plates directly and BSA-coupled nucleosides were added (see chapter 4.2.3.3 for ELISA protocols). After Cryo conservation and determination of subclass and titer, the antibody hybridomas of around 10-60 different antibody clones per nucleoside were ready to be tested further. The complete record of these antibody candidates is listed in Table 16 in the appendix (chapter 5.2.1). Following the workflow in Figure 13, the hybridoma clones were subjected to dotblot experiments for first containment of specificity (chapter 2.1.2). The positively tested antibodies were then subcloned and produced in larger amounts. After purification, the antibodies were validated further, regarding specificity and sensitivity (chapters 2.1.3 – 2.1.7). Subsequently, several different applications for the antibodies were tested and are shown in chapter 2.1.8.

2.1.2 Validation of antibodies in Dot blot analysis

All positive candidates from the ELISA tests were first tested in dot blot experiments for validation. For that 100 µg BSA-coupled modified and non-modified nucleosides were cross-linked to a nylon membrane incubating the membrane for 1 h at 80°C. After blocking, the membrane was incubated with the hybridoma candidates listed in Table 16 and afterwards with a suitable secondary antibody. Figure 14 shows exemplary blots for this screen. Here, the

specificity of hybridoma clones, directed against m⁶A were analysed using m⁶A coupled BSA as a positive control and m₂⁶A- and A-coupled BSA as negative controls. The dotblots 1 – 4 in Figure 14 showed unspecific binding to m₂⁶A and / or A, while almost no cross-reaction could be detected in the blots 5 – 9. The positive candidates from this test were used for further validation. The hybridoma clones, directed against the 8 other nucleosides (m⁵C, Ψ, m₂⁶A, m¹A, m³C, m¹G, m⁵U and m³U), used for immunisation were screened in the same way. A summary of the numbers of positive candidates for all modified nucleosides in this test is shown in Table 2, chapter 2.1.7 in the second row ("dotblot").
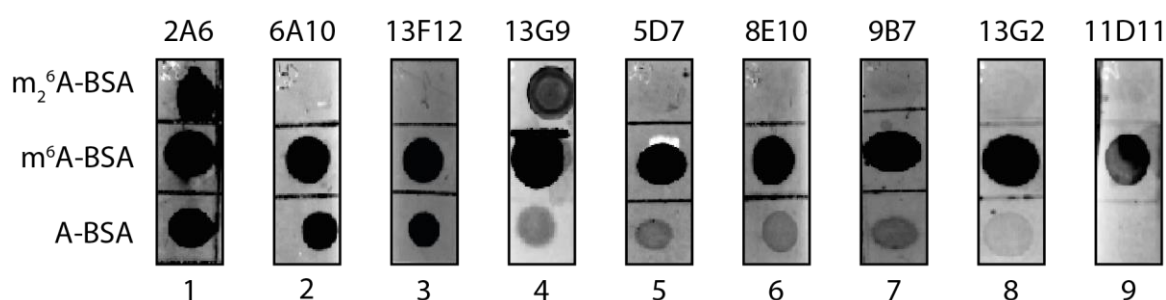
Figure 14: Dot blot analysis of several m⁶A hybridoma clones. The three BSA-coupled nucleosides m₂⁶A, m⁶A and A were used for validation and specificity studies of a number of m⁶A hybridoma clones. For some, cross reaction could be detected (blots 1-4), others showed rather specific signals (blots 5-9). In total, 63 m⁶A hybridoma clones were tested, the shown blots are examples.

For a first validation, the test using BSA-coupled nucleosides, as also used in the ELISA screens, was sufficient. However, a screen for antibody clones that can detect the modification in an RNA context would bring more application-oriented data. For that, short modified and non-modified RNA-oligos were generated or purchased and cross-linked to a nylon membrane using EDC. The membrane was subsequently incubated with the specific antibodies. The clones used for this test, were all those, found to be positive in the previous dotblot experiment from all the nine modified nucleoside antibody hybridomas (data not shown for all). To show in Figure 15, a selection of antibody clones against m⁶A, m⁵C, m₂⁶A and Ψ were chosen, as they brought forward exemplary results and some of them will be shown in further analyses in this thesis. As a loading control, the membranes were stained with methylene blue, which detects the amount of nucleic acid that was spotted.
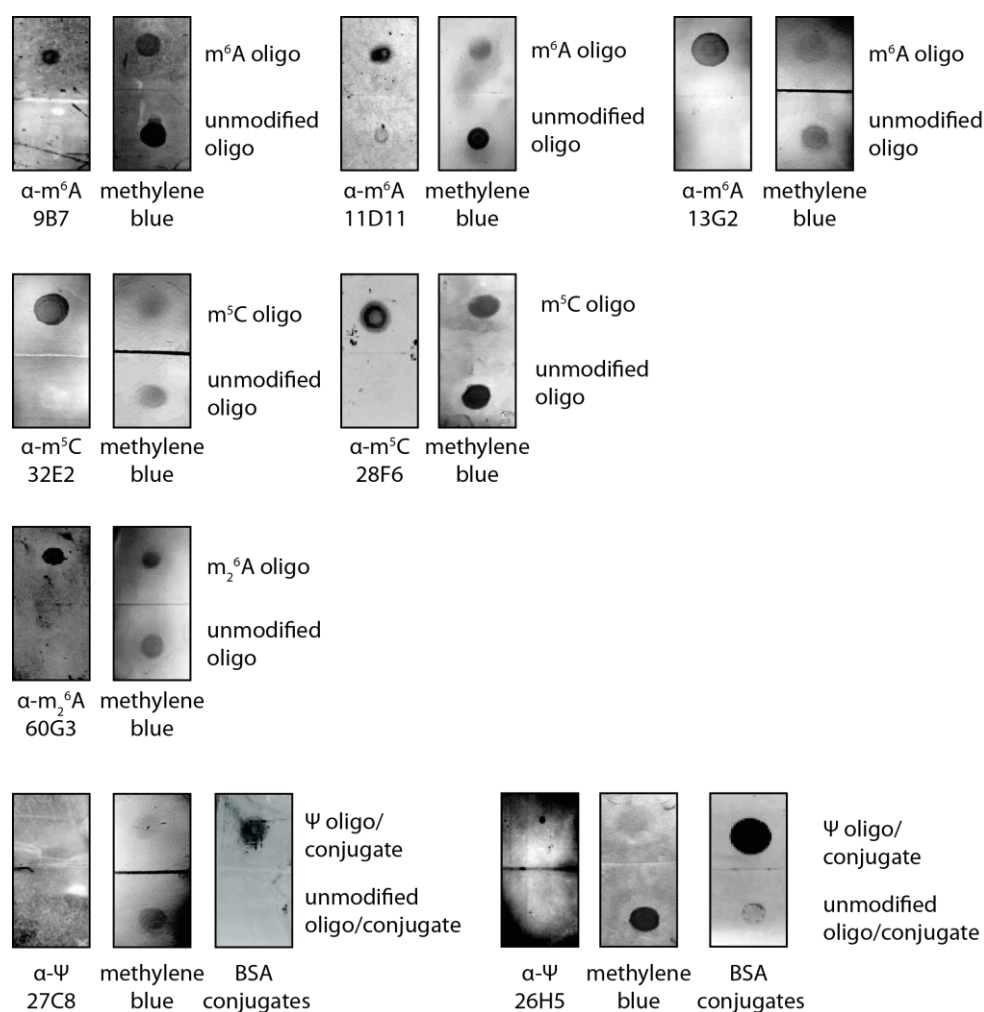
Figure 15: Dotblot analysis of antibodies using RNA oligos to verify specific binding abilities. Modified and unmodified RNA oligos were cross-linked to a nylon membrane, which was then treated with the respective specific antibody. α-m6A antibody clones 9B7, 11D11 and 13G2 are shown in the first row, α-m5C clones 32E2 and 28F6 in the second, α-m2$_2$6A clone 60G3 in the third and α-Ψ clones 27C8 and 26H5 in the last row. For the latter two, also the blots with the BSA conjugates are depicted. Methylene blue staining was performed as a loading control.

The α-m6A hybridoma clones 9B7, 11D11 as well as 13G2 are shown in the first row of Figure 15. They all show very specific detection abilities for m6A-RNA, when compared to the signal for A. The loading controls show a signal for both, the modified and the unmodified RNA oligo. The unmodified RNAs give no signal in neither of the shown dot blots. The depicted blots using the α-m5C clones 32E2 and 28F6 show similar results for detection ability, as does the blot, treated with α-m2$_2$6A clone 60G3 using the respective RNA oligos. On the blots, incubated with α-Ψ antibody clones 27C8 and 26H5, no signal was detected for the Ψ-modified RNA oligos. However also on the methylene blue stained membrane, only the unmodified oligo seems to have cross-linked to the membrane, suggesting a cross-linking problem of the RNA oligo containing Ψ. Thus, for these two antibodies also the blots, using the nucleoside-BSA conjugates are shown, which were performed analogous to the blots in Figure 14. Here, the

two antibody clones show very specific detection (Figure 15, last row). Therefore, the α-Ψ clones 27C8 and 26H5 were tested in other experiments for further validation, together with the antibody clones used for the blots in Figure 15. Positive hybridoma clones, directed against the other modified RNA bases m¹A, m³C, m¹G, m⁵U and m³U were also tested in other experiments, but the results will not be shown in further figures of this thesis. Most clones for these RNA modifications did not show as clear results in the further tests as the discussed antibody clones for the α-m⁶A, α-m⁵C, α-m₂⁶A and α-Ψ did, which will be characterised in more detail in the following chapters.

2.1.3   Establishment and optimisation of the RNA-IP protocol

A very relevant application for the produced antibodies is RNA-immunoprecipitation (RIP), because there are several sequencing approaches, where a RIP is inevitable, like MeRIP, miCLIP or PA-m⁶A-seq[52,53,278,279], as introduced in chapter 1.4.Since each antibody is unique and may require distinct IP-conditions, buffers with different pH values and salt species were tested first (Figure 16A). To examine, whether our antibody candidates are useful for IP, they were coupled to Protein G beads and incubated with total RNA from HEK293T. The precipitated RNA was then analysed in northern blot experiments using probes against endogenous RNA species that carry well known modifications. We started our buffer test with α-Ψ 26H5 using a probe against the 5.8 S rRNA for detection, because it is well established that the 5.8 S rRNA carries a Ψ-site[312]. Figure 16A shows the first buffer tests. Different salt types (NaCl, LiCl and KCl, 150 mM each; lanes 4 – 6) and pH values (pH 6.8, 7.5, 8 and 8.8; lanes 7 - 10) were titrated. According to this, LiCl at a pH of 7.5 were the buffer conditions, which gave the highest signal for this antibody clone, as seen in lane 8.
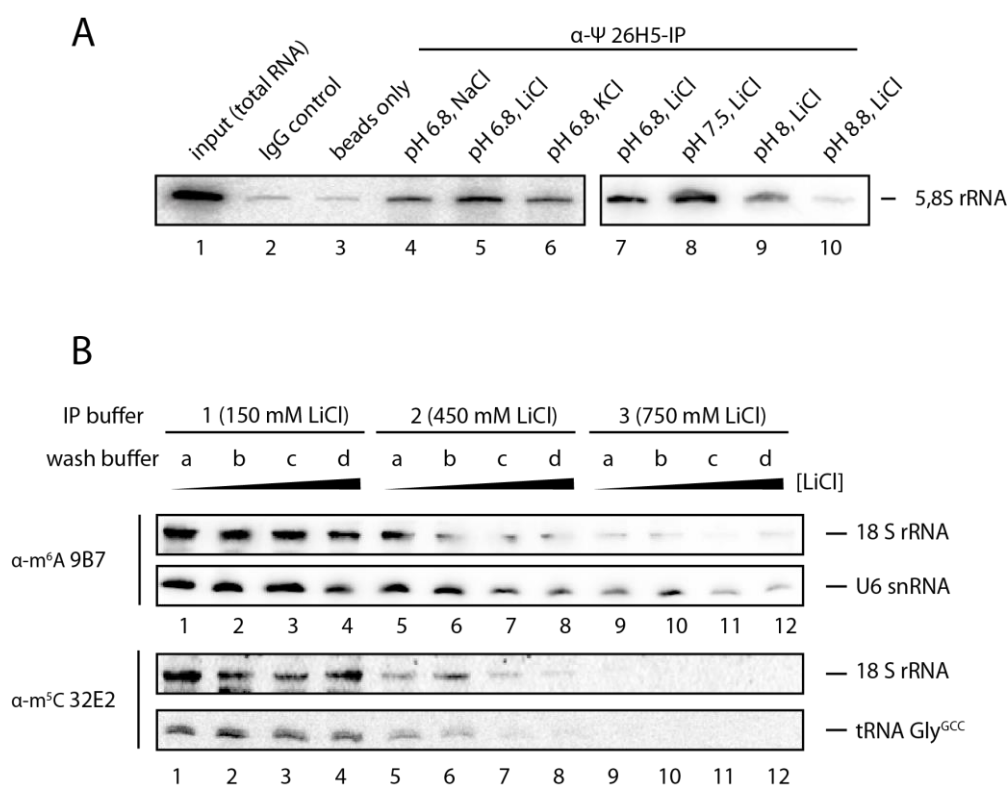
Figure 16: Buffertest for RNA immunoprecipitations.(A) For this buffer test, the antibody clone 26H5 against Ψ was used. Total RNA was loaded as a positive control (lane 1), the IgG control and "beads only" as negative controls (lanes 2 and 3). In the first IPs (lanes 4 – 6), different salts were used (NaCl, LiCl and KCl). Using the salt with the best results from this first round, the pH values were titrated from 6.8 to 8.8 (lanes 7 – 10). For detection, a probe against the 5.8 S rRNA was used. (B) The concentration of LiCl in the buffers increases from left to right. Three different LiCl concentrations in the IP buffer and 4 different washing conditions were applied. a: 150 mM – 300 mM – 450 mM; b: 300 mM – 450 mM – 750 mM; c: 450 mM – 750 mM – 1000 mM; d: 750 mM – 1000 mM – 1500 mM. As probes for the m6A IPs, the U6 snRNA and the 18S rRNA were used. For the m5C IPs, a probe against the 18 S rRNA and tRNA GlyGCC were used.

The IP buffer conditions were further optimised by titrating the LiCl concentration in IP and wash buffers. The data for the α-Ψ antibodies is not shown here, as they did not give any conclusive results. Instead, the northern blots of the IPs with the antibodies α-m6A 9B7 and α-m5C 32E2 are shown in Figure 16B, for these antibody clones seemed the most promising. IP buffers **1** (150 mM LiCl), **2** (450 mM LiCl) and **3** (750 mM LiCl) were applied for the experiments. After IPs, the beads were washed thrice with different washing buffers. The Lithium chloride concentration in the wash buffers was varied from **a** (150 mM – 300 mM – 450 mM) over **b** (300 mM – 450 mM – 750 mM) and **c** (450 mM – 750 mM – 1000 mM) to **d** (750 mM – 1000 mM – 1500 mM). For the m6A IPs, probes against the 18 S rRNA and the U6 snRNA were used to show successful precipitation, as both RNAs are known to be endogenously m6A methylated[98,99,313]. The probes, used for the m5C-IPs were directed against the 18S rRNA and the tRNA GlyGCC. For those RNAs, it is known, that they comprise at least one

endogenous m[5]C methylation[59,314,315]. The signal intensity decreases when using higher salt concentrations. However, there is a clear difference in specificity with different LiCl concentrations between the two antibodies against m[6]A and m[5]C. For the m[6]A antibody, the buffer combination **2a** seems to comprise the highest LiCl concentration to still gain a specific band for the 18S rRNA (lane 5), whereas for the m[5]C antibody, condition **1b** seems best to get a good signal for the tRNA probe (lane 2). These buffer conditions were used for further experiments. This test had to be done with all antibodies, for they all have different properties (data not shown). The best buffer condition, used for the α-Ψ antibody clones, as well as the clone α-m₂[6]A 60G3 was found to be condition **1a** (data not shown). Data for these antibodies will be shown in the course of this thesis, as they showed interesting results.

Having determined the best IP buffer conditions for each antibody, the RIP was optimised regarding the RNA and antibody concentrations. This is just shown for the antibody α-m[5]C 32E2 as an example, since it looked the same for all antibodies, tested. The total RNA from HEK293T cells for the IP was titrated from 0.1 µg to 100 µg, using the same amount of antibody (5 µg) (Figure 17A). In the next titration series, the antibody concentration was varied between 0.1 and 100 µg with the same amount of total RNA in the IP (12 µg). This is shown representatively for the antibody clones α-m[5]C 32E2, α-m[6]A 9B7 and the clone α-m₂[6]A 60G3 (Figure 17B).
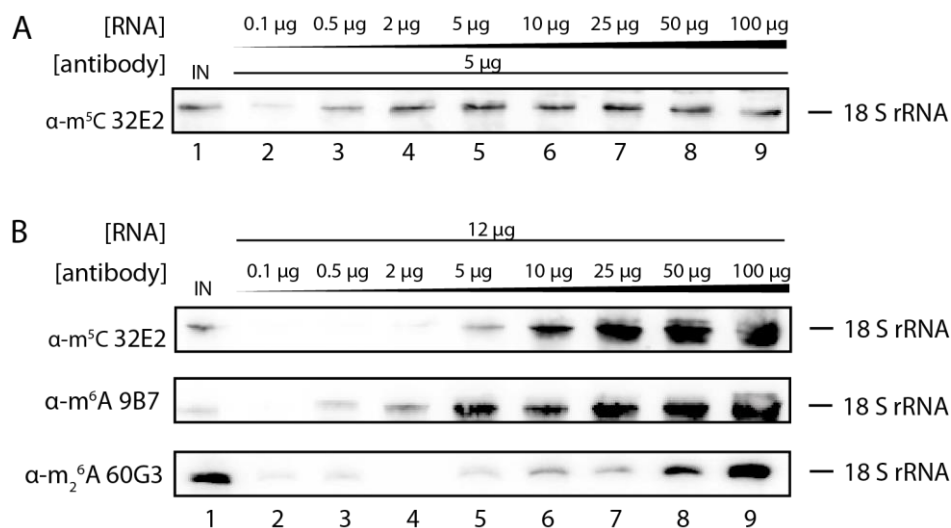
Figure 17: Titration of RNA and antibody concentrations in IP assays. (A) Titration of the concentration of total input RNA in IP experiments using the antibody α-m[5]C 32E2. A probe against 18S rRNA was used in northern blot analysis. (B) The α-m[5]C antibody 32E2 was titrated from 0.1 to 100 µg, with constant amount of RNA (12 µg) in the reaction (upper panel). The antibodies α-m[6]A 9B7 and α-m₂[6]A 60G3 were titrated the same. The RNA concentration was kept constant at 12 µg in all IPs. For detection, a probe against the 18 S rRNA was used.

The antibody titration assays using the antibody clones α-m^{5}C 32E2, α-m^{6}A 9B7 and α-m$_2^6$A 60G3 were conducted to find the best amount for each antibody individually. For detection, a probe against the 18S rRNA was used, as the respective RNA modifications endogenously occur in this RNA, as mentioned before. For m$_2^6$A, the presence in the 18S rRNA has been shown very early in several publications as well[3,17]. The titration of the RNA did not show big differences in the signal intensity. The precipitating antibody however seemed to be the limiting factor in the IP and its amount changed the signal intensity a lot. The amount of antibody, needed, had to be titrated for each antibody individually, since each clone behaved differently. For α-m^{5}C 32E2, 10 μg and for α-m^{6}A 9B7, 5 μg of antibody showed sufficient results and were used for further assays. For m$_2^6$A, even 50 μg of antibody had to be applied. Although, 2μg of RNA seemed to be sufficient to detect the ribosomal RNA, 5-10 μg of total RNA were used in most subsequent experiments to also be able to precipitate less abundant RNA.

Another optimisation test was carried out, to find out the best coupling strategy. The standard protocol for protein immunoprecipitation assays is to first couple the antibody to protein G beads, wash the unbound antibodies off and apply the mixture of proteins afterwards. This protocol can however lead to important epitope binding sites of the antibody to be occupied by the beads and thus to weaker binding of the antigen to the antibody. Therefore, two coupling methods were tested, regarding the precipitation capability. The antibody was in one case coupled as described above and afterwards incubated with total RNA (**a**). In the other case, the antibody was first incubated with total RNA and afterwards pulled out with the beads (**b**). The result is shown in Figure 18. This test was also conducted with a well-established polyclonal α-m^{6}A antibody, which was commercially purchased and is widely used in the field (α-m^{6}A antibody clone 202-003, Synaptic Systems (sysy)). For α-m^{6}A (lanes 2 and 3), α-m^{6}A sysy (lanes 4 and 5) and α-m^{5}C 32E2 (lanes 6 and 7), protocol **b** was more sufficient for precipitation. The α-Ψ antibody 27C8 did not show any preferred bead-coupling protocol (lanes 8 and 9) and the α-m$_2^6$A antibody 60G3 precipitated much better, when incubating the antibody with the beads first (protocol **a**, lanes 10 and 11)

Figure 18: Investigation to find the best mode of coupling the antibody to the beads. Antibodies against m^{6}A (9B7 and the commercial antibody from Synaptic Systems), m^{5}C (32E2), Ψ (27C8) and m$_2^6$A (60G3) were tested regarding the coupling method. In strategy a, the antibody was coupled to the beads, which were afterwards incubated with the RNA. For method b, the antibody and the RNA were mixed and incubated together, followed by precipitation with the protein G beads.

2.1.4 Competition assays for specificity and sensitivity analysis

To gain further insight into the specificity of the antibodies, a competition assay was conducted. This would show, if any unspecific interaction with the respective unmodified RNA nucleoside occurs, when using the antibodies in IP experiments. An excess of modified or unmodified free nucleosides were added to the IP sample during the binding. This was done to see, whether the free nucleosides can compete the RNA off the beads. At high sensitivity, the samples with the modified nucleosides should give no signal in northern blot analysis. The signal of the sample with the unmodified nucleoside should show the same intensity as the untreated IP, resulting in high specificity. In Figure 19, examples for these competition IP assays are shown for the antibodies m^6A 9B7 (A), m^5C 32E2 (B), Ψ 27C8 (C) and m_2^6A 60G3 (D). To have an internal negative control, an unmodified GFP mRNA was spiked into the total RNA input. In lanes 1 respectively, 200 ng of total RNA and 75 ng of GFP spike-in was loaded as input control. The IP was conducted with an IgG control antibody in parallel to the other IPs to test for background signals (lanes 2). Lanes 3 show the IP with the respective antibody. In lanes 4, 100 µM of the specific modified nucleoside was added for competition. The unmodified nucleoside was added in additional samples, which are shown in lanes 5. The upper blots for each antibody were analysed with a probe against an rRNA subunit and the lower ones show the signals for a probe against GFP. The α-m^6A directed antibody gave clear signals for the IP and the non-modified nucleoside and no signal for the IP with spiked-in modified nucleoside (Figure 19A). This shows that the antibody clone 9B7 can specifically recognise the free m^6A nucleoside, but is not directed against the non-methylated nucleoside. The same could be observed when using the α-m^5C antibody 32E2, which showed a preferential binding to the target and was competed off the total RNA m^5C-sites, when adding the specific RNA base (Figure 19B). In Figure 19C, the results for the α-Ψ antibody 27C8 is shown, which seems not to have any affinity for the unmodified nucleoside U (lane 5). However, the amount of Ψ-nucleoside was not enough to compete with the endogenous Ψ-sites that was bound by the antibody, resulting in a slight band in lane 4, suggesting low sensitivity. The α-m_2^6A antibody 60G3 also did not show impaired binding upon adding the A nucleoside (lane 5). But also here, a faint signal is detected, when adding m_2^6A nucleosides to the reaction (lane 4). This could however also be a background signal, since the IP with the IgG control antibody shows a similar signal. No unspecific binding to the unmodified spike-in GFP could be observed in neither of the conducted IPs shown in Figure 19.
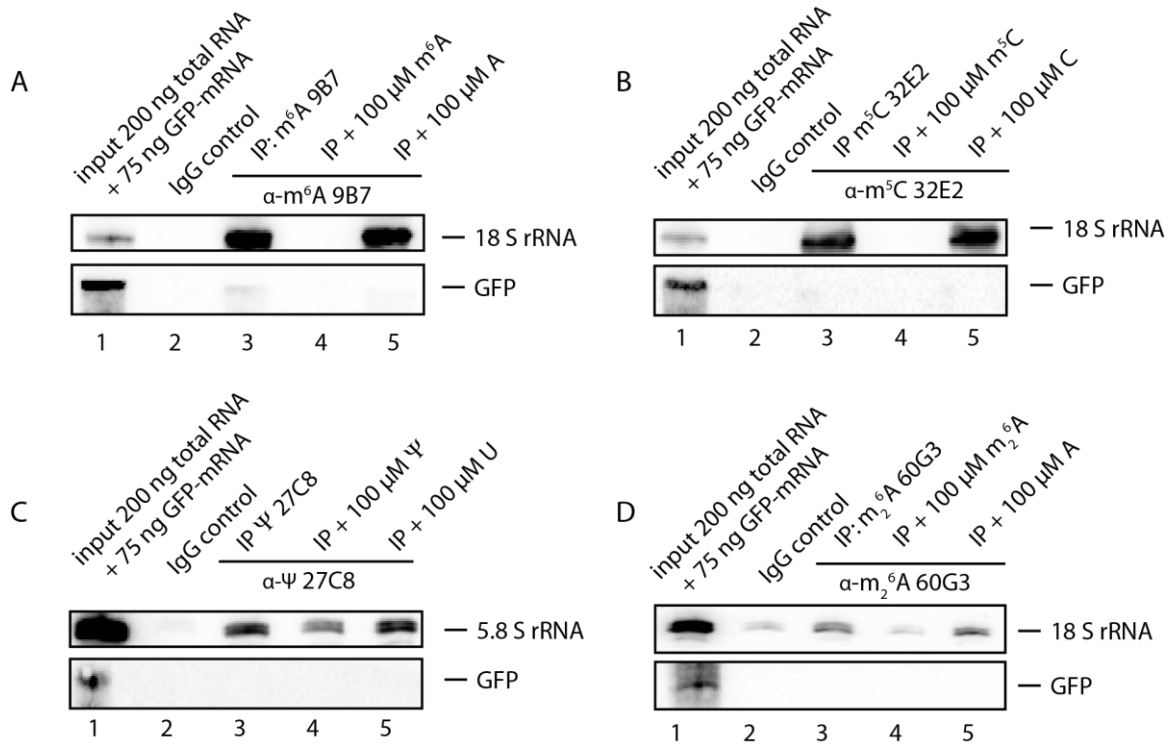
Figure 19: Competition immunoprecipitations of certain antibodies against modified RNA bases. The antibodies (A) m6A 9B7, (B) m5C 32E2, (C) Ψ 27C8 and (D) m26A 60G3 have been tested in a specificity assay, using free nucleosides to compete for the modified sites in the total RNA input. IgG controls were used to analyse a potential background signal. Unmodified nucleosides were used as a control for the competition. As a negative control, unmodified GFP mRNA was spiked-in the input before IP.

To specify at which nucleoside concentration, the competition is detectable and how much unmodified nucleoside can be added to still see no unspecific binding, a titration of nucleosides was conducted with the four antibodies shown for the previous experiment (α-m6A 9B7, α-m5C 32E2, α-Ψ 27C8 and α-m26A 60G3). The titration was performed, adding no, 10 nM, 100 nM, 1 µM, 10 µM and 100 µM of modified or unmodified nucleoside to the IPs (Figure 20). Again, probes against the ribosomal RNA subunits 18S or 5.8 S rRNA were used for detection of the endogenous modification.
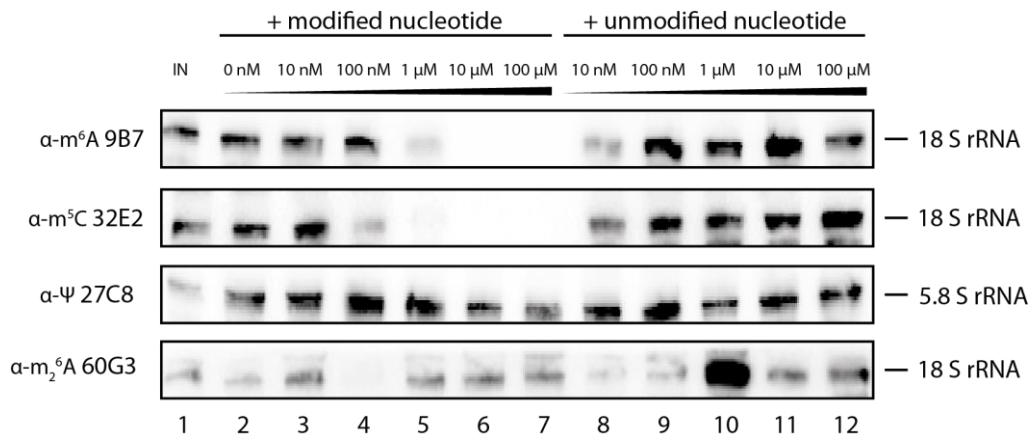
Figure 20: Titration of the competing free nucleosides. To find the nucleoside concentration at which a competition can be observed, the antibodies m6A 9B7, m5C 32E2, Ψ 27C8 and m2·6A 60G3 were subjected to a titration series with different nucleoside concentrations. Modified and unmodified nucleosides were used to investigate the competition ability for each antibody. After IPs, the resulting northern blots were incubated with probes against ribosomal RNA subunits 18S or 5.8 S rRNA.

The concentrations at which the competition with the modified nucleoside could be detected, was different for all antibodies. Also the signals for unmodified nucleoside-spike-ins were detected at different concentrations. In the IPs, using the α-m6A antibody 9B7 (Figure 20, first row), the signal of the m6A nucleoside competition vanished at around 1 μM (lane 5). The signal with the unmodified A nucleoside in the IP was detected in the IPs up 100 μM of A (lane 12). Thus, the results hint to high sensitivity as well as high specificity. In the α-m5C IPs (second row), only 100 nM of m5C nucleoside (lane 4) was need for competition and also 100 μM of C nucleosides (lane 12) could be added without unspecific binding. Sensitivity and specificity seems very high for this antibody clone as well. The amount of Ψ nucleoside in the IP (third row) was still not high enough to lose the signal, even with 100 μM in the IP (lane 7). However, for this antibody, too, up to 100 μM of unmodified nucleoside could be added without noticeable competition (lane 12). The α-Ψ antibody 27C8 seems very specific but not as sensitive. The concentration of spiked-in m2·6A nucleosides seemingly needs to be higher than 100 μM to be able to compete completely (lane 7). For the A nucleosides, the data from Figure 20 is rather inconclusive, as all, except 1 μM A nucleoside (lane 10) in the IP lead to a competition. More tests have to be conducted to validate the α-m2·6A 60G3 antibody to its full extent. Also for the other antibodies, tested here, further characterisation was performed.

2.1.5   Optimisation of the elution protocol

To enhance the specificity of the output after IP, a method for elution of specifically bound RNA was performed using modified nucleosides to elute the RNA off the antibody. This was previously done by Dominissini et al.[52]. The protocol was optimised using the antibodies against m5C (clone 32E2) and m6A (9B7), as they showed the best results in previous experiments, and is depicted in Figure 21. After IP and washing, 250 – 500 μM of modified or unmodified nucleosides were added to the beads and incubated for one additional hour while shaking. The RNA was then extracted from eluates and the beads and was loaded onto the gel. In lane 2, the conventional IP was loaded, lanes 3 – 5 show the RNA, which was still bound to the beads after elution and lanes 7 – 9 show the signals of the eluates after IP and elution. For the m6A IPs, the high signals are very clearly seen only in the IP (lane 2) and in the elution samples with the modified nucleosides (lanes 7 and 8). The elution, using this protocol seems to be applicable for the antibody α-m6A 9B7. For the m5C antibody 32E2, the signals were

weaker than detected before. A signal could be detected in the beads-fraction that was treated with the unmodified nucleosides (lane 5) and also faintly in the elution fractions with modified nucleoside (lanes 7 and 8) and unmodified nucleoside (lane 9). Thus, further optimisation work had to be conducted for the elution experiment to be able to detect the signals better.
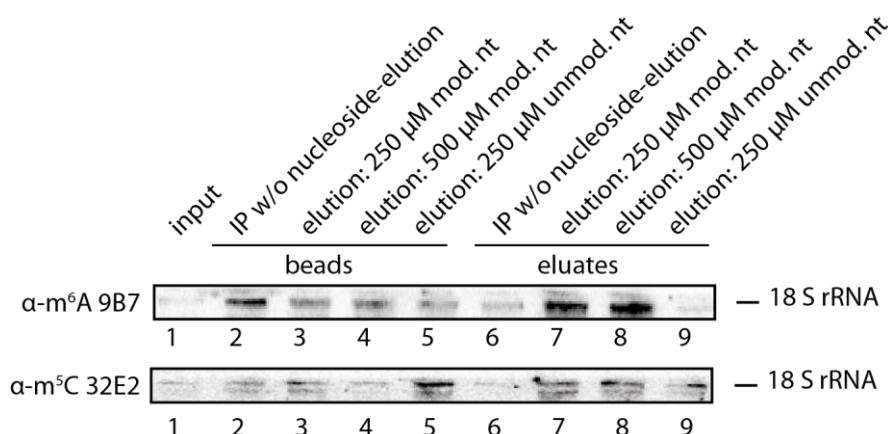
Figure 21: Specificity test via elution after the IPs. Free nucleosides were used to elute the specifically bound RNA from the antibodies α-m⁵C 32E2 and α-m⁶A 9B7. After IP and washing, modified and unmodified nucleosides were added to the beads for elution. In the left part, the RNA signals for the beads fraction are shown and in the right part, the elution signals for the two antibodies are shown.

In Figure 22, the optimisation of the elution protocol using the antibodies α-m⁶A 9B7, α-m⁵C 32E2 and α-m₂⁶A 60G3 is shown. The RNA was eluted from the beads, as it was done in the previous experiment, using 250 μM modified nucleoside. In addition to testing the most potent buffer conditions for IP and washing, *in vitro* transcribed modified or unmodified GFP mRNA was spiked in the IP for further specificity control. Of note, m₂⁶A is not incorporated in the RNA by the T7-polymerase during *in vitro* transcription and thus m₂⁶A-GFP could not be used in this experiment. A GFP probe was used to visualise the precipitated GFP amount in the northern blot (Figure 22, upper panels). As a positive control, a probe against 18S rRNA was used (Figure 22, lower panels). In lanes 1 respectively, 200 ng total RNA and 75 ng GFP mRNA was loaded as input. For Background analysis, IPs using an IgG control antibody were conducted (lanes 2).
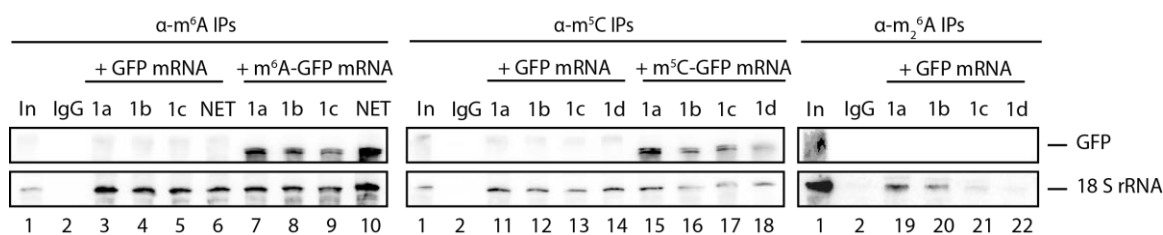
Figure 22: Optimisation of the elution protocol of antibody IPs using spike-ins. Modified and unmodified GFP mRNA was used as spike-ins to the total RNA in the IPs. The m6A antibody, which was used was 9B7 (lanes 3 – 10), for m5C, the clone 32E2 was used (lanes 11 - 18) and the m2 6A antibody clones was 60G3 (lanes 19 – 22). Different IP and wash buffers were used for each antibody. The RNA was eluted from the beads after IP, as described above. Probes against the GFP mRNA and 18S rRNA were used for northern blot detection.

The α-m6A IPs showed no signal for GFP in the IPs with unmodified spike-ins (lanes 3 to 6), whereas signals could be detected in the IPs with modified GFP spike-in (lanes 7 to 10). In previous experiments with the α-m6A antibody, there were hints that NaCl results in higher affinity to its targets, as compared to using LiCl (data not shown). Hence it was tested again in this experiment. The buffer that showed the highest signal and thus precipitated most GFP mRNA was the **NET** buffer for the m6A antibody (lane 10, upper panel), which contains NaCl instead of LiCl. The elution of m6A containing RNA with m6A nucleosides was successful in all IPs, with highest signals using buffer condition **1a** and **NET** buffer (lanes 3 and 10). The α-m5C antibody 32E2 was also able to specifically precipitate the modified GFP-mRNA (lanes 15 to 18 in contrast to lanes 11 to 14, upper panel). The signal showed highest intensity, when using the buffer condition **1a** in this elution experiment (lane 15). Also the detection of endogenous rRNA was most successful with buffer condition **1a** (lanes 11 to 18, lower panel). The α-m2 6A 60G3 antibody clone showed no precipitation of the non-modified GFP mRNA (lanes 19 to 22, upper panel). The elution protocol showed best detection of the endogenous m2 6A sites in rRNA when using the buffer **1a** (lanes 19 to 22, lower panels). In general, for IP experiments, the elution protocol can be recommended to give rise to more specific signals but always has to be tested for each antibody individually.

2.1.6 Estimation of the apparent K_D values

An important characteristic of antibodies is the dissociation constant (K_D). This index is defined as the coefficient of the propensity of a complex to separate into its components and is regularly used in various applications[316]. For the description of antibody-antigen interactions, it usually rather describes the tendency to interact (association constant). It is commonly used as a measurement of the specificity of an antibody. Here, the apparent K_D-values were determined by Robert Hett using HPLC analyses. For that, free modified and unmodified nucleosides were mixed equally in six different concentrations, subjected to

immunoprecipitations and filtered to remove the antibody from the reactions. The filtered nucleosides as well as the inputs were then analysed via HPLC (Figure 23A). For a detailed protocol of the procedure, please see chapter 4.2.3.4 in the methods section.
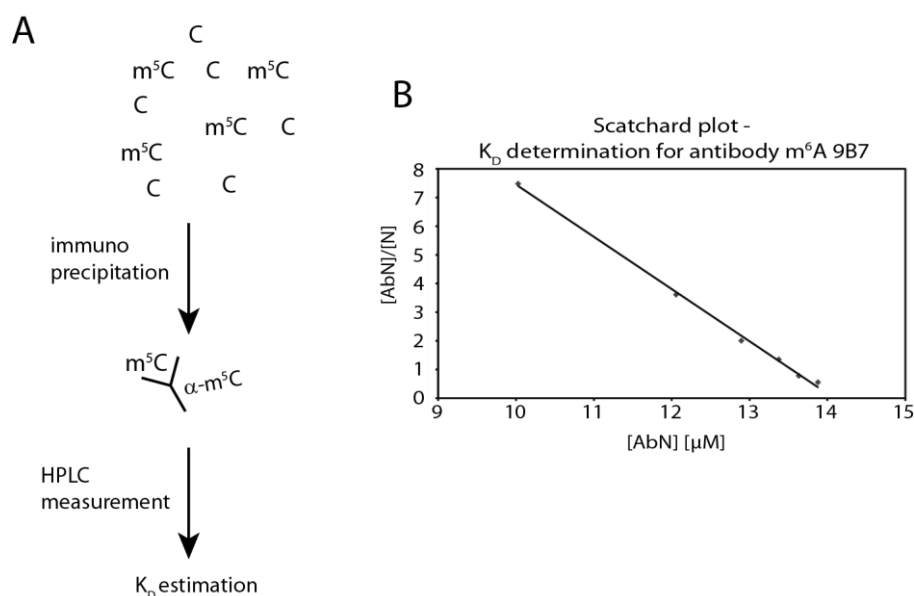
Figure 23: Estimation of the apparent K$_D$-value of antibodies. (A) Schematic overview of the experimental setup. The modified and unmodified nucleosides are mixed, immunoprecipitated with the specific antibody and analysed via HPLC. (B) Using the differences between the values for modified and unmodified, a Scatchard plot was derived. As an example, the plot for the antibody clone 9B7 against m6A is shown.

The antibody-bound and unbound fractions were determined from the HPLC measurements and the concentrations of the bound ([AbN]) and free nucleoside ([N]) were calculated. For the Scatchard plot, the ratio of bound and free nucleosides was plotted against the bound fraction[317,318]. This was done for all the potentially highly specific antibodies. The K$_D$ values were then estimated from the negative reciprocal value of the slope of the resulting line (Figure 23B). This estimation was used to deduce the binding models that describe the ratio of free and bound nucleoside (see Figure 24). These values were fitted with nonlinear regression, which is a statistical method for estimating the relationship among independent variables by successive approximations[319]. In Figure 24A, the grey squares in the upper part of each graph show the binding of the antibody to m6A with A as the control nucleoside. The black triangles in the lower part of the graphs depict antibody-m$_2$6A binding. For the m5C antibodies, m3C was used as a negative control (black triangles) (Figure 24B) and for the m$_2$6A antibodies, binding to m6A was analysed in addition to the binding to m$_2$6A (Figure 24C).
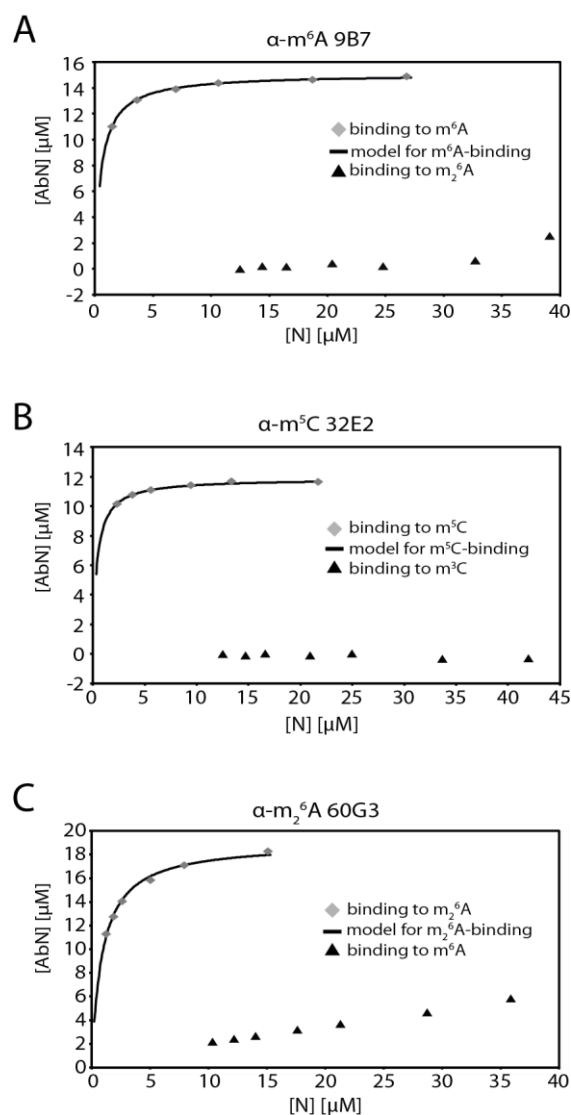
Figure 24: Binding models for the K_D-determination of antibodies against m6A, m5C and m26A. The grey squares show the binding to the specific nucleoside, the antibody was generated against. The fitted binding curve is represented in black. Unspecific binding to differently modified nucleosides is depicted with black triangles.

The antibody clone 4G10 against m1G showed unspecific binding to G, when higher concentrations were used. Thus, clone 4G10 was not further validated, but rather the α-m1G clone 6E3 (shown in Figure 43 J/K, chapter 5.2.2 in the appendix). The binding modelling was done for several antibodies and after fitting with nonlinear regression, the apparent K_D-values of the different antibodies were estimated. They are listed in Table 1.

Table 1: List of the apparent K_D-values of several antibody clones against m⁶A, m⁵C, Ψ, m₂⁶A, m¹G and m³U. The row "control nucleoside" shows the RNA bases with which the specific modified nucleoside was initially mixed, before the IP was conducted.

Modification	Antibody clone	apparent K_D-value (nucleoside) [μM]	control nucleoside
m⁶A	13G2	1.92	A
	11D11	0.59	A
	9B7	0.55	A
		0.89	m₂⁶A
		0.60	m¹A
m⁵C	31B10	1.14	C
	28F6	1.5	C
	32E2	0.39	C
		0.68	m³C
Ψ	26H5	38.12	U
	27C8	17.18	U
m₂⁶A	60G3	0.89	A
		1.15	m⁶A
m¹G	6E3	9.88	G
	4G10	0.15	G
m³U	6A2	0.52	U

The K_D-values of most of the tested antibodies are in the low μ-molar range, when using free nucleosides. Further biochemical analyses were mainly carried out with one clone for each antibody that showed the best results in this test. The respective K_D-values were more or less coinciding with the results from the RNA-IPs. The best antibody clones were α-m⁶A 9B7, α-m⁵C 32E2, α-Ψ 27C8, α- m₂⁶A 60G3, α-m¹G 6E3 and α-m³U 6A2. A compilation of all binding model curves and Scatchard plots are shown in Figure 43 in the appendix (chapter 5.2.2).

2.1.7 Determination of the antibody specificities

The capacity of the antibodies to enrich for the specific RNA base was the question of another experimental setup, which is graphically depicted in Figure 25. For that, a DNA fragment was *in vitro* transcribed on the one hand with unmodified nucleoside-tri-phosphates (NTPs) in the presence of ³²P-α-ATP and on the other hand with a mixture of specific modified NTP and

unmodified NTPs, this time in the presence of ^{32}P-α-UTP. The ^{32}P-α-ATP and ^{32}P-α-UTP RNAs were mixed in equimolar concentration and IPs with the modification-specific antibodies were performed. The precipitated RNA was then digested to nucleoside-mono-phosphates (NMPs) using Nuclease P1 and analysed by thin layer chromatography (TLC). The NMPs are separated on a TLC plate and the radioactive signal intensities, resulting from ^{32}P-AMP and ^{32}P-UMP correspond to the amount of immunoprecipitated RNAs. These were normalised to the input signals. From this, enrichment factors were calculated that allow for an estimation of the antibody specificity. For α-m^{6}A and α-m^{5}C antibodies, the signal for AMP depict the amount of immunoprecipitated unmodified RNA oligos, whereas the UMP signals are proportional to the modified RNA oligos that were enriched in the experiment.
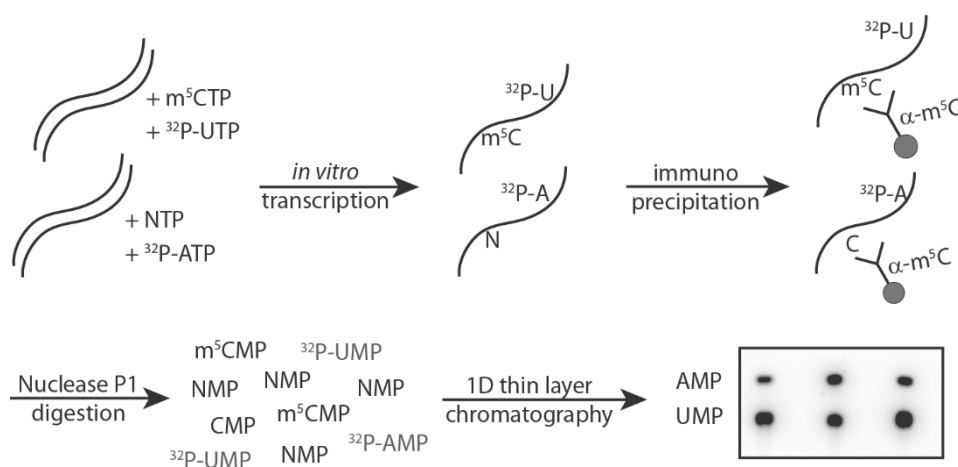
Figure 25: Schematic depiction of the experiments to determine the enrichment of antibodies. A DNA fragment was *in vitro* transcribed with modified NTPs and ^{32}P-UTP and with unmodified NTPs and ^{32}P-ATP. From this mix, an IP was performed with the respective antibodies. The output was digested to NMPs and analysed via thin layer chromatography (TLC).

Different percentages of modified NTPs were used for the *in vitro* transcription (*ivt*) to analyse the immunoprecipitation capacity of the antibody with high and low amounts of modified bases in the target RNA. This is relevant in order to see, whether the antibodies are capable of enriching only highly modified RNA or if they can comparably detect low amounts of the RNA base, which would be more application specific to use in experiments with endogenous RNA. For m^{6}A, 1 % (Figure 26A) and 50 % (Figure 26B) of m^{6}ATP was used in triplicates. The radiograms are shown in the left parts of Figure 26A and B, the quantifications are depicted in the right parts. Four different antibody clones against m^{6}A were tested in this assay: 11D11, 13G2, 9B7 and a commercially available antibody from Synaptic Systems, which is widely used in the field and was thus considered as positive control. When using only 1 % m^{6}ATP in the *ivt*, the enrichment of precipitated modified RNA over the unmodified and input RNA only amounts to 1.5 to 2-fold. This can be observed for all the tested antibody clones similarly. When 50 % m^{6}ATP were incorporated into the transcript, 4 to almost 6-fold

enrichment was observed for the different antibody clones. This demonstrates a correlation between the amount of m6A in the RNA and the precipitation ability of the antibodies, which was expected. The α-m6A antibodies that were tested here, all show comparable enrichment among each other in both experimental setups. The enrichment of the antibodies is not as high as protein-directed antibodies, which can be much higher. However the proof-of-principle setup with the commercially available and widely used antibody (Synaptic Systems) shows same results as the newly generated antibodies do. Thus, the values of enrichment of m6A RNA, gathered in this experiments are plausible and nevertheless significant.
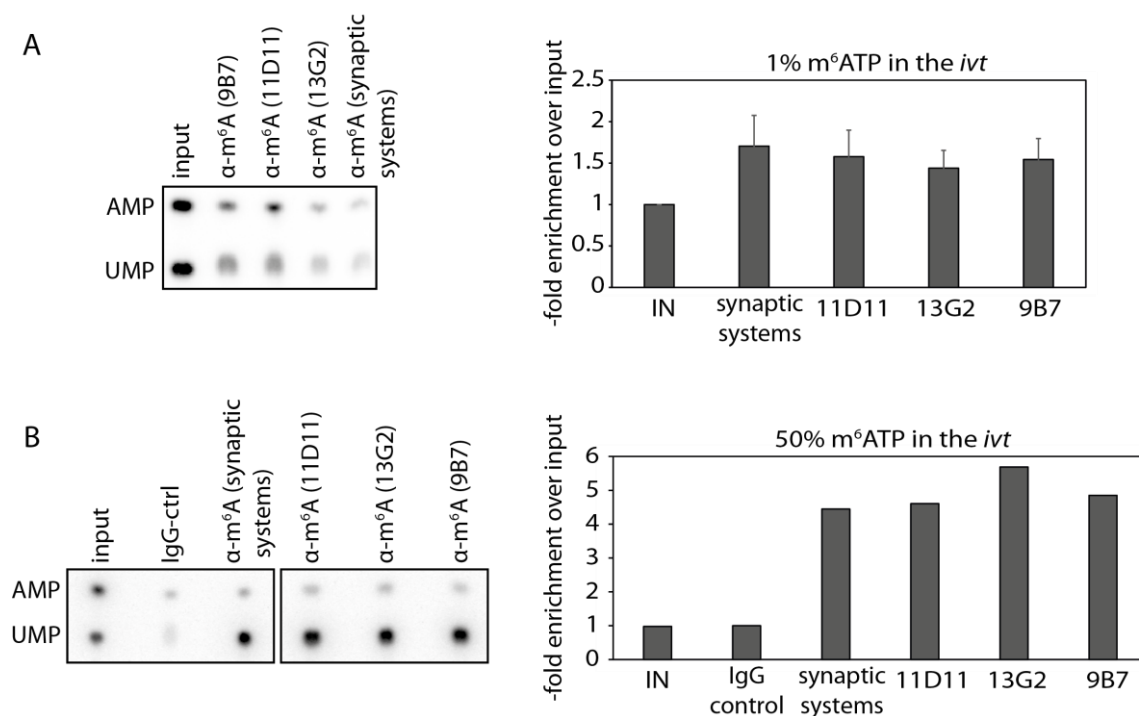
Figure 26: Enrichment of m6A in m6A-IPs using 1 % and 50 % m6ATP in the *ivt*. In the left part of the figure, exemplary autoradiograms of the TLCs are depicted, the right part shows the quantifications of the IPs in triplicates. The three m6A antibody clones 11D11, 13G2 and 9B7 were tested. Additionally, the commercially available antibody from Synaptic Systems served as a positive control. In (A), the experiments with 1 % m6ATP are shown. Part (B) comprises the experiments with 50 % m6ATP in the *ivt*.

The experiments regarding the m5C antibodies were carried out with the clones 28F6, 32E2 and the commercially available antibody from Diagenode. First, only the experiments with 1 % m5CTP in the transcription reaction were performed and analysed as described above. The calculations resulted in an enrichment of up to 6-fold for the clone 32E2, 2.5-fold for clone 28F6 and almost none for the antibody from Diagenode (Figure 27).
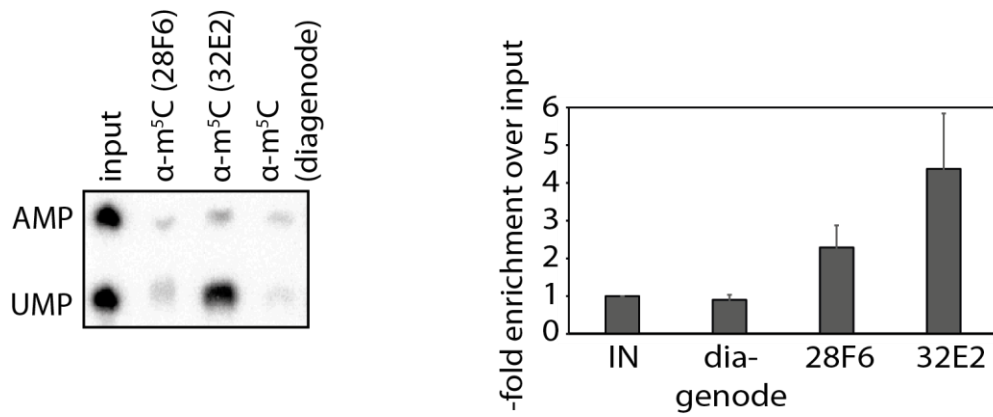
Figure 27: Enrichment of m5C in m5C-IPs using 1% m5CTP in the *ivt*. Results from the *ivt* and TLC experiments, analysing the m5C antibody enrichment capacity. An antibody from Diagenode (commercially available) and the clones 28F6 and 32E2 were tested in this experiment, using 1 % m5CTP in the transcription reaction.

Since the antibody α-m5C 32E2 showed very high enrichment factors and was moreover promising regarding the very high specificity compared to the commercial antibody, further TLC-based experiments were conducted. A titration of the m5CTP in the reaction was performed, using 10%, 30 % and 50 % of m5CTP in the reaction. Furthermore, the input RNA was titrated as well from 2.5 µg to 16 µg for each NTP-percentage. The signals of these IPs on TLC plate are shown in Figure 28 in the upper part. The lower part shows the evaluation of these signals in separate graphs. This suggests 12 µg of RNA to be the best concentration for these assays. Furthermore, no significant difference concerning enrichment capacity can be seen, when using 10, 30 or 50 % of m5CTP in the transcription reaction, as the enrichment factor using 12 µg varies only from 4.5- to 4-fold. In conclusion, the high enrichment capacity of the antibody α-m5C 32E2 is relatively independent of the amount of modified nucleotides in the RNA since all the enrichment curves shown in Figure 28 are similar in appearance and thus the resulting enrichment factors are reproducibly significant.
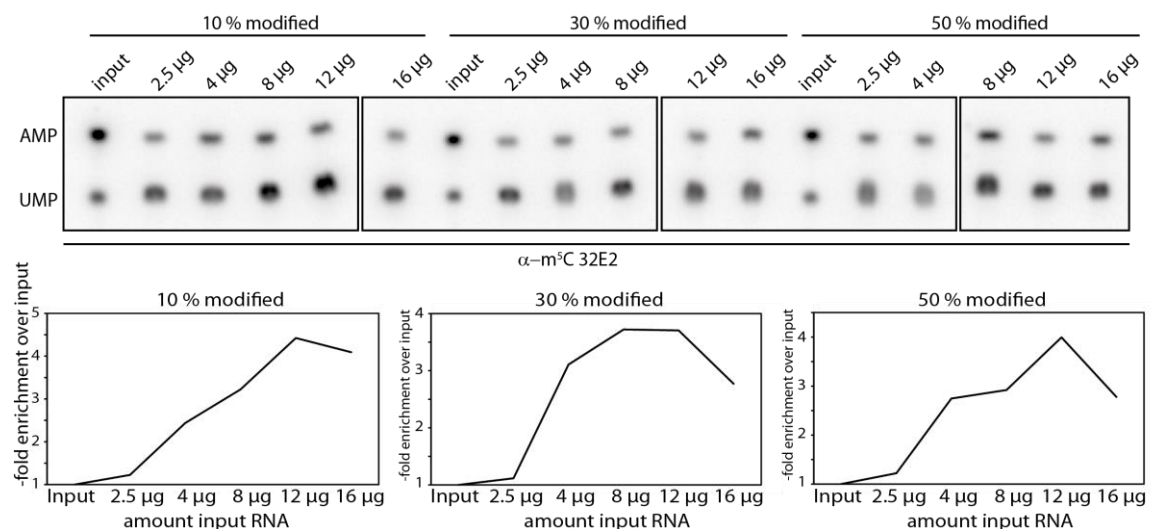
Figure 28: Titration of the m⁵C antibody clone 32E2 and input RNA in TLC experiments. The upper part shows the radioactive signals on TLC plates after the experiment. 10, 30 or 50 % of m⁵CTP was used in the *ivt* and the reaction was done with 2.5 to 16 µg of RNA. The lower part shows the calculated –fold enrichments in three graphs, divided in the different m⁵CTP amounts, used in the transcription.

Subsequently, the pseudouridine antibody clones 25C6, 26H5 and 27C8 were tested in this experimental system. Different to that, in IPs using α-Ψ antibodies, the signal for UMP is proportional to the enriched unmodified RNAs and the AMP signal represents the modified RNAs that were precipitated. This is done to avoid a competition between Ψ and UMP for the U-sites in the RNA, when using them together in the *ivt*. For a more detailed protocol, see chapter 4.2.2.10 in the methods section. The results are shown in Figure 29. In part A, again only 1 % ΨTP was used in the *ivt*. Here, no significant enrichment could be measured, for none of the antibody clones. In Figure 29B, however, 50 % ΨTP were used and up to 6-fold enrichment was measured for the clone 27C8, which was thus chosen for further analyses because it showed specificity and affinity in the experiments carried out so far.
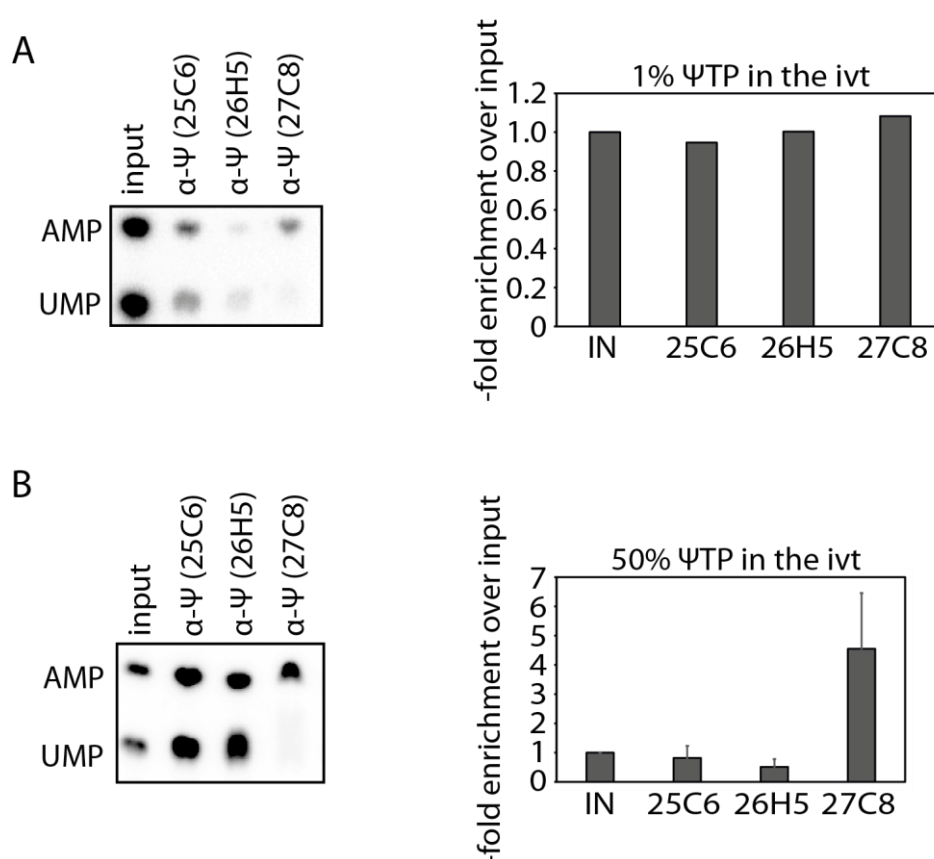
Figure 29: Enrichment of Ψ in Ψ-IPs using 1 % and 50 % ΨTP in the *in vitro* transcription. (A) 1 % of ΨTP was used for these experiments. The left part shows the signals on the TLC plate. Antibody clones 25C6, 26H5 and 27C8 were tested in this experiment. (B) Here, 50 % of ΨTP were used in the *ivt*. The right graph shows the calculated enrichment factors. The experiments were conducted in triplicates.

Due to the inability of incorporating m_2^6A in an *in vitro* transcription using the T7 RNA polymerase, these experiments could not be performed for the α-m_2^6A antibodies.

To investigate performance under more competitive conditions, a second experimental strategy for assessing modified RNA enrichment by our antibodies was designed. Short RNA fragments of 10 nucleotides in length were designed, containing either Ψ, m^5C, m^6A or m_2^6A. As negative control, an unmodified RNA oligo was used. With the best antibody clones from the previous experiments, immunoprecipitation experiments were conducted using all the differently modified RNAs for each antibody. For each antibody clone, γ-AT^{32}P-labelled Ψ-oligos, m^5C-oligos, m^6A-oligos, m_2^6A-oligos and unmodified oligos were used for IP. The cpm (counts per minute) values of the input RNA and the samples after IP were measured with a Scintillation counter. From triplicate experiments, enrichment factors were calculated, normalised to the input and the signal for the unmodified oligo. In Figure 30A, the enrichment for the α-m^6A antibody clones 9B7 and the commercial antibody from Synaptic Systems are shown. Part B shows the m^5C enrichment of the antibody clone 32E2. In C, the experiment with the pseudouridine antibody clone 27C8 is shown and in D, the m_2^6A antibody 60G3 enrichment is depicted. The enrichment ability of the two antibodies against m^6A, 9B7 and Synaptic Systems clone are comparable. Both antibodies are able to enrich for the m^6A-oligo, by approximately 6-fold over the input, not having a very high affinity to the other modified oligos (Figure 30A). The anti-m^5C antibody 32E2 enriched around 120-fold for the m^5C oligo and has no high affinity for the other oligos (Figure 30B). Anti-pseudouridine clone 27C8 shows relatively high affinity for the Ψ-oligo, but even higher for the m^5C-oligo. While having a high sensitivity for its target RNA base, this antibody seems to have no high specificity (Figure 30C). The α-m_2^6A antibody is able to enrich mainly for the m_2^6A-oligo and with an enrichment of 8-fold over the input, this antibody seems highly specific (Figure 30D).
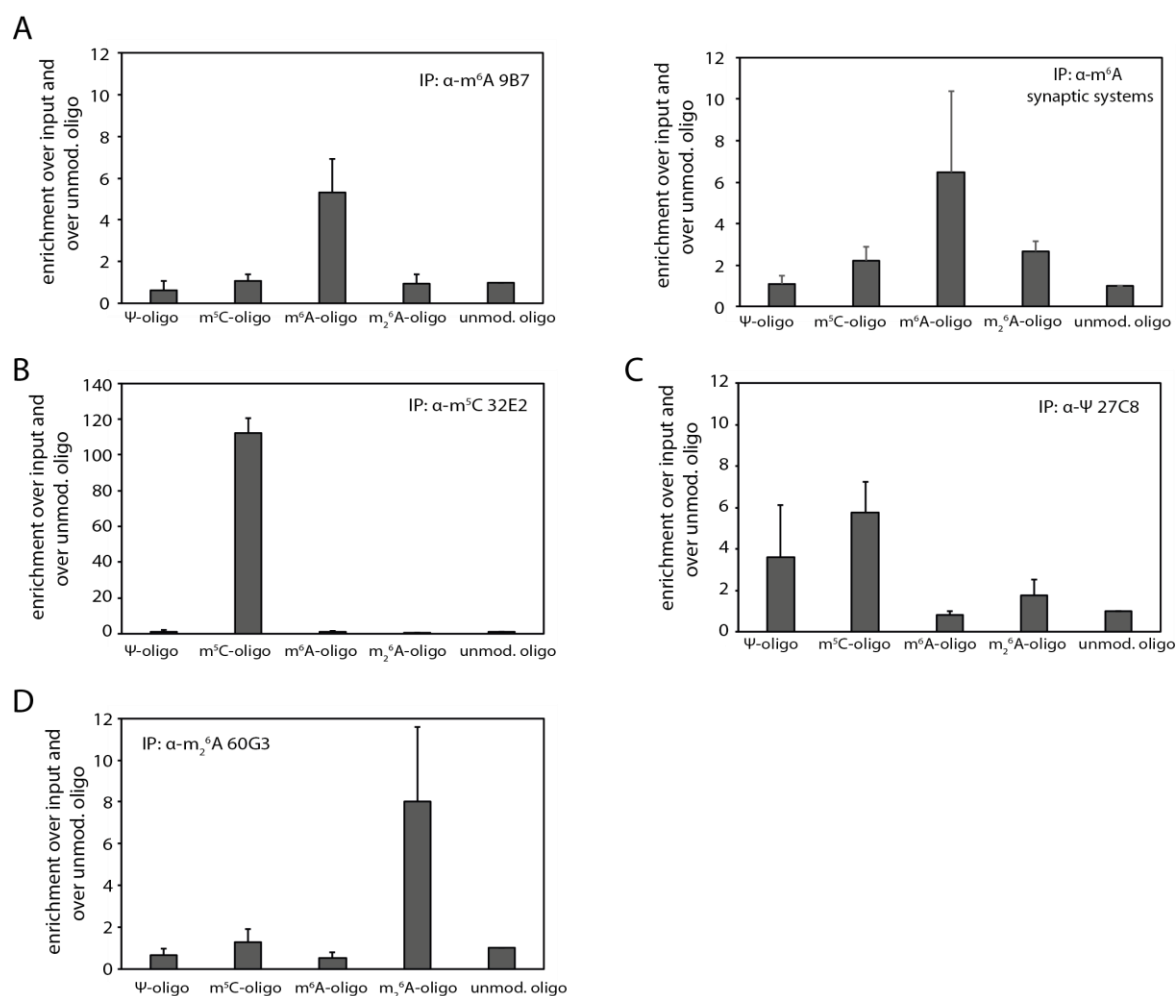
Figure 30: Determination of the enrichment of RNA oligos with different antibody clones. IPs using different radioactively labelled oligos as input were performed with different antibodies. The enrichment factor was calculated, normalising the cpm-value of the IP to the input and the signal with unmodified oligo. (A) The enrichment factors of antibody clone α-m6A 9B7 and the polyclonal antibody from Synaptic Systems for differently modified oligos are shown. (B) The enrichment results for the antibody clone 32E2 against m5C are depicted. (C) Pseudouridine antibody specificities are shown in this graph. (D) The enrichment ability of the antibody against m26A, 60G3 is shown.

Table 2 sums up the number of specific antibody clones that showed positive results in the different experimental setups. This comprises all antibodies, including the ones, for which the results are not shown in this thesis. The antibodies were first tested in ELISA experiments, then in dot blots. After that, an RNA-IP analysis was performed and for three modifications, an *ivt*-TLC experiment was developed and conducted. The last row shows the established clones, which are now stable hybridoma cells, expressing the antibody, which can be purified.

Table 2: Hybridoma fusion screen and candidate validation.

Modification	ELISA Capture ELISA	dot blot	RNA-IP	TLC	established clones
m^{5}C	10	9	3	2	3
m^{6}A	63	20	11	3	4
Ψ	6	4	2	1	3
m$_2^6$A	8	6	3	-	3
m^{1}G	28	7	3	-	3
m^{1}A	36	4	4	-	2
m^{5}U	5	3	2	0	2
m^{3}U	20	10	6	-	5
m^{3}C	33	17	6	-	3

2.1.8 Further applications of the antibodies

Having developed a functional set of tools, the next step was to apply the antibodies in biologically relevant experiments. We used the antibodies to immunofluorescently stain the modified RNA bases in C643 cells (chapter 2.1.8.1). Another application, which was applied was miCLIP, a crosslinking method to analyse RNA, which is bound by the specific antibodies for investigation of methylation sites on nucleotide resolution by possible subsequent sequencing (chapter 2.1.8.2).

2.1.8.1 Visualisation of modified RNA by Immunofluorescence experiments

Immunofluorescence assays using the α-m^{6}A antibody 9B7 were carried out in C643 wildtype (WT) and METTL3 knock-out (KO) cells (gratefully provided by Dr. Stefan Hüttelmaier, Halle). The aim of this experiment was to investigate, whether and to which extent m^{6}A can be detected in such assays. Since METTL3 only catalyses m^{6}A on mRNA and the m^{6}A marks on the rRNA, tRNA and other non-coding RNAs are not affected by the KO of METTL3, only a reduction of the signal can be expected. Nevertheless, a difference between the fluorescence signals of WT and METTL3-KO cells using the α-m^{6}A antibody is likely. Additionally, it would be benefiting for the community, working with m^{6}A to have established antibodies that can be operated in IF experiments as well, to be able to investigate this RNA mark also through this methodology. The first investigation, however that had to be done, was to verify the knockout of METTL3, since this cell line was not published before and a characterisation was not provided. For that, a western blot with WT and METTL3 KO cell lysate was loaded on a SDS gel and stained with METTL3 antibody and α-Tubulin antibody as loading control (Figure

31). The α-tubulin band is clearly visible and comparable in signal intensity. The signal for METTL3 is clearly visible in the WT lane and lost in the knock-out cells. However, a very faint and smaller band appears in the KO.
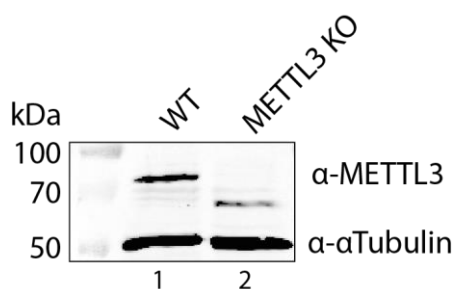
Figure 31: Validation of the METTL3 knock out (KO) in C643 cells via western blot. Western blot of C643 wildtype (WT) and METTL3 KO cell lysate. An antibody against METTL3 was used for detecting the specific protein, α-tubulin immunostaining serves as a loading control.

Having confirmed the knockout of METTL3, the m^6A levels in the two different cell lines were compared via HPLC analysis. For that, poly-(A) RNA from WT and KO cell total RNA was enriched using oligo-dT capturing. Enrichment efficiency was verified by measuring the depletion of ribosomal RNA as seen in Figure 32. The left chromatogram shows the input total RNA, whereas in the right part, the chromatogram for poly-(A) enriched RNA is shown, which clearly lacks the high peaks of 18 S and 28S rRNAs.
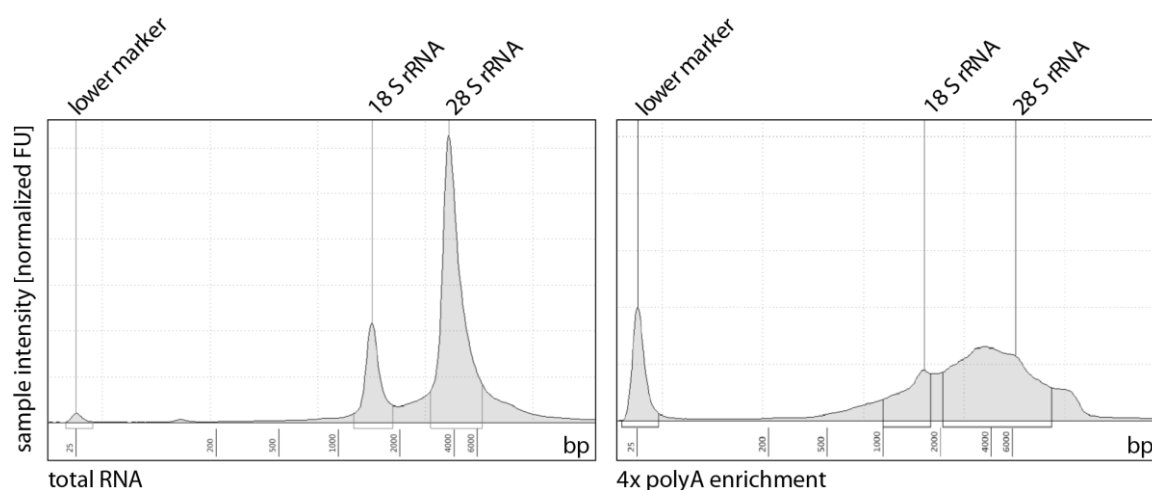
Figure 32: Enrichment of poly-(A) RNA from total RNA. Total RNA from C643 cells was used as the input for the enrichment reaction. The TAPE station analysis of input total RNA is shown on the left side. Apart from the lower marker at 25 nucleotides, the most prominent peaks are the 18S and the 28S rRNA. On the right, the RNA after mRNA enrichment is depicted, with strongly decreased rRNA peaks.

The poly(A) RNA was then digested into single nucleosides with an enzyme mix consisting of Benzonase and Phosphodiesterase I for 3 to 4 hours at 37°C. After this treatment, the nucleoside mix of WT and KO RNA were loaded onto a HPLC Hypercarb column (Thermo

Scientific), applying also an m6A nucleoside as a standard (Figure 33A). The quantification of the integrated area of the m6A/A ratio peaks, normalised to WT is shown in Figure 33B. HPLC analysis was performed by Robert Hett. The m6A peak in the wildtype cells was found to be 70% higher than the peak of the mRNA from METTL3 KO cells.
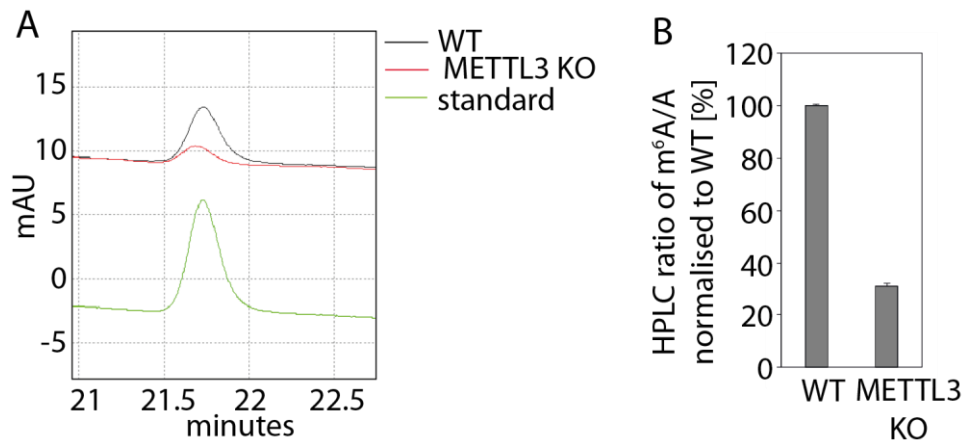
Figure 33: Validation of the METTL3 knock out (KO). (A) HPLC curves of the m6A peak measure in C643 WT (black), METTL3 KO (red) poly-(A)-RNA. The green line, which has a small subset is the curve for the m6A standard nucleoside. The m6A peak is detected after 21.75 minutes of HPLC run. (B) Quantification of the HPLC measurement of WT and METTL3 KO C643 cell mRNA shown in B.

The decrease in the amount of m6A in KO cells, which was seen in the HPLC analysis was then investigated in immunofluorescence staining. C643 WT and KO cells were treated with the α-m6A antibody clone 9B7 and the polyclonal antibody from Synaptic Systems, following the protocol, described in 4.2.5.6 (Figure 34A). Using ImageJ (Wayne Rasband, NIH), the signal intensities were quantified for 30 cells for each antibody staining (Figure 34B). Using the antibody clone 9B7, a signal decrease of approximately 40% in the KO was observed. Staining with the Synaptic Systems antibody, the signal decreased by 30%. These results suggest that real m6A signals were detected in the experiments and that the antibody can be used in analyses like the presented.
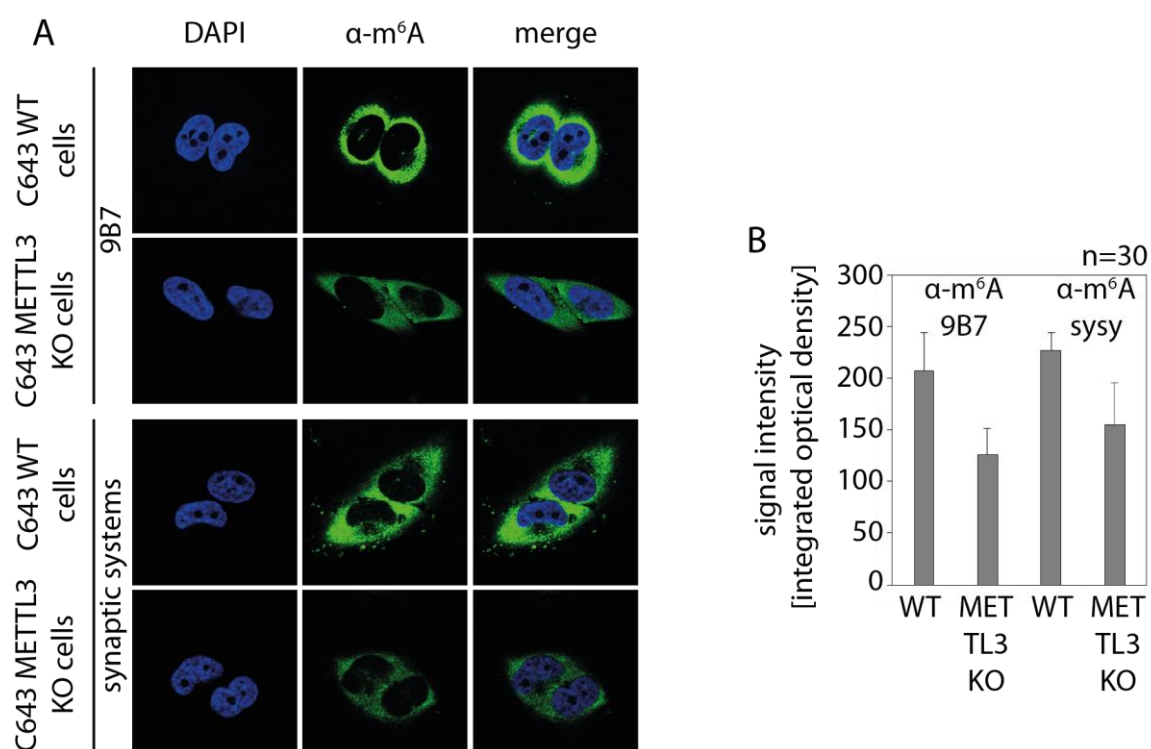
Figure 34: Immunofluorescence staining of C643 WT and METTL3 KO cells. (A) The C643 cells were stained with two different α-m6A antibody clones (9B7 and Synaptic Systems polyclonal). (B) Quantification of the immunofluorescence staining shown in (A).

2.1.8.2 miCLIP analysis

A very commonly used method for RNA-base directed antibodies is miCLIP analysis that allows for base-resolution mapping (m6A individual-nucleotide-resolution cross-linking and immunoprecipitation)[193,278]. For that, total RNA is extracted and the antibody is cross-linked to the specific RNA sites using UV light at 254 nm. The antibody and bound RNA is then precipitated with protein G-coupled magnetic beads. After radioactive labelling of the RNA, the antibody-RNA complex is loaded onto a SDS-gel and blotted on a nitrocellulose membrane. The experiment was done using α-m6A antibodies 9B7, 19B7, 11D11 and the commercially available one from Synaptic Systems. Also α-m5C antibody clones 32E2 and the commercially available one from Diagenode were used. Lastly, the α-Ψ antibody clone 27C8 and the m2 6A-directed clone 60G3 were applied in this experiment. The respective autoradiograms of the blots, which show antibody-bound RNA fragments are presented in Figure 35.
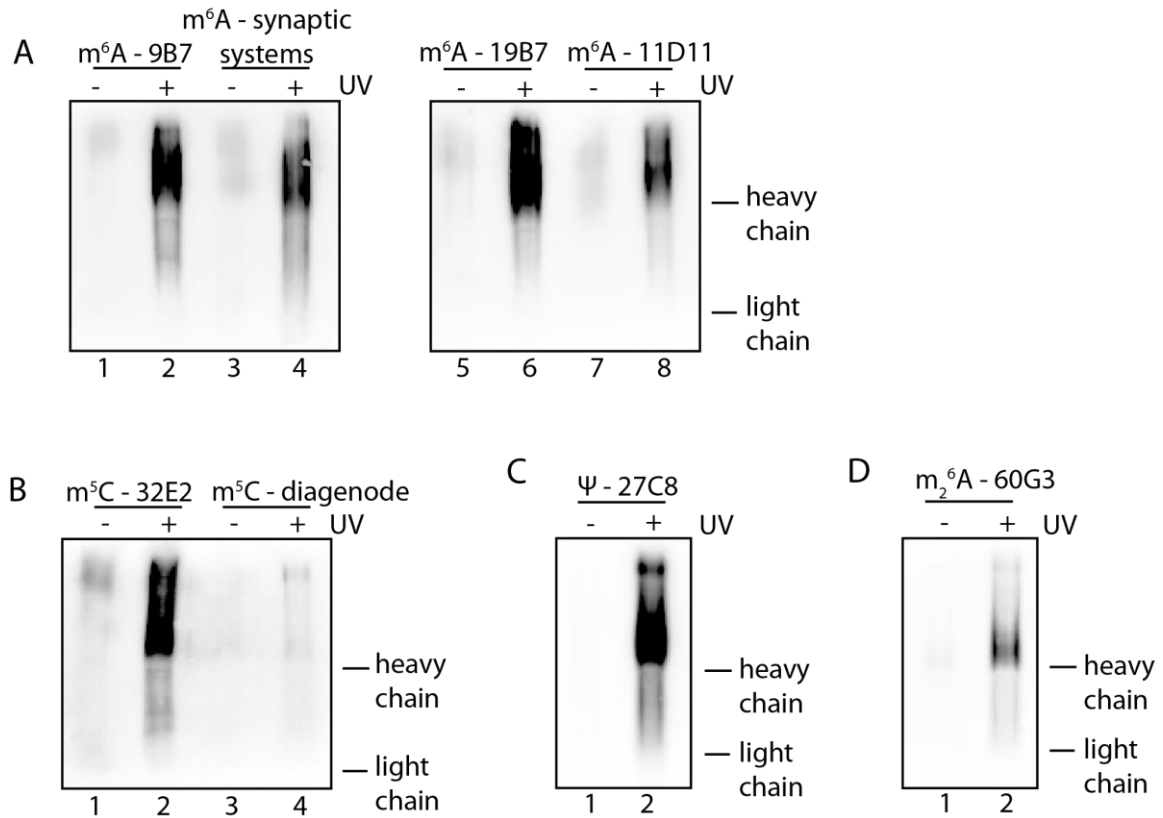
Figure 35: Autoradiograms of miCLIP analyses using different antibodies. miCLIP experiments were conducted using (A) m6A antibodies, (B) m5C antibodies, (C) Ψ- antibodies and (D) m26A antibodies. The (-) lanes shows the non-crosslinked negative control, the lanes with a (+) were UV-crosslinked. The heights of heavy (50 kDa) and light chains (25 kDa) of the antibodies are labelled on the side.

Heavy and light chain of the antibodies are marked as size markers. The RNA, which was immunoprecipitated by the specific antibodies is found as fragments, smearing from the light (25 kDa) and heavy (50 kDa) - but mostly from the heavy - antibody chains in all experiments. Also, in almost all +UV-setups, the antibodies seem to be able to precipitate RNA (lanes 2, 4, 6 and 8) in contrast to the UV–negative controls (lanes 1, 3, 5 and 7). The RNA signals could then be cut out of the gel and be subject to a cDNA library preparation and a subsequent RNA-sequencing.

Most of the shown figures and other content of this chapter are part of the manuscript *Generation and validation of monoclonal antibodies specific to modified nucleotides, Saller, F. et al.,* which was under revision for publication at the time of writing this thesis.

2.2 Detection of RNA modification binding proteins

The aim of the following chapter was to identify specific reader proteins of the base modifications m^6A, m_2^6A and m^1A. As an initial screening strategy, a biochemical pulldown approach was developed.

2.2.1 Principle of the pulldown

Several laboratories already made more or less successful attempts to find interactors of modified RNA bases, so-called reader proteins. Different approaches have been made, including SILAC and other mass-spectrometry-based methods[243,320]. However, a lot of functions of modified RNA bases in the cell can still not be explained and moreover, for most of the modified RNA bases, no reader or interacting protein has yet been found. To be able to affect downstream processes, most probably, the bases however have to be bound by certain effector proteins. Thus, a lot of effort is being made by several groups to find reader proteins, specific for RNA base modifications.

A well performing RNA pulldown method was already well-established in our group[321]. To tackle the problem of detecting reader proteins, in this study, a variation of this pulldown strategy was applied. Magnetic beads, coupled to streptavidin were used to first be bound to a biotinylated 2'-O-Methyl-RNA linker. This RNA oligo is complementary to an RNA-hairpin, based on a pre-microRNA. In the loop of this hairpin, the modified base of interest was placed for better accessibility for possible specific reader proteins (Figure 36). This coupled hairpin was then incubated with different cell lysates and was washed stringently to get rid of unspecific binding. Subsequently the samples were loaded on an SDS-gel and finally the whole precipitate was cut out and prepared for mass spectrometric analysis.
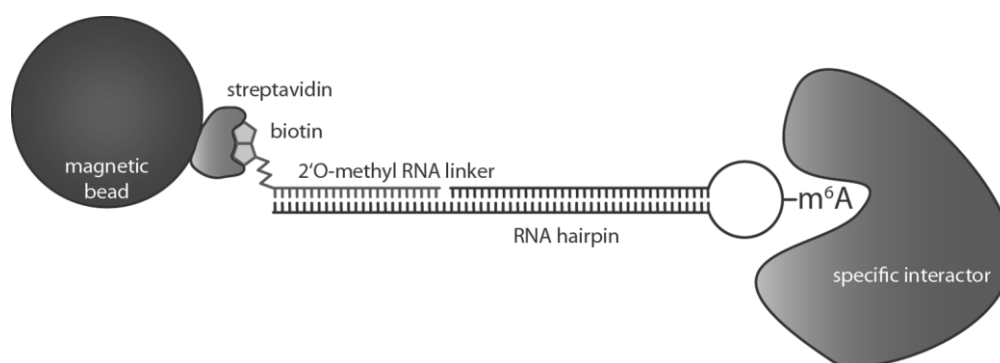
Figure 36: Scheme of the hairpin-pulldown approach to find modified RNA base binding proteins. Magnetic streptavidin beads were coupled to a biotinylated 2'-O-Methyl-RNA linker which can bind complementary to a hairpin, containing the modified base in the loop region. This setup was used to precipitate specific interactors which were identified by mass spectrometric analysis.

2.2.2 Ligation of the hairpins for the pulldown

In order to perform pulldown experiments, the hairpins were obtained in two different ways. The unmodified part was cloned and *in vitro* transcribed. The modified part was purchased from Axolabs GmbH. These two RNA-oligos were then ligated to generate the full hairpin (Figure 37A). The first ligation attempt included a splint-involving ligation to aid the two free ends find each other and ensuring a more efficient ligation. Several optimisation trials were conducted, including buffer tests, titration of the reactants and other components of the reaction, usage of different ligases, incubation times and temperatures and much more (Data not shown). In Figure 37B, the resulting hairpins of the optimised protocol are shown. In lane 1, the fully *in vitro* transcribed unmodified hairpin was loaded as size standard. Lane 2 – 4 show the individual fragments without ligation. In the lanes 5 – 8, the produced ligation products of the pre-let7f2-based hairpin are shown, lanes 9 – 12 show the different pre-mir29b2-based hairpins.
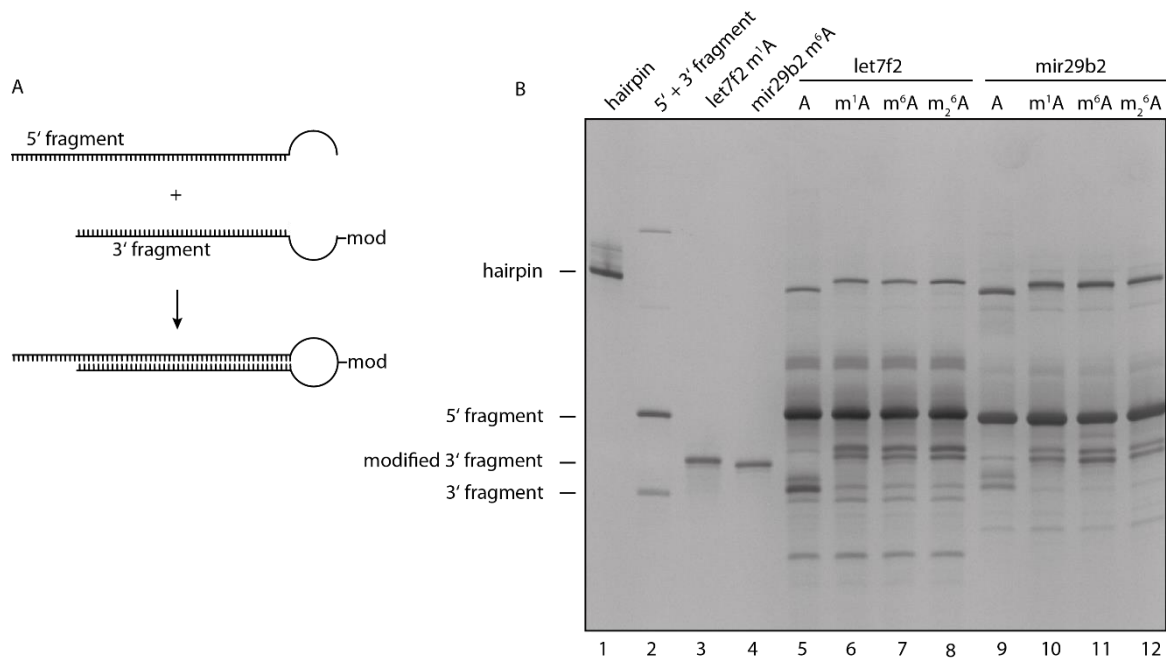
Figure 37: Ligation reaction of the two fragments to gain a hairpin. (A) Schematic depiction of the ligation of the two RNA fragments. (B) Urea gel showing the hairpin and the 3' and 5' fragments as size markers and the ligation products of the optimised protocol.

Finally, a suitable protocol was established and the hairpins were produced in a larger scale for further application in pulldown experiments.

To make sure, the RNA hairpins were ligated in the right way, a test-pulldown was conducted, comparing ligated and *in vitro* transcribed pre-miRNA hairpins. Thereby, it could be verified, if the ligated hairpins behaved in the same way as the endogenous pre-miRNAs do. Binding between modified pre-miR-29b2 (ligated and *in vitro* transcribed as a whole) and its binding

protein YBX1 was investigated (Figure 38). Pre-miR-21 was used as a negative control, but showed a faint band of the protein as well. The signal for YBX1 could clearly be detected in the positive control and also in the test pulldown with the ligated hairpin. The ligated product showed another unknown precipitated band, but the hairpin was also able to specifically bind the protein of interest. Thus, the ligated hairpin was intact and could be used in further experiments.
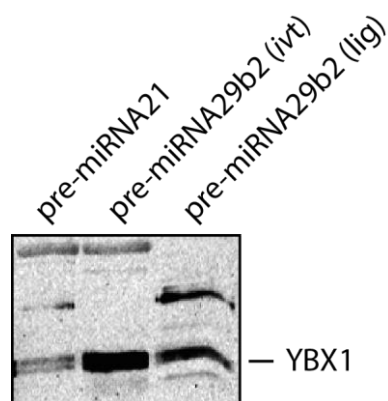
Figure 38: Protein binding pre-test of transcribed versus ligated hairpin. The hairpin pre-miR-29b2 was tested in a pulldown assay using its binding protein YBX1. The experiment comprised a negative control (pre-miR-21), the *in vitro* transcribed pre-miR-29b2 and the ligated pre-miR-29b2.

2.2.3 RNA pulldown of modified RNA binding proteins

The RNA pulldown experiments were conducted in the three human cell lines HEK293T, NTera2 and HepG2. Furthermore, the setup was conducted with 2 different pre-miRNA hairpin templates pre-let7f2 and pre-miR29b2. The RNA modifications m^1A, m^6A and m_2^6A were chosen to be analysed in this study. Thereby, m^6A was used as positive control, for a lot of m^6A readers are already known[224,322–325]. M^1A and m_2^6A on the other hand were chosen, since not much is known about these RNA base modifications and at least m^1A is a potential mRNA modification[326], which suggests that also some readers for this modification should exist.

 After the pulldown, the proteins were eluted from the beads, run on 10 % SDS gels (NuPAGE, Invitrogen) and the entire lane was cut into several pieces for mass spectrometry analysis (see Figure 39 for an example).
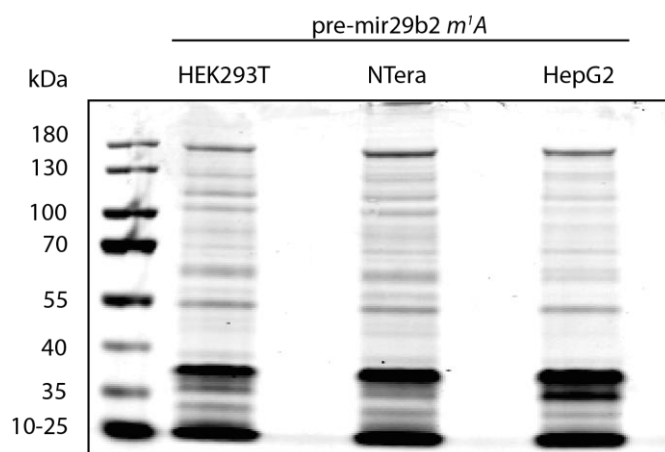
Figure 39: SDS gel of the pulldowns with pre-mir29b2 m¹A in three different cell lines, as examples. The gel was stained with Coomassie blue. The bands were cut out and prepared for mass spectrometry analysis. This was done for the other lanes of the different hairpins and cell lines as well.

The gel pieces were then trypsin-digested and prepared for mass spectrometric analysis (see 4.2.4.5). This analysis resulted in a list of around 2400 binding proteins for all three nucleosides, which had to be sorted into true binders and false positive candidates. Of this long list of proteins, it is very likely that the vast majority shows only background binding. To distinguish the unspecific binders, a preclear experiment has been conducted independently and analysed as well. Therefore, only the streptavidin beads coupled to the biotin-linked RNA oligo, was incubated with the cell lysates without the use of the hairpin-RNA. For analysis, several leverage points were used to examine the data. On the one side, the peptide scores were taken into account. Proteins with a lower score than 50 were not considered further, unless the protein was a known reader protein. To be considered as 'positive', the protein in question had to reveal a higher score for one of the modifications than for the other two base methylations. Also, proteins, which showed a higher score in the preclear measurement than in a pulldown were not regarded specific. It was further checked, if a protein was detected in more than one replicate or in samples with both pre-miRNA backgrounds. The hits were counted, compared with all other pulldown sample results and also taken into consideration. In Table 3, the potential binding proteins with the highest mass spectrometry peptide scores are listed, ranked by their abundance in the data set.

Table 3: Sorted proteins found in the pulldown for the different RNA base modifications. The shown list comprises the potential binders, which showed the highest scores in the mass spectrometry data for the m^1A-, m^6A- and m_2^6A pulldown. The protein names represent the "uniprot" nomenclature (www.uniprot.org).

m^1A		m^6A		m_2^6A	
TBA4A	SPF27	TBB6	CPNE9	H2B1O	PLEC
H2B1M	RN3P2	TADBP	SRRT	H2B2F	PP1B
FXR1	RBBP6	FMR1	PSIP1	IF2B3	RIF1
FXR2	EXOS8	XPO1	TF2H4	PLOD1	NDUS3
VSIG8	RCC1	UBA1	FLNA	FUBP2	IKIP
YTDC2	UN45A	H2B2D	GBB1	TUT4	STT3A
SYTC2	AMYP	NSUN2	MIC60	YLPM1	PLIN3
MCA3	DMBT1	DDX20	MRCKB	VIGLN	TMA16
FUBP3	G45IP	CPSF6	UBP10	RBM15	AL1A2
DICER	WDR55	CAPR1	YTHD2	SF3B4	CDK5
1433G	RALA	SF01	ICAM1	H32	FANCI
PLAK	DI3L2	PI51A	IGJ	NOLC1	RM04
NACAM	BT1A1	SF3B6	CCDC8	RL36L	GMPPA
TGM3	PADI4	HBA	DCAF7	LAT1	PON2
TNIK	RBM40	MSH2	DDB1	AMPN	NDUS1
NUCB1	UCHL5	MECP2	RPP38	SMC2	PPHLN
TPM2	FEN1	ATD3B	VIR	PRS6A	DHX40
RADI	MET17	ERLN1	S30BP	PDIP3	RPC1
EZRI	PEF1	TF2H2	YTDC1	MD12L	GALK1
DIM1	THOC7	ZC11A	AGO2	CS047	SUN2
LAP2A	CASC3	EI2BB	TRM2A	PLOD3	METL8
PINX1	GSTP1	CD11A	NSUN5		
S10A3	PEX19	EIF3G			
LYG2	L2HDH				
MYO15	THUM1				
PHF5A	ZC3H8				
TBL2	NMNA1				
RT18B	ZCHC8				
INCE	ALKB5				

In Table 17 to Table 18 (chapter 5.2.3), the scores and peptide amounts for all the proteins are shown. The next step was to verify the data, gained from mass spectrometry. For that, electro mobility shift assays (EMSAs) and western blots were performed. EMSAs, conducted with YTH proteins and m^6A oligos were used as a positive control experiment, the EMSA with the protein c9orf114 showed weak binding to the m^1A oligo (data not shown). All other westernblots and EMSA assays, which were executed did not show any clear results. Thus, it remained unclear whether the identified proteins are specific binders and therefore, these proteins were not investigated further as part of this study.

3. DISCUSSION

3.1 Antibodies against modified RNA bases

One central aim of this work was to generate highly specific and sensitive antibodies against various modified RNA bases. This was achieved with the help of Robert Hett and in collaboration with the group of Dr. Regina Feederle from Helmholtz Center, Munich.

3.1.1 The selection of the coupling reaction method

For the first step of antibody generation, the synthesis of the antigens was chosen following a protocol established by Erlanger and Beiser[291]. This was executed in the laboratory by Robert Hett. The reaction was followed photometrically and showed a shift of the conjugate in the expected range. To increase the efficiency of the reaction, ovalbumin was cationised. Thus, the lysines of the protein are transformed into iminium cations, which consist of a mesomere-stabilised nitrogen-carbon bond. These iminium cations are very reactive and the nucleosides are more likely to be bound by these lysine sites of ovalbumin. Using a carrier protein for immunisation is commonly used for the generation of antibodies against small compounds[327]. However, this antigen strategy was not the only one that could have been applied. There are approaches from other laboratories (i.e. Prof Dr. Thomas Carrell, Munich) to couple not only a nucleoside to the carrier protein but an RNA-oligo, containing the modified base. Thereby, the antibody would be directed against the modification in an RNA context and not only against the single nucleic acid base. There are, however, no published antibodies that were successfully generated by the use of this method. The reaction that was chosen for this work, resulted in potent and useful antigens since the number of positive antibody hybridoma clones was relatively high.

3.1.2 The importance of the right immunoprecipitation conditions

In chapter 2.1.3, several conditions are described for optimising the RNA IP protocol. For the specificity of an antibody, the right pH and the type of salt in the IP buffer seems to be crucial. LiCl, which has shown to precipitate the RNA best in these experiments, is a known RNA interacting and stabilising salt[328,329] (Figure 16A). Furthermore, the salt concentrations in the wash buffers have a high influence on the precipitated RNA (Figure 16B). The stringency of the washing steps has to be perfectly balanced to gain only specific bound RNA species, without immunoprecipitating unmodified RNAs. Additionally, especially the amount of antibody changes the amount of precipitated RNA tremendously (Figure 17). It seems that the application of a high excess of antibody in the immunoprecipitation experiment leads to a

higher yield in precipitation, as the antibody with its restricted binding sites represents the limiting factor. Then there is the effect of the mode of coupling that seems to be very important for the ability to bind the RNA properly (Figure 18). It is not easy to distinguish if a signal is specific or not. For that, competition with free nucleosides as well as the use of unmodified spike-in RNAs are good tools as seen in Figure 19. The buffer conditions can be very clearly determined, when using unmodified and modified mRNA spike-ins, since there, the signal should be very distinctly positive or negative (Figure 22). For every antibody clone however, the protocol had to be optimised separately, since the conditions vary immensely from antibody to antibody. Particularly for sequencing approaches, highly specific enrichment of RNA transcripts is of great importance, as otherwise, the data cannot be trusted and worked with.

3.1.3   One important annotation

A relevant point that must not be forgotten, when dealing with results from these antibody-based methods is that the antibodies, generated here, are only directed against the base and not the whole RNA-nucleoside, since the ribose ring is destroyed during the coupling reaction (Figure 9). This means that our antibodies cannot distinguish between the modified RNA bases, they have been generated against or additionally 2'-O-methylated modified RNA nucleosides (methylation at the 2'-OH-group of the ribose ring). Even modified DNA nucleosides could be detected by the antibodies. To avoid misinterpreting data, gained from an antibody-based experiment, the input can be DNase treated before. To identify any unwanted co-immunoprecipitated 2'-O-methylations is a more complicated problem to address and is not easily solved. Deep-sequencing and bioinformatical-based setups like RiboMethSeq, 2'OMe-Seq, RibOxiSeq, Nm-Seq or meTH-seq can help detect the 2'-O-methylations[330,331]. For detection of 2'-O-methylations, biochemical properties of the structure can be taken advantage of. 2'-O-Methylations have an increased resistance against alkaline/enzymatic hydrolysis, the reverse transcription stops at low NTP concentrations at these sites and when located at the 3' end, enzymatic activity can be altered[331].

3.1.4   Challenges in K_D determination

A very important characteristic of antibodies is the affinity to their antigens (K_D index), as mentioned in 2.1.4. The apparent K_D-values were determined using mixtures of free modified and unmodified nucleosides (see 2.1.4). The samples were then separated using filter tubes. The modified nucleosides, bound by the antibody were then assumed to be retained on the filter (bound fraction), whereas the unbound nucleosides were measured via HPLC. The ratio of bound and unbound was then used to determine the K_D value. There are several caveats to

this method. The filter-separation is not an error-free technique, since antibody-nucleoside complexes could slip through the membrane or too much free nucleosides could remain in the supernatant. To make sure, these potential shortcomings are negligible, six different dilutions of the nucleosides were prepared for the experiment. The mathematical approach of K_D determination also has its downsides. The numbers that are calculated are graphical approximations and, although arithmetically correct, still estimations. These K_D index numbers also may vary depending on the substrate. Furthermore, all the experiments to determine the K_D value presented here, were conducted with nucleosides. Nucleosides are however not the final target of these antibodies in subsequent applications. Thus, a similar experiment was attempted with RNA-oligos. For that, the concentration of the RNA was measured before and after IP and the same mathematical evaluation as before with the nucleosides was performed. However, the obtained outcome was not as clear as the experiment with the nucleosides. Although conducted in triplicates with 4 different dilutions each, the Scatchard plots did not emerge as a straight line. Also the binding models did not show a clean curve. In some cases, to obtain a reasonable value, particular data points had to be purged. The K_D-values, identified with the RNA oligos (Table 4) vary from the ones, obtained with nucleosides and show increased values for the affinity constants. Nevertheless, for most antibodies tested, the values are still in a low µmolar range. These K_D-values are however only an estimation and not to be taken for granted for the above-mentioned reasons.

Table 4: Comparison of the K_D-values of the antibodies against modified RNA bases using nucleosides and RNA oligos for determination of the affinity. The first three rows show antibody clones and the K_D-values, determined with the nucleoside method, like in Table 1. In the last row, the apparent K_D-values obtained, using RNA oligos are listed.

Modification	Antibody clone	apparent K_D-value (nucleoside) [µM]	apparent K_D-value (RNA oligo) [µM]
m⁶A	13G2	1.92	12.7
	11D11	0.59	21.4
	9B7	0.55	14.7
		0.89	
		0.60	
m⁵C	31B10	1.14	23.8
	28F6	1.5	14.9
	32E2	0.39	20.5
		0.68	

Ψ	26H5	38.12	59.4
	27C8	17.18	6.7
m$_2^6$A	60G3	0.89 1.15	1.66
m^{1}G	6E3	9.88	-
	4G10	0.15	-
m^{3}U	6A2	0.52	-

3.1.5 Further quantitative characterisations of the antibodies

The affinity was further tested in several other quantitative experiments like the *in vitro* transcription/TLC experiments or the IPs with radioactive and modified RNA oligos. Here, the antibodies were tested in a more application-oriented examination, using them for enriching RNA oligos. These setups were particularly important for the antibody characterisation to validate their specificity and enrichment abilities. The TLC experiments showed very clear results regarding the enrichment capability. In these experiments, the newly generated antibodies against m^{6}A (clones 11D11, 13G2 and 9B7, equally) showed approximately the same results as the commercial antibody did (Figure 26). This proof of principle setup shows that the attempt for generating highly specific antibodies was successful. The antibody clone 32E2 against m^{5}C even yielded higher enrichment as the commercial α-m^{5}C antibody (which did not enrich at all) did and showed overall a very good enrichment capacity (Figure 27 and Figure 28). The α-Ψ antibodies on the other hand were not enriching their target RNA as much. Only when using a highly modified RNA oligo, the antibody clone 27C8 had good enrichment abilities (Figure 29). Unfortunately, not all the antibodies could be tested in this highly informative experiment, as the *in vitro* transcription cannot be executed with all modified NTPs. This is because the RNA polymerase, used for *in vitro* transcription is not able to incorporate every modified NTP in the RNA. Thus, another experiment was designed to investigate the enrichment capability as well as the specificity towards differently modified RNA oligos that were purchased. Here, the generated α-m^{6}A antibody (clone 9B7) showed slightly reduced enrichment, compared to the commercial one (Synaptic Systems). However, the background enrichment for the clone 9B7 was lower, thus the specificity for this clone is higher. A very interesting notation is that the m$_2^6$A-oligo seems not to be enriched more than other RNA transcripts, even though the difference in the structure between m^{6}A and m$_2^6$A is very little (see Figure 40). That an antibody can distinguish between such small epitopes was not entirely clear before and is striking.
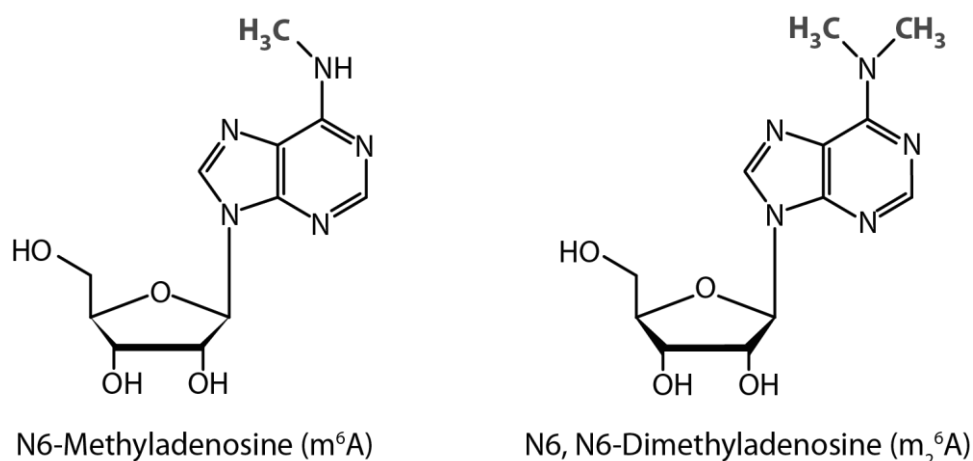
Figure 40: Structures of N6-Methyladenosine and N6, N6-Dimethyladenosine. When comparing the two structures, the only difference is one methylation group at the nitrogen atom at the 6th position of the purine ring. M^{6}A has only one and m$_2$^{6}A harbours two methylation groups.

Even more astonishing is the tremendous enrichment of m^{5}C-oligos using the α-m^{5}C antibody 32E2. To display the enrichment of the other RNA oligos using this antibody, the y-axis of the chart is depicted non-continuously in Figure 41B. This antibody seems to be very specific and also very sensitive as it enriches the same amount of modified RNA bases 100-fold more effectively than the other antibodies.
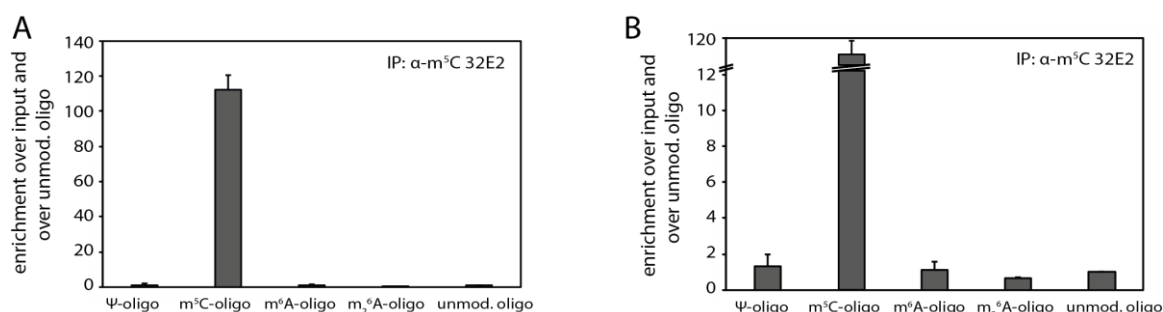
Figure 41: Enrichment of modified RNA oligos using the antibody clone α-m^{5}C 32E2. (A) Enrichment of the oligos like it was shown in Figure 24B. (B) Different y-axis application to visualise the enrichment of the other modified RNA oligos.

The assay, done with the α-Ψ antibody 27C8 showed enrichment for the Ψ-oligo but unfortunately, it enriched the m^{5}C-oligo even more (Figure 30C). This fits to other results for this antibody, being not as specific as other antibodies that were generated. The α-m$_2$^{6}A-antibody clone 60G3 enriches very specifically for the m$_2$^{6}A-oligo and not for any other modification. Again, the expected potential cross-reaction with the m^{6}A-oligo cannot be seen here (Figure 30D).

3.1.6   Antibodies from other laboratories and companies

In the introduction, several groups were mentioned, that also developed antibodies against RNA base modifications (1.5.4). Among them, the groups of Munns and Sawicki were the first ones to establish such of tools for application in RNA biology[298,332]. They used the same approach as was described here. Several m5C antibodies have been originally generated against DNA, but have later also been applied for RNA-specific questions[56,306–308,333]. One example is the m5C antibody from Diagenode, which was tested in the *ivt*-TLC experiments as well. Several labs used this antibody for different experiments with the aim of detecting m5C in RNA. However, the results presented here (chapter 2.1.7) do not show very specific binding of this antibody to m5C in the context of RNA. The antibody against m6A by Synaptic Systems is very widely used for several applications, as discussed in chapter 1.5.4. Many sequencing experiments have been conducted using this antibody. From our data, this antibody displays very sensitive and specific properties. Data, generated with this antibody can indeed be trusted, according to our results. A very positive outcome of our research was that the antibody clones α-m6A 9B7, 11D11 and 13G2 seem to be as specific as the α-m6A clone from Synaptic Systems. In a very recent publication, the efficiency of RIP-Seq protocols was to be optimised[311]. Three different commercially available α-m6A antibodies were tested and compared. These were antibodies from Synaptic Systems, which was also tested here, from NEB and Millipore. The latter showed the lowest signal-to-noise ratio and overall had the best performance[311]. This however is a polyclonal antibody, whereas the presented antibody clones are monoclonal, thus directed only against one epitope, which commonly leads to a higher specificity. Studies like these show that there is a very high urge to find highly specific and sensitive antibodies. As they also conclude in their discussion to aim optimising RIP-Seq protocols for m5C and m1A as well, "when good antibodies become available"[311].

3.1.7   Nucleobase directed antibodies in different applications

3.1.7.1   Immunofluorescences

The generated and rigidly tested antibodies have subsequently been applied in several biochemical and molecular biological experiments. When using the α-m6A antibody clone 9B7 in immunofluorescence assays, well detectable signals can be seen, however only in the cytoplasm (Figure 34). Non-coding RNAs such as rRNAs and snRNAs, which localise to the cytoplasm harbour m6A-marks and are detected by the antibody. Strangely, no signal is detected in the nucleus, even though the U6 snRNA, as well as several mRNAs that are bound by nuclear YTHDC1, have been reported to harbour m6A sites and localise to the nucleus[98,131]. An explanation could be that the reader protein is bound to the RNA modification and the

antibody cannot access its target. The same could be true for the U6 snRNA, which could be too deeply buried in the spliceosome to be accessible for the antibody. Nevertheless, a signal can be detected for the cytoplasmic RNAs, so in principle, the antibody seems to be sufficient for immunofluorescence experiments. The commercial antibody from Synaptic Systems shows very similar intensity and patterns as the clone 9B7. Thus, our newly generated antibody can stain as sufficiently as the widely used and trusted antibody clone. In the immunofluorescences, the knock-out (KO) of METTL3 clearly leads to a reduction of the m^6A signal intensity. The remaining 70 % of the m^6A signal originates like abovementioned, most likely from rRNA, snRNA and other cytoplasmic RNA species. The analysis of the KO of METTL3, which was demonstrated in Figure 31 shows a shorter and less abundant band in the western blot. This could be a truncated version, hinting to a non-complete knockout. But since the m^6A abundance is reduced by around 30% in HPLC measurements of poly-A RNA (Figure 32), the expressed protein seems to be non-functional. Altogether, the immunofluorescence stainings represent another very useful application of the generated antibodies and open the way to new exciting experimental insights.

3.1.7.2 miCLIP analysis

The described miCLIP technique (m^6A/methylation individual-nucleotide-resolution cross-linking and immunoprecipitation) was developed for the analysis of RNA-methylation at a nucleotide resolution[193,278]. Here, it was tested, if certain antibody clones against m^6A, m^5C, Ψ and m_2^6A are applicable for such approaches (chapter 2.1.8.2). The resulting autoradiograms are shown in Figure 35. Several other groups have already applied this or analogous methods for subsequent sequencing of the RNA[193,278,334,335] . The different m^6A antibody clones used here, show varying results (Figure 35A). Clones 9B7 and 19B7 show the most intense RNA signals. The signal intensities when using the antibody clones from Synaptic System and 11D11 are similar to each other. When comparing the autoradiograms using the newly generated antibodies to those, presented e.g. by Grozhik et al.[334] (Figure 42), the signal pattern seems to be similar. In the paper, it is not exactly specified if the autoradiogram shown was performed with polyclonal α-m^6A antibody from Synaptic Systems or from Abcam. In any case, the signal of Figure 42 can be compared with the data, produced with the generated α-m^6A-antibodies.
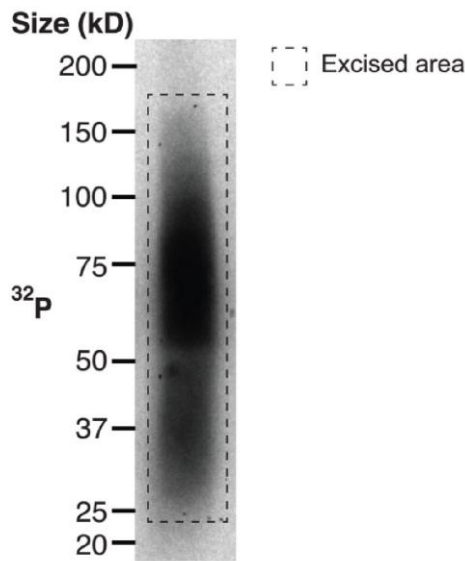
Figure 42: Autoradiogram of a miCLIP experiment, performed by Grozhik et al.[334]. The group used poly(A)-RNA, crosslinked to an α-m6A antibody. After the described miCLIP protocol (chapter 2.1.8.2 and 4.2.3.5), the crosslinked RNA fragments can be seen on the nitrocellulose membrane as smears extending from light and heavy chains of the reduced antibody.

The α-m5C antibody clone 32E2 precipitates a high amount of RNA, whereas the one from Diagenode does not (Figure 35B). Again, the commercial α-m5C antibody appeared to be not as sensitive as the antibody, generated in this thesis. The α-Ψ antibody 27C8 also shows a very high signal for precipitated RNA (Figure 35C). This, however, is most probably due to unspecific binding of the antibody to RNA and not restricted to the Ψ-modification. This non-specificity could also be seen in the enrichment-experiment, shown in Figure 30, where the α-Ψ antibody bound to any oligo. The m_2^6A-antibody showed very little signal in the experiment (Figure 35D). This might be due to low m_2^6A-modified RNA concentrations, present in the analysed total RNA or low sensitivity of the antibody. To really draw a conclusion out of all the miCLIP-experiments, the RNA would have to be sequenced to gather and compare solid data. In chapter 1.3.3, it was already mentioned that several different sequencing data sets are published, which all differ a lot from one another. Especially m5C, m1A and Ψ sites in mRNA are under debate[54,55,57,149,151,253]. But even m6A sites are not fully explored. Regularly, computational or biochemical tools are published for better discrimination between real sites and background signals. Rigidly tested tools like the antibodies presented here can definitely help to figure out, which modified sites are real.

Apart from the presented data, the antibodies have been used in different experimental setups by other groups. The group of Prof. Dr. M. Cristina Cardoso (Technische Universität Darmstadt) performed immunofluorescence experiments using the α-m5C antibody 32E2 to

stain DNA in mouse embryonic fibroblast (MEF) cells. The signal could clearly be detected in nucleoli and showed much higher intensity than the α-m⁵C antibody from Active Motif clone 33D3. Another experimental setup, using the α-m⁶A antibodies generated here, was Fluorescence-Activated Cell Sorting (FACS) analysis in MEF cells, performed by the group of Prof. Dr. Vigo Heissmeyer (Ludwig-Maximilians-Universität München). There, m⁶A-modified RNA could be detected in solution using biotinylated antibody clones. In detail, the difference of detected m⁶A in wildtype compared to WTAP-deficient cells could be made visible clearer by the newly generated antibodies, when compared to the commercial antibody from Abcam. The data for both experiments is not shown, but can be found in Figure 5 and 6 of the manuscript *Generation of monoclonal antibodies specific to modified nucleotides, Saller, F. et al.* (under revision at the time of submission of this thesis). Taken together, possibly new experimental approaches could be accomplished, when using the antibodies in setups like this.

3.1.8 The anti-Pseudouridine antibodies

Before working with the antibodies, dot blot analysis was pursued to get a first glimpse on how the antibody hybridomas perform in general (Figure 14). For some of these antibody clones, the chosen method did not show a positive result, like the α-Ψ antibody shown in Figure 15, even though it performed better in other experiments. However, the overall performance of the α-Ψ was not very convincing. For certain applications, the antibodies seemed to be sufficient, especially when immunoprecipitating highly Ψ-modified RNA (TLC experiment with 50% ΨTP in the reaction, Figure 29B). Another experiment, where the antibodies showed reasonably good specificity, was a CMC-analysis (data not shown). Here, total RNA was treated with a chemical that binds specifically to Ψ (CMC) and thus prevents antibody binding. Indeed, a reduced binding and thus reduced signal intensity was observed when using the presented antibody clones 27C8 and 26H5 to precipitate CMC-treated RNA. This hints to specific binding, since uridine is not bound by CMC and could thus be bound by the antibody, when unspecific. In the K_D analysis, the antibodies seem rather high, except for the clone 27C8, which shows a K_D of 6 µM in the RNA-oligo based measurements. It is therefore always crucial to test the antibody of interest in the experiment of choice rigidly before believing the produced data.

3.1.9 Recapped conclusions for the generated antibodies

Antibodies are biochemical tools with biological background and thus can have several caveats compared to engineered proteins. Thus, the rigid testing for sensitivity and especially specificity are crucial for every experiment that is to be done with these valuable tools. The optimisation of several applications for the respective antibody is of great importance. The antibodies have been keenly characterised and their functions tested in different experiments to make sure that data, produced with the help of these antibodies can be relied on. Judging from the executed experiments, a set of highly specific and sensitive antibodies have been successfully generated, as it is depicted in Table 5.

Table 5: Summary of the different antibody validation results. K_D: dissociation constant, IP: immunoprecipitation, TLC: thin layer chromatography experiment, IF: immunofluorescence, FACS: fluorescence-activated cell sorting; +: medium performance in the experiment, ++: good performance in the experiment, +++: very good performance in the experiment, n.a.: not analysed.

Modification	Antibody clone	apparent K_D-value	RNA-IP	TLC	IF	Crosslink	FACS
m⁶A	13G2	+	n.a.	++	n.a.	n.a.	n.a.
	11D11	+++	++	++	-	+	++
	9B7	+++	++	++	++	+++	+++
	19B7	n.a.	+	n.a.	+++	+++	+++
m⁵C	31B10	++	n.a.	-	-	n.a.	n.a.
	28F6	++	n.a.	+	-	n.a.	n.a.
	32E2	+++	+++	+++	+++	+++	n.a.
Ψ	26H5	-	n.a.	n.a.	n.a.	n.a.	n.a.
	27C8	-	-	+	n.a.	++	n.a.
m₂⁶A	60G3	++	++	n.a.	n.a.	+	n.a.

3.2 Detection of RNA modification binding proteins

3.2.1 Ligation difficulties

To ligate two DNA fragments is a common procedure during every cloning experiment. Ligation of two RNA fragments however, is not as trivial. There are several RNA ligases that have been tested, including T4 DNA ligase, RNA ligase, a truncated version of the T4 RNA ligase and the Circ-ligase (Plasmid thankfully provided by Dr. Jan Medenbach), which was eventually applied. Furthermore, different strategies have been approached, like splint-ligation, where a short RNA fragment was used to bring the 3' and the 5' ends together by base pairing. Another approach was the direct ligation with dephosphorylated 5'-fragment and phosphorylated 3'-fragment. Different RNA, $MnCl_2$/$MgCl_2$, PEG, ATP and ligase concentrations, different incubation times and reaction temperatures have been tested and the conditions were optimised for each hairpin individually. Up-scaling was not applicable for this reaction, so it was conducted in several smaller batches (Figure 37). Aside from a lot of unspecific side products, the desired bands were finally obtained and could be used for the pulldown experiment. That the ligated hairpin can be used for the pulldown experiment was shown in Figure 38, where the ligated and the *in vitro* transcribed hairpin were compared regarding their precipitation efficiency. Here, the protein of interest could be detected with both hairpins equally.

3.2.2 Reader proteins

Finding reader proteins is a task that is not easy to accomplish. Although being RNA binding proteins, they don't always have a familiar RNA binding domain like KH-domain, zinc finger, RRM (RNA recognition motif) or dsRBM (double-stranded RNA-binding motif)[336]. The first family of RNA modification binding proteins that was discovered, were the m6A-readers of the YTH domain family, which all share the YTH domain[219,220]. This domain, which is located in the C-terminal part of the proteins has been shown to be able to bind m6A in an RNA context[133]. With a K_D of around 26 µM, this protein-RNA binding is however comparably weak[219]. This is one reason, why finding new reader proteins can be challenging. Furthermore, the field of readers is very diverse and all kinds of differently assigned proteins can function as a modified RNA base binding protein. Heterogenous nuclear ribonucleoproteins (hnRNPs) for example, are involved in pre-mRNA processing and transport, such as alternative splicing or nuclear export. They comprise an RRM domain, with which they can bind the RNA. Just recently, HNRNP-A2B, -G and –C have been found to bind m6A in RNA, thus also affecting splicing or mediating primary miRNA processing[103,244–246]. IGF2BP is another example of reader proteins with several functions in the cell. It comprises 2 RRMs as well as 4 KH

domains, binding mRNAs and targeting them to cytoplasmic RNPs[337,338]. Both HNRNP as well as IGF2BP proteins have been found in the data, acquired for m6A (Table 6).

In the experimental approach (Table 3 in chapter 2.2.3) executed here, not all the YTH proteins could be detected. These proteins can be taken as positive controls. In the m6A pulldown, only YTHDF2 and YTHDC1 were detected to be specific reader proteins. Another YTH protein, YTHDC2, was detected to bind more specifically to m1A than to m6A. YTHDF1 and 3 could not be detected in this approach. Their binding to the modified base might be less strong. Also, they were not found to be the most abundant m6A reader proteins in this analysis, compared to other proteins, detected. However, several other known reader proteins could be found in the data. These proteins, found in other studies as well, are discussed in chapter 3.2.3. Additionally, several methyltransferases were found in the data, like DIMT1, METTL17 (both as m1A reader), METTL8 (supposedly binding to m_2^6A) or NSUN5 (found in the m6A data). Here again, the binding affinity of the proteins is different to what was expected, as NSUN5 for example, is known to methylate C to gain m5C in rRNA[178]. METTL8 was found to install a m3C modification, other than m_2^6A[339]. METTL17 was very recently described as acting on mitochondrial ribosomal RNA, namely installing m4C(840) and m5C(842) in the 12S mt-rRNA[340], but a methylation activity for m1A is not described. For DIMT1, a N6-dimethylating action on adenosine was observed[341]. Also methyltransferase-interacting proteins, like RBM15 (in the m_2^6A data) or KIAA1429/Virma (Virilizer) (m6A-binding) were found. Even a demethylase, like ALKBH5 was found in the data from the m1A pulldowns. This is in contrast to what has been found before: ALKBH5 was referred to as m6A demethylase[141](see chapter 1.3.1.1). However, the other known m6A-demethylase FTO was recently shown to act on m1A and m6Am as well[256]. The finding of this work could be a hint for a similar function of ALKBH5. Most of the proteins that have been found are not known to bind to modified RNA base modifications. The validation attempts were not completely convincing. This could partly be, due to the weak binding of reader proteins as discussed above. Another reason might of course be that the proteins are no real readers, but merely bind unspecifically to the modified RNA base or the RNA hairpin as such. The binding could also be sequence-dependent, having nothing to do with the altered RNA base. To get a better idea of the real binding situation, a deeper investigation has to be accomplished. The project however could not be followed in that extent at the time.

3.2.3   Comparison with the results of other reader-finding attempts

As already introduced in chapter 1.3.2, a lot of effort from other labs already went into the finding of RNA modification binding proteins and the research is not at all at its end. For m6A, the most reader proteins have been found. The groups of Gideon Rechavi and Michiel

Vermeulen have conducted similar, but only m⁶A-regarding mass spectrometry-based high-throughput analyses, as presented in this study[52,243]. The comparison between the two data sets and our findings are listed in Table 6. Proteins that have been found were marked with (✓), proteins that did not come up in the analysis were labelled with (✗). In the data from this work, it occurred that proteins were found in the pulldown data, derived with a different base modification (m^{1}A or m$_2^6$A). They are assigned accordingly. (∼) is written, when the data is not significant for one modification.

Table 6: Comparison of three different data sets of m⁶A reader proteins. In the left column, the proteins are listed. The data from the papers Dominissini *et al.,* 2012 and Edupuganti *et al.,* 2017 and ours were compared regarding their detection of the proteins, binding to m⁶A[52,243]. (✓: found in the data, ✗: not found in the data, m^{1}A / m$_2^6$A: differently assigned proteins, ∼: found in the data, but not significant).

Protein	Rechavi Data	Vermeulen Data	Our Data
YTHDC1	✗	✓	✓
YTHDF2	✓	✓	✓
YTHDC2	✗	✓	✓
RBBP6	✗	✓	m^{1}A
YTHDF3	✓	✓	✗
CPSF6	✗	✓	✓
HNRNPH2	✓	✓	∼
TARDBP	✗	✓	✓
FUBP3	✗	✓	m^{1}A
FMR1	✗	✓	✓
KHSRP	✗	✓	m$_2^6$A
HNRNPH1	✗	✓	∼
IGF2BP3	✗	✓	m$_2^6$A
FXR1	✗	✓	m^{1}A
HNRNPF	✗	✓	∼
COLGALT1	✗	✓	✗
CNBP	✗	✓	✗
FXR2	✗	✓	m^{1}A
ALKBH5	✗	✓	m^{1}A
YTHDF1	✗	✓	✗
ZCCHC8	✗	✓	m^{1}A
SF3B4	✗	✓	m$_2^6$A

XRN1	✗	✓	✗
NMT1	✗	✓	✓
EDC4	✗	✓	✗
PATL1	✗	✓	✗
LSM1	✗	✓	✗
ELAVL1	✓	~	✓
DHX36	✓	~	m^1A
DBN1	✓	✗	~
HNRNPA2B1	✓	✗	m_2^6A
GNAI3	✓	✗	✓
HNRNPR	✓	✗	✓
FUBP1	✓	✗	~

The relatively great deviation between the three data sets derive from different approaches and its data analyses. The group of Vermeulen also found m^6A-repellent proteins, which in turn positively regulate the mRNA stability. Of these proteins, some have also been found in our data set.

Overall, the presented data, produced for this work may not be completely trusted. The pulldown conditions would have to be optimised and further analysis has to be conducted.

3.3 Outlook

Although first discovered in the early twentieth century, research in the direction of epitranscriptomics is relatively young. The great majority of interconnections between modified RNA bases and the resulting effect has not been elucidated yet. More and more new techniques, methods and tools are developed to help seek links in different regions. The antibodies, described in this work are just one example of endless attempts to tackle the remaining questions. The applied pulldown method was another trial to bring more light into the unknown correlations in this field. Every day, new data is produced in the RNA modification area. Thus, one of the greatest tasks is to distinguish the truth from misleading hints. It will be very interesting to see, where the research in this field heads and what great discoveries will be made in the future. It is very likely that a number of these RNA base modifications have great implications on cellular levels and to follow publications in this area is greatly recommended.

4. MATERIAL AND METHODS

4.1 Material

4.1.1 Reagents and consumables

The chemicals and reagents were purchased in the highest standards (*pro analysis*) from the following suppliers: AppliChem (Darmstadt, Germany), Biorad (Hercules, USA), Fermentas (St. Leon-Rot, Germany) GE Healthcare (Buckinghamsire, UK), Merck (Darmstadt, Germany), New England Biolabs (Ipswich, USA), PAA (Pasching, Austria), Roche Diagnostics (Penzberg, Germany), Roth (Karlsruhe, Germany), Serva (Heidelberg, Germany), Sigma-Aldrich (St. Louis, USA) and Thermo Fisher Science (Waltham, USA).

Enzymes and respective buffers were obtained from Thermo Scientific (Waltham, USA), unless stated differently. The T7 RNA Polymerase was recombinantly expressed, purified and provided by Dres. Treiber.

Radio chemicals were purchased from Hartmann Analytics GmbH (Braunschweig, Germany) and American Radiolabeled Chemicals, Inc. (St. Louis, USA).

Other consumables were purchased from: Sarstedt (Nümbrecht, Germany), GE Healthcare (Buckinghamshire, UK), Biorad (Hercules, USA), Eppendorf (Hamburg, Germany), Invitrogen (Carlsbad, USA) and CAWO (Schrobenhausen, Germany).

Peptides, used as antigens were bought from Peps4LS GmbH (Heidelberg, Germany).

The Kits were purchased as stated in Table 7.

Table 7: Kits

Kit name	Supplying company
NucleoSpin® Gel and PCR Clean-up	Macherey-Nagel (Düren, Germany)
NucleoSpin® Plasmid	Macherey-Nagel (Düren, Germany)
NucleoBond® Xtra Midi	Macherey-Nagel (Düren, Germany)
NucleoSpin® RNA Midi	Macherey-Nagel (Düren, Germany)
Illustra MicroSpin G-25 Columns	Fermentas (St. Leon-Rot, Germany)
First Strand cDNA Synthesis Kit	GE Healtcare (Buckinghamsire, UK)
Rotiphorese Sequenziergel	Roth (Karlsruhe, Germany)
MEGAclear™ transcription clean-up Kit	Invitrogen (Carlsbad, USA)
Oligo Clean & Concentrator™-5	Zymo Research (Freiburg, Germany)
Oligo d(T)$_{25}$ Magnetic beads	New England Biolabs, NEB (Ipswich, USA)

4.1.2 Antibodies

Commercial Antibodies were obtained as seen in Table 8.

The tested antibodies against base modifications, which are a main part of this thesis, are displayed in the result section and the appendix (Table 5 and Table 16). These were generated in a collaboration with the laboratory of Dr. Regina Feederle in Helmholtz Centre Munich (Neuherberg, Germany). Another antibody, which was generated in collaboration with the Helmholtz Centre Munich was the antibody α-METTL3 clone 29C8, which was presented in Schöller et al.[173].

Table 8: Commercial antibodies

Antibody	Source organism	Purpose of use	Supplying company
α-Flag M2	mouse	Immunofluorescence	Sigma-Aldrich (St. Louis, USA))
α-GFP	mouse	Western blot	Roche (Penzberg, Germany)
α-HA 16B12	mouse	Western blot	Covance (Princeton, USA)
α-Myc	rabbit	Western blot	Sigma-Aldrich (St. Louis, USA)
α-m^{5}C (33D3)	mouse	RIP	Diagenode (Ougrée, Belgium)
α-m^{6}A, polyclonal	rabbit	RIP	Synaptic Systems (Göttingen, Germany)
α-m^{6}A, monoclonal	mouse	RIP	Synaptic Systems (Göttingen, Germany)
Alexa 488 α-mouse	goat	Immunofluorescence	Invitrogen (Carlsbad, USA)
Alexa 555 α-rabbit	goat	Immunofluorescence	Invitrogen (Carlsbad, USA)
α-mouse IgG	goat	Western blot	Licor (Bad Homburg, Germany)
α-rabbit IgG	goat	Western blot	Licor (Bad Homburg, Germany)

4.1.3 Oligonucleotides and Plasmids

The DNA-oligonucleotides were purchased at Metabion GmbH (Martinsried, Germany). RNA-nucleosides were purchased from Carbosynth (Oxford, UK). RNA-oligo nucleotides were obtained from Metabion GmbH (Martinsried, Germany), Dharmacon (Lafayette, USA), Biomers GmbH (Ulm, Germany) and individually synthesized by Axolabs GmbH (Kulmbach, Germany).

Table 9: DNA oligonucleotides

Name	Sequence (5' to 3')
Cloning primers	
Hairpin cloning	
HH_Adaptor_for_7f2-1	CGGTACCCGGTACCGTCGGGAGACCTAGCCTTGTGG
HH-7f2-1_rev	ACTGACCCTAAAACTATAC
HH-Adaptor_for_end	AATCCATGGTCTCCCCTGATGAGTCCGTGAGGACG
HH-7f2-2_for	CGGTACCCGGTACCGTCTTGGAGATAACTATACAG
HH-7f2-2_rev	ACCGTGGGAAAGACAGTAG
HH-7f2-2_for_end	AATCCATGGCTCCAACTGATGAGTCCGTGAGGACG
Splint-7f2-1	CTCCAAGATGNGGTATGACCC

Splint-7f2-2	GATGNGGTATGACCCTAA
HH-Adaptor_mir29b2-1	CGGTACCCGGTACCGTCGGGAGACCTAGCCTCTTCTG
HH-29b2-1_rev	ACAAAAATCTAAGCCACCATG
HH-29b2-2_for	CGGTACCCGGTACCGTCTGTATCTAGCACCATTTG
HH-29b2-2_rev	ACTCCTAAAACACTGATTTC
HH-29b2-2_for_end	AATCCATGGGATACACTGATGAGTCCGTGAGGACG
Splint-29b2-1	GATACAAAGANTGGAAAAAT
Splint-29b2-2	AAGANTGGAAAAATCTAAG
HH-Adaptor_mir1-2-1	CGGTACCCGGTACCGTCGGGAGACCTAGCCTACCTAC
HH-1-2-1_rev	ACTCATATGGGTACATAAAG
HH-1-2-2_for	CGGTACCCGGTACCGTCATGCTATGGAATGTAAAG
HH-1-2-2_rev	ACGCCTACCAAAAATACATAC
HH1-2-2_for_end	AATCCATGGTAGCATCTGATGAGTCCGTGAGGACG
RNA binder cloning	
YTHDC1_BamHI_TEV_F	ATAGGATCCGAAAACCTGTATTTTCAGGGAATGGCGGCTGACAGTCGGGAGG
YTHDC1_SalI_R	AAAGTCGAC TTATCTTCTATATCGACCTCTCTCC
YTHDC1_BamHI393TEV_F	ATAGGATCCGAAAACCTGTATTTTCAGGGA TCTGCAAGGAGTGTTATCTTAA
METTL17_EcoRI_TEV_F	ATAGAATTCGAAAACCTGTATTTTCAGGGAGGCGGCGCGGCGGCACTGAAGTGTC
METTL17_SalI_R	AAAGTCGAC TCAACTCTCAGAGGGATCCTGAGCC
DIMT1_BamHI_TEV_F	ATAGGATCCGAAAACCTGTATTTTCAGGGAGGCGGCCCGAAGGTCAAGTCGGGG
DIMT1_SalI_R	AAA GTCGAC CTAGGAAAAATGAATACCTTCTGCG
TFB1M_BamHI_TEV_F	ATAGGATCCGAAAACCTGTATTTTCAGGGAGGCGGCGCTGCCTCCGGAAAACTCAGC
TFB1M_SalI_R	AAA GTCGAC CTAGAGTCTGTAATTCTCTGCG
TOMM22_BamHI_TEV_F	ATAGGATCCGAAAACCTGTATTTTCAGGGAGGCGGCGCTGCCGCCGTCGCTGCT
TOMM22_SalI_R	AAAGTCGACCTAGATCTTTCCAGGAAGTGAGG
YTHDF1_BamHI_TEV_f	ATAGGATCCGAAAACCTGTATTTTCAGGGA TCGGCCACCAGCGTGGACAC
YTHDF1_BamHI_365_TEV_f	ATAGGATCCGAAAACCTGTATTTTCAGGGA AGCGTCGAATCCCACCCCGTC
YTHDF1und2_SalI_rev	AAAGTCGACTCATTGTTTGTTTCGACTCTGCCGTTC
YTHDF2_BamHI_TEV_f	ATAGGATCCGAAAACCTGTATTTTCAGGGA TCGGCCAGCAGCCTCTTGGAGC
YTHDF2_BamHI_383_TEV_f	ATAGGATCCGAAAACCTGTATTTTCAGGGA TCAGAACCCCACCCAGTGTTGGAG
YTHDF3_BamHI_TEV_f	ATAGGATCCGAAAACCTGTATTTTCAGGGATCAGCCACTAGCGTGGATC
YTHDF3_BamHI_388_TEV_for	ATAGGATCCGAAAACCTGTATTTTCAGGGAAGTGTAGAAGTGCATCCCGTG
YTHDF3_SalI_rev	AAAGTCGACTTATTGTTTGTTTCTATTTCTCTCCCT
VP5_METTL17_F	CGATGCTAGCATGGCGGCGGCACTGAAGTG
VP5_METTL17_R	CGATGAATTCTCAACTCTCAGAGGGATCCTG
VP5_DIMT1_F	CGATGCTAGCATGCCGAAGGTCAAGTCGG
VP5_DIMT1_R	CGATGCGGCCGCCTAGGAAAAATGAATACCTTCTGC
VP5_TFB1M_F	CGATGCTAGCATGGCTGCCTCCGGAAAACT
VP5_TFB1M_R	CGATGAATTCCTAGAGTCTGTAATTCTCTGCG
VP5_TOMM22_F	CGATGCTAGCATGGCTGCCGCCGTCGCTGC
VP5_TOMM22_R	CGATGAATTCCTAGATCTTTCCAGGAAGTGAG
Northern blot probes	
5,8S rRNA probe2	GACGCTCAGACAGGCGTAGCCC
18S rRNA probe1	CATGCATGGCTTAATCTTTGAGACAAGC
18S rRNA probe2	CTAAACCATCCAATCGGTAGTAGCGAC
28S rRNA probe1	GGTTAGTTTCTTTTCCTCCGCTGAC

28S rRNA probe2	GGCTGACTTTCAATAGATCGCAGCG
7SK	ACTCGTATACCCTTGACCGAAGA
U6 snRNA	GAATTTGCGTGTCATCCTTGCGCAGGGGCCATGCTAA
U2 snRNA	GAGGTACTGCAATACCAGGTCGATGCGTGG
qPCR primer	
NDUFB7_qPCR_FW	CCTCATCCGGCTGCTCAAGT
NDUFB7_qPCR_REV	GCAGTAGTCCCAGTCGTGC
SZRD1_qPCR_FW	CTCCTGACCAGCAGATACGTT
SZRD1_qPCR_REV	GAGCCTGTGAGACTCAGCTTG
SCO1_qPCR_FW	CTATTGCCTGGGAACCCG
SCO1_qPCR_REV	CTTCCAGGAAACAGGCCC
RTN3_qPCR_FW	AAAGTGGGACTGAGAGGGAGT
RTN3_qPCR_REV	AAACCACTTTCCCAAATGGCG
RTN3_qPCR_FW2	GGTCACTCCCTCTGCCACTA
RTN3_qPCR_REV2	TCAGAACCGGTGTCCAGTGA
OSBPL8_qPCR_FW	ACTGATGAGCCACAGAACTTCA
OSBPL8_qPCR_REV	CTGACCAGTGGTAGTGCTTGA
UBR4_qPCR_FW	TGGCTGAGCAGATGCAAGAA
UBR4_qPCR_REV	TGGCATGTGCACTCCAAGAT
PCSK1_qPCR_FW	GGAGTGGAATCACACGGACA
PCSK1_qPCR_REV	GTCCCGTGTTTGTTCTCGTT
SYT12_qPCR_FW	GCAGTATCGGGTCCGTTTTT
SYT12_qPCR_REV	GGCTCTTGATGACGCTCAGAT
TET2_qPCR_FW	TCCCATCTTGCAGATGTGTAG
TET2_qPCR_REV	GTCCAAACCTTTCTTCCATGATT
SUGP2_qPCR_FW	TCCAGGAGCCAAAAGTCCAT
SUGP2_qPCR_REV	TATCGGTCAGCTTCTGCTGG
FIBIN_qPCR_FW	TCTCCTACGACCTAGACGGG
FIBIN_qPCR_REV	TTGGAGTAGGCATCCCCGAT
tRNA-Gly GCC-fw	TGCAGGTCTTTAGCTGACAGT
tRNA-Gly GCC-rev	GAGAAAAAGAATTGAAATGGATCGG
AC008870.1-fw	GCCATACTGACCTGTGCCAT
AC008870.1-rev	CCTTTTCAGTTCCTGGGGCT
RIMBP3B-fw	AAAGCCCTGCTCCAGGATTC
RIMBP3B-rev	TTGGGCATCTTGCTTTTGCC
AP000295.1-fw	CACACACGAGGCCTATGTCA
AP000295.1-rev	GCCAGCCAGAAATTGTGTGAG
NUTM2E-fw	CGTGCTTCCTCATCCCAGTT
NUTM2E-rev	ATCCGGTCAAAGTTGCTCGT
FP565260.2-fw	GTGTCTCGCCACCTGGAAT
FP565260.2-rev	GTGCACCAGGATCAGTTTCG
AC011511.4-fw	CTTCGACTACCCCTCGGACA
AC011511.4-rev	GTGGGCGAGCCTGAATAGAA
HNRNPH2-fw	CAAGTGGGGGGTGCTTACGAT

HNRNPH2-rev	TAAGCCCATCCCTCCCATCA
CSPG4P11-fw	CCTCCTCCAGGCAAGAATCTG
CSPG4P11-rev	TTCGGGTTGGGACATGGAGA
ATP5MPL-fw	GAACTCGCGGGTCAGACATT
ATP5MPL-rev	TCTTTTATCAGCAGCCCGGA
PTBP1-fw	CTGCGCATCGACTTTTCCAA
PTBP1-rev	TGCATACGGAGAGGCTGAGA
SNORA70-fw	CGCAGCCAATTAAGCCGAC
SNORA70-rev	AGGTCCCTTAGAGCAACCCA
AC010733.2-fw	TAGAATTGGTGATCCAGGCCG
AC010733.2-rev	GCAGGCTGGGTATTACCTGA
SNORD10-fw	ATGCGTGTCATCTGAGCCTCT
SNORD10-rev	AACAGCCCTGGGAAGTAGGAC
RNU12-fw	ATAACGATTCGGGGTGACGC
RNU12-rev	ACCTTGAGGGCGACCTTTAC
BIVM-ERCC5-fw	CTTTCTGCACAAGTGCCTCA
BIVM-ERCC5-rev	GAGCGGGATGGATTTGGAGT
SNORA40-fw	CGTGGACAAAGACTTACAGATAGG
SNORA40-rev	ACTGAACAATGAGTTCTGGGTTG
TMEM189-UBE2V1-fw	GCATGTCATCCTGCCACGTA
TMEM189-UBE2V1-rev	ACCCCAGCTAACTGTGCCAT
BLOC1S5-TXNDC5-fw	GATAACAGCAGCATCTCGACC
BLOC1S5-TXNDC5-rev	CTGTAACATTGAAGGAAAGACCAG
HIST1H4J-fw	CGCTAAGCGCCACCGTAAAG
ALY2 fw	ATGCGATGTGGCAAAACGAC
ALY2 rev	CTCGATAGACGAGCCACCAC
ALY3 fw	CCATAAACAAGCTTGCCCGC
ALY3 rev	CTGTGGTTCCGACTTCCACT
ALY4 fw	GGCTGAAGAGGACGGTTGTT
ALY4 rev	GCGACTGACAGTAGGAGCTG
MOS11 fw	TGGTATTGGATCGACGGCTG
MOS11 rev	CGCTTCTCCTCTTCGGTCAA
U2AF65 fw	GCGGAAAGTTTGGTGCTTTGA
U2AF65 rev	CGAGCCATCTGTATCGGCAT
Firefly fw	TCGAAAGAAGTCGGGGAAGC
Firefly rev	CGGTTTATCATCCCCCTCGG
Renilla fw	TGATAACTGGTCCGCAGTGG
Renilla rev	TAAGAAGAGGCCGCGTTACC
GFP fw	TCGTGACCACCCTGACCTA
GFP rev	TCTTGTAGTTGCCGTCGTCC

Table 10: RNA oligonucleotides

Primer name	Sequence (5' to 3')

Hairpin project

Let7f-2 scaffold-m6A	UACC m6A CAUCU UGGAGAUAAC UAUACAGUCU ACUGUCUUUC CCACG
Let7f-2 scaffold-m1A	UACC m1A CAUCU UGGAGAUAAC UAUACAGUCU ACUGUCUUUC CCACG
Let7f-2 scaffold-m62A	UACC m62A CAUCU UGGAGAUAAC UAUACAGUCU ACUGUCUUUC CCACG
Mir-29-b2 scaffold –m6A	UCCA m6A UCUUU GUAUCUAGCA CCAUUUGAAA UCAGUGUUUU AGGA
Mir-29-b2 scaffold –m1A	UCCA m1A UCUUU GUAUCUAGCA CCAUUUGAAA UCAGUGUUUU AGGA
Mir-29-b2 scaffold –m62A	UCCA m62A UCUUU GUAUCUAGCA CCAUUUGAAA UCAGUGUUUU AGGA
mir7f2-nonmod	ACCNCAUCUUGGAGAUAACUAUACAGUCUACUGUCUUUCC
mir1-2-nonmod	ACAUNACAAUGCUAUGGAAUGUAAAGAAGUAUGUAUUUUU
mir29b2-nonmod	CCANUCUUUGUAUCUAGCACCAUUUGAAAUCAGUGUUUUA

Antibody project

ELISA-biotin-RNA-m1A	NN(m1A) NNN (m1A)NN N -Biotin
ELISA-biotin-RNA-A	NNA NNN ANN N -Biotin -
ELISA-biotin-RNA-C	NNC NNN CNN N -Biotin
ELISA-biotin-RNA-dU	NN(2-Deoxyuridine) NNN (2-Deoxyuridine)NN N -Biotin
ELISA-biotin-RNA-T	NNT NNN TNN N- Biotin
PseudoU-RNA-oligo	AGCCUACCΨACUCAG
random m26A-RNA-oligo	NNNNNm26ANNN
random ctrl-RNA-oligo	NNNNNNNNN
m5C-RNA-oligo	ACGCGUAm5CUUGA
m6A-RNA-oligo	ACGCGUm6ACUUGA
control-RNA-oligo	ACGCGUACUUGA
m1G-RNA-oligo	ACGCm1GUACUUGA

Table 11: Vectors

Plasmid	Resistance	Tag
pcDNA5	Amp	none
pCS2-Myc6-FA	Amp	Myc
pSuperior	Amp	none
VP5	Amp	Flag/HA
pET	Amp	His
pGex	Amp	GST

4.1.4 Technical equipment

Table 12: Equipment

Equipment	Supplying company
MyiQ SingleColor Real-Time PCR Detection System	Bio-Rad (Hercules, USA)
UV Stratalinker 2400	Stratagene (Santa Clara, USA)
Odyssey Infrared Imaging System	LI-COR Biosciences (Lincoln, USA)

Personal Molecular Imager (Phosphor-imager)	Bio-Rad (Hercules, USA)
Agilent 4200 TapeStation System	Agilent Technologies (Waldbronn, Germany)
Confocal laser scanning microscopy platform Leica TCS SP8	Leica Microsystems (Wetzlar, Germany)
MaXis Mass Spectrometer	Bruker Corporation (Billerica, USA)

4.1.5 Biological Material

Table 13: Cell lines

Cell line	Specification
HEK 293T	human embryonic kidney cell line
HeLa	human cervical epithelial adenocarcinoma cell line
HeLa suspension	human cervical epithelial adenocarcinoma cell line
Mcf7	human metastatic breast adenocarcinoma cell line
NTera2	human metastatic embryonal carcinoma cell line
HepG2	human hepatocellular carcinoma cell line
C643	human thyroidea carcinoma cell line

Table 14: Bacterial Strains

Bacterial strain	Genotype
Escherichia coli XL 1 blue	F- recA1, endA1, gyrA96, thi-1, hsdR17, supE44, relA1, lac F'[proAB lacI qZΔM15 Tn10 (Tet^R)]
Escherichia coli BL21	F- dcm+ Hte ompT hsdS(rB- mB-) gal endA Hte
Rosetta	F- ompT hsdS$_B$(r$_B^-$ m$_B^-$) gal dcm (DE3) pRARE (Cam^R)

4.2 Methods

4.2.1 Preparation of DNA constructs

4.2.1.1 PCR and Cloning

For the cloning attempts, different variations (e.g. classical PCR, two-step PCR and colony PCR) of the Polymerase Chain reaction (PCR) were pursued. During this reaction the gene of interest is amplified. The applied DNA-oligonucleotide primers were designed to anneal to the flanking regions of the gene of interest. The DNA-polymerase extends the DNA oligonucleotide through the addition of dNTPs. Thus, the DNA fragment is amplified exponentially. The following steps were performed in a thermo-cycler: 30sec at 98°C; for 20 – 35 cycles: 10 sec at 98°C, 0 – 1 min at 55 – 65°C, 30 sec/kb at 72°C; then 10 min at 72°C. The pipetting scheme was as follows: 1 µg cDNA (HEK 293T or HeLa) or gDNA or cells from a colony, 10 µl 10xBuffer HF/GC, 2.5 µl Primer F (10µM), 2.5 µl Primer R (10µM), 2.5 µl dNTPs (10 mM each), up to 5 µl DMSO (optional), 1 µl DNA Polymerase (Phusion) (2 U/µl), fill up to 50 µl with water. After amplifying, the PCR products were analysed on 0.5 – 2 % agarose gels. The fragment of interest was then isolated from the gel using the "PCR clean-up kit" from Macherey & Nagel according to the manufacture's protocol. The purified PCR products, as well as the vector were then used for a restriction reaction. After a 2-4 hour incubation at 37°C and kit clean-up, the digested vector and insert were ligated for 1 h at RT: 1.5 µl T4 ligase, 1.5 µl T4 ligase buffer, 350 – 450 ng vector, 1 – 1.8 µg insert, fill up to 15 µl with water. After this, the product was transformed into competent *E. coli* cells, using 15 µl ligase reaction and 50 µl competent *E. coli* cell suspension. The sample was incubated at 42°C for 1 minute then at 4°C for 1 minute. After plating the cell suspension on a LB-Amp-plate, it was incubated overnight at 37°C. Several colonies were then picked, inoculating 5 ml of liquid LB-Amp media. The test tubes were incubated overnight at 37°C under agitation. 1.5 ml of each clone was subjected to a boiling lysate test. For that, the cell pellet was resuspended in 40 µl of Easy Prep buffer (10 mM Tris/HCl, pH 8, 1 mM EDTA, pH 8, 15 % sucrose, 2 mg/ml lysozyme, 0.2 mg/ml RNaseA and 0.1 mg/ml BSA) and incubated for 1 min at 99°C, then 1 min at 4°C and finally spun down for 15 min at full speed in a table centrifuge. 10 µl of the supernatant was used for a test digest with the restriction enzymes used for cloning for approx. 1 hour at 37°C. The product of this reaction was then separated on an agarose gel. The band pattern should now show the vector and the insert with the correct size. If so, the tested clone is considered potentially positive. Using 3 ml of the inoculated LB-Amp media, the DNA was purified using the "NucleoSpin Plasmid mini-prep kit" of Macherey-Nagel. The resulting product was then sequenced with the help of the sequencing service "Macrogen" to check if the sequence is correct without any

undesired mutations. To yield higher amounts of DNA and for subsequent experiments, 100 ml of LB-Amp media were inoculated with the positive clone and a "Midi Prep" (NucleoBond® Xtra Midi, Macherey-Nagel) was performed according to the manufacturer's protocol.

4.2.1.2 Agarose Gel Electrophoresis

The agarose gel electrophoresis is a method to separate a mix of nucleic acids. Generally, 0.5 – 2 % agarose gels were prepared. Therefore, the appropriate amount of agarose is dissolved in 1 x TBE (10 x TBE: 890 mM Tris, 890 mM boric acid and 20 mM EDTA) via heating. The hot agarose is poured into an already prepared and sealed agarose chamber. In addition, approx. 1 µl of ethidium bromide is dissolved in the solution to make the nucleic acids visible. A specific DNA band of interest can then be cut out of the gel. The DNA is then purified via a gel purification kit of Macherey-Nagel and can be used for further analysis.

4.2.2 Working with RNA

4.2.2.1 RNA Isolation

HEK 293T or HeLa cells from a confluent 15 cm plate were harvested and spun down at 500 x g for 5 minutes. One approach was to use the RNA Midi kit by Macherey & Nagel following the manufacturer's protocol (NucleoSpin® RNA Midi). The other way, applied, was to use TRIzol™ (Invitrogen) for RNA preparation. 1 ml TRIzol and 200 µl chloroform were added to the cell pellet and then the mixture was vortexed thoroughly for 15 seconds. The sample was centrifuged at 4 °C at 12.000 x g for 15 minutes. Subsequently, another chloroform step was executed or the RNA was directly precipitated using 600 µl isopropanol and 1 µl glycogen. This mixture was then either incubated for 1 hour at -80 °C or several hours at -20 °C. The sample was centrifuged for 30-60 min at 4 °C at full speed. The pellet was washed twice with 75% ethanol and resuspended in RNase-free water. The concentration was measured using the NanoDrop (Thermo Fisher).

4.2.2.2 RNA-Immunoprecipitation

Total RNA from HEK293T cells was isolated like it was described in the previous chapter. Several optimisation tests have been conducted for the RNA-immunoprecipitations. Thus, wide ranges of RNA, antibody and buffer concentrations and amounts were used and are given in this protocol. Two different protocol setups for the RNA-immunoprecipitations were tested for the antibodies. For a part of the experiments, 0.1 – 100 µg of the respective antibody was coupled over night at 4 °C to 15 – 40 µl Protein G Sepharose beads (GE Healthcare) or Dynabeads™ Protein G (Invitrogen). The coupled beads were washed thrice in RNA-IP buffer

(150 – 750 mM LiCl, 0.5 % NP-40, 10 mM Tris-HCl, pH 7.5) or NET buffer (50 mM Tris, pH 7.5, 150 mM NaCl, 5 mM EDTA, 0.5 % NP-40, 10 % glycerol). Using 0.1 - 100 µg of the total RNA or 0.5 – 1 nmol of the RNA-oligos, the immunoprecipitation was conducted for 2 hours in 0.5 - 1 ml RNA-IP buffer. For the other setup, the antibody was incubated with the RNA in RNA-IP buffer or NET buffer for 2 hours. Protein G Sepharose beads or Dynabeads™ Protein G were added and incubated for additional 2 hours. For the nucleoside-competition assay, 5 µM - 5 mM nucleoside (end concentration) was added and incubated for 1 additional hour. The setups were then washed once each with RNA-IP buffer, wash buffer I (RNA-IP buffer with 300 - 1000 mM LiCl) and II (RNA-IP buffer with 450 - 1500 mM LiCl) or NET buffer and twice with NET wash buffer (NET buffer with additional 150 mM NaCl). For isolation of the RNA from the beads, 500 µl TRIzol® was used and the RNA was precipitated afterwards.

4.2.2.3 Fragmentation of RNA

The fragmentation was conducted following the protocol of Dominissini and colleagues[342]. 180 µg total RNA was incubated with 10x fragmentation buffer for 5 min at 94 °C. 2 µl EDTA was added immediately and the samples were put on ice. After precipitation with 0.1 x NaAc and 2.5 x EtOH at 20 °C over night, the RNA samples were used for RIP.

4.2.2.4 CMC-treatment of RNA

CMC (*N*-Cyclohexyl-*N*′-(2-morpholinoethyl)carbodiimid-methyl-*p*-toluolsulfonat) treatment of RNA can be used to block Pseudouridine sites[273]. Total RNA was denatured in 5 mM EDTA for 2 min at 80 °C followed by incubation with 30 µl BEU-buffer plus CMC (0.3 M CMC, 50 mM bicine, pH 8.3, 4 mM EDTA and 7 M urea) for 30 min at 40°C and afterwards precipitated. Using a basic buffer (50 mM sodium-carbonate, pH 10.4, 2 mM EDTA) for 2 h at 50 °C, the G- and U-sites of the RNA were reconstituted [57,273]. After another precipitation, the RNA was used. As mock samples, the samples were incubated with BEU-buffer without CMC.

4.2.2.5 cDNA Preparation

To perform a (quantitative) PCR, complementary DNA (cDNA) is needed. CDNA is reverse transcribed from RNA, using an RNA dependent DNA polymerase (Reverse Transcriptase). First, the genomic DNA (gDNA) has to be removed from the preparation: 1 – 5 µg extracted RNA, 1 µl 10x buffer with MgCl2, 1µl DNase I, filled up to 10 µl with water was incubated for 30 minutes at 37°C. After that, 1 µl 50 mM EDTA was added and the setup was denatured at 65°C for 10 minutes. For the Reverse Transcriptase reaction the following reagents were added to the 11 µl gDNA free RNA: 1 µl random hexamer primer (or oligo (dT)$_{18}$ primer), 4 µl 5x reaction

buffer, 2 μl 10 mM dNTP Mix and 2 μl Reverse Transcriptase. The mix was then transferred into a cycler and the following program was used: 5 min at 25°C, 60 min at 37°C, 5 min at 70°C.

4.2.2.6 Quantitative Polymerase Chain Reaction (qPCR)

The quantitative polymerase chain reaction is a type of PCR where the amplification of the targets can be observed in real time. The RNA of interest first had to be reversely transcribed into cDNA. The intercalating agent (SsoFast™ Eva Green, Bio-Rad or Takyon™ SYBR® Mastermix blue, Eurogentec) interacts with the double stranded DNA and is excited via a Laser. Triplicate measurements were performed. The relative quantification was carried out, using the method of Pfaffl (2001)[343]. 7.5 μl of the qPCR mix, 1 μl of a 10μM primer mix and 4.5 μl H$_2$O were mixed and 2 μl of the cDNA was added. The samples were then analysed on the qPCR machine MyiQ SingleColor Real-Time PCR Detection System (Bio-Rad).

4.2.2.7 Urea Polyacrylamide Gel Electrophoresis for RNA Analysis

For the analysis of RNAs, an urea polyacrylamide gel electrophoresis was performed. Thereby, an RNA mix is separated into the different species of RNA when an electric current is applied. Depending on the size of the RNA of interest, a 4 – 20 % urea polyacrylamide gel was used, the percentage indicating the degree of branching. The solutions used, were provided by Roth (Rothiphorese Sequencing Gel System) and include a Urea gel Concentrate and Diluent. Freshly added to the mix are APS and TEMED. When the gel is polymerised, it should be prerun at 400 V for 20 – 30 minutes using 1 x TBE. To avoid a smiling effect, a metal plate is clamped to the back of the gel to ensure a good heat distribution. Approximately 10 – 20 μg of the RNA sample is mixed with 10 – 15 μl RNA loading dye (formamide with bromophenol blue and xylene cyanol) and incubated for 5 minutes at 95°C. The pigments run depending on the percentage of the gel at the height corresponding to a certain length of RNA. Thus, the running time needed, can be estimated. The wells have to be cleaned with a syringe, directly before loading, since the urea is settling down in the wells. The gel runs at 400 V. After the run, the gel can be stained with ethidium bromide for 10 minutes.

4.2.2.8 Semi-dry Northern Blot with Urea Polyacrylamide Gels

The urea polyacrylamide gel were placed between two stacks of whatman papers and onto a membrane. The nylon membrane used here is specifically suitable for the blotting of nucleic acids (Hybond-N by GE Healthcare). The size of the membrane and the whatman papers should be the same as the gel's size. Everything was first dipped into ddH2O before assembling the "sandwich", avoiding air bubbles during assembly. The blot ran for 20-60 minutes (depending on the size of the RNA of interest) at 20 V (constant voltage used).The

RNA was then crosslinked to the membrane via the UV-Stratalinker at 254 nm with the AutoCrossLink function, when the RNA of interest is larger than 75 nucleotides. Small RNA was crosslinked using EDC (l-ethyl-3-(3-dimethylaminopropyl) carbodiimide), following Pall et al[344]. The membrane was then prehybridised in hybridisation solution (5 x SSC, 7 % SDS, 1 M Na_2HPO_4 pH 7.2 and 1 x Denhardt's solution; 50 x Denhardt's solution: 1 % albumin fraction V, 1 % polyvinylpyrrolidone K30, 1 % Ficoll 400; 20 x SSC: 3 M NaCl, 0.3 M Na citrate) and incubated for 1 hour at 50 °C in a rotating oven. Meanwhile, the probe was labelled using radioactive γ-^{32}P-ATP. For this, the following setup was prepared: 14μl H_2O, 1μl 20 μM Oligonucleotide, 2μl 10 x PNK buffer A, 1μl PNK (polynucleotide 5'hydroxyl-kinase) and 2 μl γ-^{32}P-ATP. The mixture was incubated at 37 °C for 30 – 60 minutes. To stop the labelling reaction, 30 μl 30 mM EDTA was added. Using a MicroSpin G-25 Column (Illustra, GE Healthcare), all the free γ-^{32}P-ATP was filtrated out of the sample. The probe was then added to the hybridisation solution in the hybridisation flask containing the membrane. After an incubation overnight, the membrane was washed using 30-50 ml of the washing solutions. The wash solution I (5 x SSC and 1 % SDS) was used twice, the wash solution II (1 x SSC and 1 % SDS) once. Subsequently, the membrane was wrapped in saran foil and exposed onto a Phosphoimager screen. The detection was done using the Phosphoimager.

4.2.2.9 Standard *in vitro* transcription

The reaction was prepared in various sample sizes, ranging from 50 μl to 10 ml. 10 μg PCR product/linear vector/other DNA fragment was used for a 200 μl *in vitro* transcription (ivt) reaction. 20 μl of 10 x ivt-buffer (10 mM DTT, 0.01% Triton-X-100, 2 mM Spermidine and 30 mM Tris-HCl, pH 8), 10 μl of NTP mix (0.2 M each), 5 μl of $MgCl_2$ (1 M), 0.2 μl of Pyrophosphatase (Thermo) and 20 μl of a T7-RNA polymerase (2 mg/ml, purified by Dr. Thomas and Dr. Nora Treiber in the lab) were added. The setup was filled up to 200 μl with H_2O. The ivt sample was incubated for 4 hrs at 37°C. Then, 1 μl DNase I (50 U/μl) was added, incubating for additional 15 min at 37°C. After that, the RNA was purified using Urea gels with acryl-amide concentrations depending on the RNA size. For that, the ivt setup was mixed equally with 2x RNA loading dye (formamide with bromophenol blue and xylene cyanol). The bands were then cut out at the right size using either UV-fluorescence from Ethidium Bromide staining or through UV shadowing at 254 nm which can be seen when using high amounts of RNA.

4.2.2.10 *In vitro* transcription with ^{32}P-labelled and modified NTPs, immune precipitation and digestion

RNA oligos with different lengths (880 bp, 100 bp and 50 bp) were *in vitro* transcribed in four different setups. For the first two reactions, modified NTPs of interest in different ratios (0.1%

to 50 %) of the total NTPs were used. In one transcription mix, additional ^{32}P-UTP was added, the other was non-radioactively transcribed. The second two control setups were transcribed using unmodified NTPs. For one of them, the radioactive sample, ^{32}P-ATP was used. The four different samples were then DNase-digested and purified using the MEGAclear™ Transcription Clean-Up Kit (Ambion). For the non-radioactive samples, the concentration was determined using a NanoDrop Photometer, for the radioactive samples, the cpm-values were determined using the Cerenkov setting at a Scintillation-counter. The different RNA-solutions were then mixed to obtain equal cpm-values as well as same amounts (1.25 µg – 8 µg) for the modified and unmodified samples. These setups were then used for immune precipitation (see chapter 4.2.2.2). The precipitated RNA was digested using Nuclease P1 over night at 37°C. The single nucleotides were afterwards analysed via 1D thin layer chromatography. This method was elaborated together with Prof. Dr. Mark Helm and his PhD students Kaouthar Slama and Jasmin Hertler from the Johannes-Gutenberg University in Mainz.

4.2.2.11 Thin layer chromatography (TLC)

The digestion with nuclease P1 and the TLC was conducted as described earlier (*e.g.* Grosjean, Keith and Droogmans, 2004). The digested RNA was spotted on a TLC-plate which ran in 66 % isobutyric acid and 1 % conc. ammonia for 3 – 4 hours. After drying, the signals were detected by exposure to a screen and scanning using a Phosphoimager (PMI, Bio-Rad).

4.2.2.12 Electro Mobility Shift Assay (EMSA)

For the EMSA, a native gel was prepared (6 %-gel: 12 ml 30 % acrylamide, 3 ml glycerol, 6 ml 10 x EMSA, 480 µl 10 % APS, 48 µl TEMED and 39 ml H_2O). As running buffer, 1 x EMSA buffer (45 mM Tris and 45 mM Borat) was used. The samples consisted of 1µl tRNA, a titration set of protein (usually from 0 to 500 ng) and 1 µl of the radioactively labelled RNA, filled up to 20 µl with gel-shift-buffer (GSB) buffer (1 x GSB: 100 mM MOPS, pH 7, 50 mM KCl, 5 mM $MgCl_2$, 5 - 10 % glycerol, 0 - 30 µg/ml heparin and 1 mM DTT). The samples were incubated on ice for 15 min. The gel ran approximately 1 - 2 h at 260 V in the cold room.

4.2.2.13 Dot blot

8 µg of RNA-oligo were spotted on a nylon membrane. The RNA was EDC (1-ethyl-3-(3-dimethylaminopropyl) carbodiimide hydrochloride) cross-linked to the membrane. When using BSA-nucleoside conjugates, 20 µg was spotted and the membrane was baked at 80°C for 1 h to crosslink. In both cases, the membrane was blocked in 1x TBS-T (150 mM NaCl, 10 mM Tris, pH 8.0, 0.1 % Tween) containing 5 % skimmed milk powder for 1 h at 4°C. The first antibody (hybridoma) was diluted 1:5 in a 5 % skimmed milk solution in TBS-T and incubated

over night at 4°C, shaking. The secondary antibody (α-mouse or α-rat [Licor]) was diluted 1:10,000 in TBS-T and incubated for 1 hour. The documentation was conducted using the Odyssey scanner system (LI-COR Biosciences).

4.2.2.14 Ligation of RNA fragments for the pulldown

Before the ligation, the 5'-end of the *in vitro* transcribed 5'-fragments had to be dephosphorylated, since they are synthesized with a triple-phosphate by the T7-polymerase. This was done, using FastAP (Thermo Fisher Scientific) and the appropriate buffer. The 3'-fragments, which were purchased by Axolabs had to be phosphorylated, since they are sent without 3'-phosphorylation. Here, PNK (Thermo Fisher Scientific), the PNK-buffer and 10 mM ATP (Thermo) were used. Both reactions were conducted at 37 °C for 1 h. After this preparation, the RNA was isolated and precipitated using P/C/I-solution (Roth). For the ligation, 40 µg of the 5' fragment and 10µg of the 3' fragment, 1 x Circligation buffer (10x: 0.5 M MOPS, pH 7.5, 0.1 M KCl, 50 mM MgCl$_2$, 10 mM DTT), 50 µM ATP (Thermo), 20 % PEG6000 (Thermo) and 1.5 µl/20 µl Circligase (purified in the lab, plasmid kindly provided by Dr. Jan Medenbach) were mixed and incubated for 3 hrs at 50 °C for the let7f2-hairpin and 5 hrs at 40 °C for the mir29b2 hairpin. These temperatures and times were found to be the best in several optimisation experiments. The ligated products were then purified over an urea-gel using UV-shadowing and subsequently used for pulldown experiments (see 4.2.4.4).

4.2.2.15 Digestion of poly-A RNA and subsequent HPLC analysis of nucleosides

After poly-A purification of total RNA, using oligo dT magnetic beads (NEB, following the manufacturer's protocol), the RNA was digested into single nucleosides using an enzyme mix, consisting of Benzonase and Phosphodiesterase I for 3 to 4 hours at 37°C. The nucleosides were resolved on a Hypercarb-column (5 µm, 100 x 2.1; Thermo Scientific) using the HPLC-system "WellChrom" from Knauer, equipped with Pump K-1001, Diode Array Detector K-2800, column oven and a Vacuum Degasser from Techlab GmbH (Germany).The experiments were done, detecting at wavelengths ranging from 260 to 280 nm. The resulting chromatograms were analysed with the software ChromGate Client/Server Vers. 3.1.7. Gradients, using the buffers A (50 mM NH$_4$CH$_3$CO$_2$, pH 5.0), B (20% 50 mM NH$_4$CH$_3$CO$_2$, pH 5.0 / 80% acetonitrile) and C (50% acetonitrile) were applied at different temperatures (25°C, 55°C) and flow rates (0.2 ml/min, 0.25 ml/min), see Table 15 for details. For quantifying the percentage changes of the nucleoside concentrations between different samples, an equimolar amount of an internal standard (unmodified nucleoside) was added to the solution of the modified nucleoside. The peak area of the modified nucleoside was then normalized to the internal standard to correct

for loading errors and/or unspecific binding during processing. The HPLC analysis was performed by Robert Hett in the lab.

Table 15: HPLC gradient protocols for analysis of nucleosides

Time (min)	Flow (ml/min)	Buffer A (%)	Buffer B (%)	Buffer C (%)
Gradient 1 (for purine analysis)				
0	0.25	100	0	0
2	0.25	100	0	0
2.1	0.25	65	35	0
7	0.25	65	35	0
22	0.25	0	100	0
52	0.25	0	100	0
Gradient 2 (for pyrimidine analysis)				
0	0.2	100	0	0
2	0.2	100	0	0
30	0.2	65	35	0
35	0.2	65	35	0
35.1	0.2	100	0	0
45	0.2	100	0	0
Gradient 3 (for Ψ analysis)				
0	0.2	100	0	0
2	0.2	100	0	0
30	0.2	44	0	56
35	0.2	44	0	56
35.1	0.2	0	100	0
55	0.2	0	100	0

4.2.2.16 Quality measurement of RNAs using the TAPE Station System

The quality of RNAs with the Agilent 4200 TapeStation System (Agilent Technologies, Waldbronn) was determined according to the protocol *Agilent High Sensitivity RNA ScreenTape System Guide*. 2 μl of RNA (concentration between 0.5 and 10 ng/μl) or HS RNA ladder were mixed with 1 μl HS RNA Sample buffer, vortexed for 1 min, heated to 72°C for 3 min and directly put on ice for 2 min. After centrifugation, the samples were loaded into the TapeStation instrument and measured using the High Sensitivity RNA ScreenTape.

4.2.3 Antibody-related methods

4.2.3.1 Coupling of the nucleosides to ovalbumin

The coupling protocol of nucleosides to ovalbumin (OVA) and bovine serum albumin (BSA) was conducted similar as described before (Erlanger & Beiser, 1964). 25 mg of the nucleoside were dissolved in 1.25 ml 0.1 M $NaIO_4$ and incubated for 20 minutes at room temperature. 75 µl 1 M ethylene glycol were added and incubated for 5 minutes at room temperature. 50 mg of OVA/BSA were dissolved in 5 ml H_2O. The pH was set to 9 using a 5 % K_2CO_3 solution. After adding the oxidized nucleoside to the ovalbumin solution, the setup was stirred for 45 minutes, whereby the pH had to be kept at 9. A freshly prepared reduction solution (75 mg $NaBH_4$ in 5 ml H_2O) was then added to the conjugate and incubated overnight at room temperature. Using 1 M formic acid, the pH was set to 5 – 6 and incubated for another hour at room temperature. The pH was then set to 8.5 using 1 M NH_3. The setup was gel filtrated on a Superose 12 column (GE Healthcare) in 0.2 M ammonium formate, pH 8.5 (see Figure 9) For analysis, the absorption of a defined amount of the conjugate was measured via UV spectroscopy. The molar ratio of bound nucleoside per carrier protein was estimated by measuring the absorbance of the conjugate at 5 different wavelengths (250 nm, 260 nm, 270 nm, 280 nm and 290 nm) and fitting the measured data to the corresponding calculated absorption values. The spectrum of the conjugate was hereby assumed to be the sum of nucleoside and carrier protein spectra, so that the absorbance could be easily calculated by the extinction coefficients at the different wavelengths and the composition of the constituents. To find the "best fit"-composition of nucleoside and carrier protein, a grid search with a resolution of 0.1 µg was conducted using the sum-of-squares of the differences between measured and calculated absorption values as fit indicator. The reaction setup as well as the analysis was conducted by Robert Hett.

4.2.3.2 Immunization and hybridoma cell culture

Immunization, the work with hybridoma cells and ELISA screening was performed in the laboratory of Dr. Regina Feederle, our collaboration partner in Helmholtz Center in Munich. Approximately 50 µg of modified nucleobases coupled to ovalbumin (OVA) were dissolved in PBS, emulsified in an equal volume of incomplete Freund's adjuvant (Sigma) supplemented with 5 nmol CpG oligonucleotides (TIB Molbiol, Berlin), and injected both intraperitoneally (i.p.) and subcutaneously (s.c.) into Wistar rats (OVA-m^{6}A) and C57BL/6N mice (OVA-m^{5}C; Ova-Ψ). After 6 weeks, a boost with 50 µg of nucleobase-conjugated OVA without Freund's adjuvant was given 3 days before fusion. Fusion of the myeloma cell line P3X63-Ag8.653 with splenic B cells of immunized rat or mouse was performed according to standard

procedures[289]. P3X63-Ag8.653 cells were cultured at 37°C in a humidified 5 % CO_2 incubator in standard medium RPMI 1640 (Sigma/GIBCO), supplemented with 1% glutamine, 1 % non-essential amino acids, 1 % sodium pyruvate, 1 % penicillin/streptomycin (Sigma), and 2.5 % FCS (PAN). Hybridoma cells were cultured in standard medium supplemented with 20 % FCS and 2 % HT supplement (Life Technologies).

4.2.3.3 ELISA screening

Hybridoma supernatants were tested in a solid-phase enzyme-linked immunoassay (ELISA) using the corresponding modified nucleobase coupled to BSA and non-modified nucleobase also coupled to BSA as a negative control. To identify m^6A-specific candidate supernatants, 96-well polystyrene plates were coated with the m^6A-conjugated BSA overnight at room temperature (m^6A-BSA: 2.5 µg/ml). In parallel, 96-well plates were coated with m_2^6A and A (conc: 2.5 µg/ml). To identify m^5C-specific antibodies, screening plates were coated with m^5C (positive screen) and C (negative screen), for Ψ screening plates were coated with Ψ as well as C and U. For the other nucleosides, the coating was performed accordingly. After coating, the plates were washed once with PBS and unbound sites were blocked with 2 % FCS in PBS for 20 min. After washing off unbound nucleobase BSA-conjugates, hybridoma supernatants (1:10 diluted) were added and incubated for 30 min. After another wash with PBS, plates were incubated for 30 min with a mix of HRP-coupled subclass-specific mouse α-rat secondary antibodies or rat α-mouse secondary antibodies, depending on the organism, the antibody was generated in. After five washes with PBS, TMB substrate (1 Step Ultra TMB-ELISA; ThermoFisher Scientific Inc.) was added and the absorbance was measured at 650nm with a microplate reader (Tecan). To determine the subclass of all antibodies specific for the respective nucleoside, the BSA-nucleobase conjugates were coated onto 96-well polystyrene plates as described above, incubated with the hybridoma supernatants and then detected with HRP-linked antibodies specific for the different IgG subclasses of rat and mouse respectively. Selected hybridoma cells of supernatants, specific for the nucleoside were cloned at least twice by limiting dilution.

4.2.3.4 Determination of the K_D of the antibodies

For the determination of the antibody bound fraction (BF) of a modified nucleoside, 6 samples of an equimolar mixture of the modified nucleoside with an internal standard were prepared in 6 different concentrations. The concentrations ranged from 75 µM to 250 µM. In order to maintain a constant ratio between the amount of the modified nucleoside and the internal standard, the dilutions were prepared out of a premixed stock solution with a concentration of 0.5 mM for each nucleoside. A volume of 20 µl of each of these mixtures were pipetted to

100 µl PBS (= Input sample) and to 100 µl PBS containing exactly the same amount of antibody for each sample (∼ 150 µg) leading to initial nucleoside concentrations in the range of 12.5 µM to 41.7 µM. After incubation of the mixtures for 2 h at 4°C, the unbound nucleosides of the antibody-containing samples were separated by centrifugation (2 min., 14,000 g) using a 10 kDa cut-off spin filter (Roti-Spin MINI, Roth). A volume of 40 µl of each input and filtrate-sample was then applied to the HPLC with one replicate (see *HPLC analysis of nucleosides*).

The two peaks of each chromatogram were integrated. The peak area of the modified nucleoside normalized to the peak area of the internal standard eventually gave the normalized peak areas of the modified nucleoside in the input sample (nucleoside input, NI) and in the filtrate of the antibody sample (nucleoside-antibody, NA) at the various concentrations. The antibody-bound fraction (BF) of the modified nucleoside can then be calculated by: BF = (NI – NA)/NI, which can be used to derive the concentrations of bound ([AbN]) and free nucleoside ([N]) from the initial Nucleoside concentration ([N_0]): [AbN] = BF x [N_0] and [N] = (1 – BF) x [N_0]. To get a first estimation of the values for K_D and the maximal concentration of binding sites of the antibody ([B_{max}]), the ratio [AbN]/[N] was plotted against [AbN] to obtain a Scatchard plot[317,318]. From this, the K_D (dissociation constant) was estimated using the negative reciprocal value of the slope of the resulting regression line. The maximal concentration of binding sites is represented by the intersection point of the regression line with the x-axis. These estimates were then used to describe the binding with the following model: $[AbN] = \frac{[Bmax] \ast [N]}{K_D + [N]}$. To enhance the accuracy of the model-parameters, the measured data points were fitted with nonlinear regression, whereby the residual sum-of-squares between model and measured data points was minimized using Excel solver. Finally the 95%-confidence limits of the model parameters were determined via the model comparison-approach (F-test) as described by Motulsky and Christopoulos[345]. These measurements as well as the calculations were again performed by Robert Hett.

4.2.3.5 miCLIP analysis

The miCLIP experiments were executed largely following the protocol of Grozhik et al., 2017[334]. The fragmentation of the total RNA was performed with $ZnCl_2$ at 94°C for 5 min as it is described in Dominissini et al., 2013[342]. The fragmented total RNA was incubated with the antibody of interest for 2 h, rotating and afterwards UV-crosslinked, using 254 nm and 150 mJ/cm^{2}. Using protein G dynabeads (Invitrogen), the crosslinked RNA was precipitated for 2 h while rotating. After several washing steps, the RNA, attached to the antibody and beads was dephosphorylated and 5'-radiolabeled with γ-^{32}P-ATP. The beads were then resuspended in SDS-loading dye for elution. After SDS-PAGE, the gel was wet-blotted onto a nitrocellulose

membrane at 90 V for 90 min. The radioactive signals were then detected using a Phospho-imager (PMI, Bio-Rad).

4.2.4 Protein analysis

4.2.4.1 Protein immunoprecipitation

Cells transfected with plasmids encoding proteins of interest or untransfected cells were harvested and lysed using lysis buffer (25 mM Tris/HCl pH 7.4, 150 mM KCl, 0.5 % NP-40, 2 mM EDTA, 1 mM NaF, 0.5 mM DTT, 0.5 mM AEBSF). Of this filtrate, 1 % input was removed for western blot analysis. For the bead preparation, 30 µl protein G coupled Sepharose beads were washed twice in cold 1xPBS (140 mM NaCl, 2.7 mM KCl, 10 mM Na_2HPO_4 and 1.8 mM KH_2PO_4, pH 7.5). The antibody of interest was added to a final concentration of 5 µg antibody per 50 µl bead slurry, diluted in 500 µl 1xPBS per setup. This setup was incubated overnight at 4°C under agitation. The next day, the beads were washed three times with lysis buffer and left in the last washing buffer until the lysates were ready. 200 µl of washed beads were added to each setup and incubated at 4°C for 3 hrs under agitation. Using the completed Co-IP wash buffer (50 mM Tris/HCl pH7.4, 300 mM KCl, 1 mM $MgCl_2$, 1 % NP-40, 0.5 mM DTT, 0.5 mM AEBSF) , the beads were washed 4 times including a change of reaction tubes. Between the steps, the beads were centrifuged at 1000 x g for 1 min. To elute the proteins off the beads, the supernatant was taken off completely and 5x Lämmli buffer + β-mercaptoethanol was mixed to the beads and the input and IP samples were loaded onto a SDS-gel for subsequent western blot analysis. For northern blot analysis, TRIzol (Invitrogen) was added directly onto the beads to elute the RNA off the beads.

4.2.4.2 SDS Polyacrylamide Gel Electrophoresis

The samples were mixed with 5 x Lämmli buffer (300 mM Tris/HCl pH 6.8, 10 % SDS, 62.5 % glycerol, 0.05 % bromophenol blue, 10 % β-mercaptoethanol) and incubated at 95 °C for 5 min. For pouring the gel, first the separation gel (380 mM Tris/HCl pH 8.8, 6-15 % Acrylamide/Bis solution (37.5 : 1), 0.1 % SDS, 0.1 % TEMED, 0.05 % APS) and later the stacking gel (125 mM Tris-HCl pH 6.8, 5 % Acrylamide/Bis solution (37.5 : 1), 0.1 % SDS, 0.15 % TEMED, 0.05 % APS) were prepared. The gel ran at 180 to 200V in SDS Running buffer (25 mM Tris, 192 mM glycine, 1 % SDS). To evaluate the separated protein bands, western blot analysis, Coomassie or silver staining was performed.

4.2.4.3 Semi-dry Western Blot

The proteins from an SDS-gel were transferred directly onto a PVDF (polyvinylidenfluorid) membrane via semi-dry blotting. Three whatman papers and a nitrocellulose membrane of the exact same size as the gel were soaked with 1 x Towbin buffer (25 mM Tris, 192 mM glycine, 20 % methanol, pH 8.6) and placed onto the blotting surface. Then, the gel and another three whatman papers were soaked with Towbin buffer and put onto the membrane. The voltage must not exceed 25 V. The current in mA was determined by multiplying the size of the gel (in cm^2) by 2. The blot ran for 90 minutes. After blotting, the membrane was incubated in 5% milk (analytical milk powder in 1 x TBS-T (10 mM Tris, 150 mM NaCl, 0.05 % Tween, pH 8.0)) for an hour to block the unspecific protein binding sites. The primary antibody, diluted in 5% milk was incubated for an hour on the membrane. The membrane was then washed trice with TBS-T. The secondary antibody was then incubated for a further hour. After another three washing steps, the membrane was analysed using the Odyssey analyser by Licor.

4.2.4.4 Pulldown of RBPs using RNA hairpins

First, 50 µl Dyna beads Streptavidin M270 (Invitrogen/Thermo Fisher) per experiment were washed twice with pulldown buffer (50 mM Tris, pH 8, 150 mM NaCl, 5% Glycerine) using a magnetic rack. The beads were resuspended in 200 µl pulldown buffer and 4 µg of the RNA-Hook (2'O-biotinylated RNA fragment) were added. This setup was incubated for 2 hrs at 4°C, shaking. Subsequently, the beads were washed thrice with pulldown buffer. Half of the beads were taken for the preclear and stored until needed. 10 µg RNA-hairpin were added to the beads in 500 µl buffer and incubated overnight at 4°C, shaking. Since the ligation of the hairpin was not as productive, RNA had to be reused for saving purposes. Thus, the supernatant of the first coupling was used for two more rounds of fresh beads. 1 – 2 15 cm plates of the cells, in this case HEPG2, N-Tera2 and HEK293T cells, were sonified in pulldown buffer with additional 1 mM AEBSF and 1 mM DTT (completed pulldown buffer). The setting of the sonicator was 50 % duty cycle, output 4 with 2 x 20 pulses. After that, the cell suspension was centrifuged at 32,000 x g for 10 min at 4°C. From the lysate, a Bradford test should show around 5 – 10 mg/ml protein. The next step was the preclear, where the hook-coupled beads were incubated with the lysate for 4 hrs. Afterwards, the pulldown was conducted. The precleared lysate was incubated with the hook-RNA-coupled beads overnight at 4 °C, shaking. The last steps were the washing, first with completed pulldown buffer with additional 150 mM NaCl, then completed pulldown buffer with 0.1% Triton-X100 and lastly with completed pulldown buffer. The elution was done using NuPAGE LDS-sample buffer (Invitrogen). The analysis was carried out on NuPAGE Bis-Tris Gels (Invitrogen).

The protocol for the pulldown of RBPs using RNA hairpins was developed and optimised by Dr. Nora Treiber and Dr. Thomas Treiber[346,347]. For more background, see chapter 2.2.1.

4.2.4.5 Sample preparation for mass spectrometry analysis

The SDS gel was washed twice with pure H_2O, stained with p.a. Coomassie and destained with p.a. ethanol and acidic acid. Small pieces of the gel band of interest were cut out and transferred into 2 ml Eppendorf tubes and washed with 500 μl 50 mM NH_4HCO_3 for 15 - 30 min, shaking vigorously. The gel pieces were washed the same way with 50 mM NH_4HCO_3 : acetonitrile (3 : 1), then 10 mM NH_4HCO_3 : AN (3 : 1) and finally with 10 mM NH_4HCO_3 : acetonitrile (1 : 1), discarding the supernatant at every step. After removing the liquid completely, the samples were lyophilized for 1 h. The gel pieces were then covered with 100 μ of 1 mg/ml DTT in 100 mM NH_4HCO_3, pH 8 and incubated at 50°C for 1 h. After taking off the supernatant, free Cystein-Thiolgroups were alkylated using 200 μl of 5mg/ml Iodoacetic acid (IAA) in 50 mM NH_4HCO_3. The reaction was conducted for 35 min at RT in the dark. Subsequently, the gel samples were washed four times and lyophilized like it was done before. The next step was the Trypsin digestion. 5 g Trypsin powder (Sigma) was solved in 750 μl 1 mM HCl. Of that, 30 μl were mixed with 70 μl of 50 mM NH_4HCO_3 and the gel pieces were rehydrated using this solution and incubated at 37°C overnight. The Elution was conducted for 1 – 2 hrs at RT. It was eluted twice with 100 μl 100 mM NH_4HCO_3 and once with NH_4HCO_3 : acetonitrile (2 : 1). The samples were then lyophilized again and measured at the Mass spectrometer MaXis (Bruker) by Eduard Hochmuth at the chair of Dr. Astrid Bruckmann in Regensburg.

4.2.5 Cell culture work

The human cell lines used for this thesis are listed in Table 13.

4.2.5.1 Preparation of Whole Cell Lysates from Human Cell Lines

A plate of confluent cells were washed once with cold 1xPBS. Using a cell scraper, the cells were scraped off the plate and transferred into a reaction tube. To pellet the cells, they were centrifuged at 500 x g for 5 min at 4°C. The cell pellet was thoroughly resuspended in 1 ml of lysis buffer (25 mM Tris-HCl, pH 7.4, 150 mM KCl, 0.5 % NP-40, 2 mM EDTA, 1 mM NaF). After incubating for 20 minutes on ice, the sample was centrifuged at full speed for 20 minutes at 4°C. The supernatant was then subjected to immunoprecipitation experiments or directly loaded onto a SDS gel.

4.2.5.2 Cultivation and Passaging of Human Adherent Cell Lines

The adherent cell lines used for this thesis were cultivated at 37°C and 5 % CO_2. The growth media was DMEM (Dulbecco's modified eagle media) containing 10 % FBS (fetal bovine

serum) and 1 % Penicillin/Streptavidin. For splitting and passaging the cells, the old media was aspirated and the cells were washed cautiously with 1 x PBS. 1 - 2 ml of Trypsin were added in order to cleave cell-cell and cell-matrix contact proteins. Completed DMEM, was added to the trypsinated cells to stop the reaction. This cell suspension was then partially passaged into a new sterile plate.

4.2.5.3   Cultivation and Passaging of HeLa suspension cells

HeLa S3 suspension cells were cultivated in Joklik's medium (1.1 % Minimum Essential Medium Eagle (MEM) powder, 20 mM L-Glutamine, 1 % Penicillin/Streptavidin, 1 % Non-Essential Amino Acid Solution (NEAA), 24 mM $NaHCO_3$ and 10 % FBS) in various sizes of spinner flasks at 37°C and 5 % CO_2.

4.2.5.4   Transfection of HEK 293T Cells with Calcium Phosphate

To overexpress a protein, a vector containing the respective DNA has to enter the nucleus of the cell. To accomplish this, calcium phosphate precipitation transfection was used. For a 15 cm plate the following reagents were pipetted into a tube: 860 µl H_2O, 122 µl $CaCl_2$, 4-10 µg DNA, 1 ml 2 x HEPES buffer (115 mM NaCl, 1.2 mM $CaCl_2$, 1.2 mM $MgCl_2$, 1.2 $MgCl_2$, 2.4 mM K_2HPO_4, 20 mM HEPES, pH 7.4). The tube was mixed thoroughly after addition of each component. After a short incubation at room temperature, the solution was pipetted onto the adherent cells.

4.2.5.5   Transfection of HeLa Cells with Lipofectamine

For subsequent usage in immunofluorescence, transfection of HeLa cells was performed with lipofectamine to avoid $Ca_3(PO_4)_2$-precipitates. The transfection was done at a cell confluency of 70-90 % in DMEM-media without any antibiotics. Lipofectamine 2000 was used for the transfection of DNA. For a 6 well (2 cm diameter), two tubes each containing 250 µl OptiMem were prepared. In one, 1 µg of the DNA was added and in the other 5 µl of Lipofectamine 2000 were added. The samples were mixed and incubated for 5 minutes at room temperature. After pipetting the lipofectamine sample to the DNA sample, the setup was incubated for 20 min at room temperature and then pipetted onto the cells. To knock a gene down, siRNAs (small interfering RNAs) were used. The transfection reagent for the RNAi (RNA interference) was Lipofectamine RNAi Max. 50 µM siRNA and 5 µl Lipofectamine RNAiMax were added to 500 µl OptiMem. The following steps were the same as in DNA-transfection with Lipofectamine 2000.

4.2.5.6   Immunofluorescence

For localization of proteins in the cell, the proteins can be visualised using antibodies and a fluorescence microscope. The cells were split into 24-well plates using DMEM without antibiotics. The next day, the cells were transfected with Lipofectamine 2000. The following day, the cells were split onto cover-slips (12 mm), so that they had a confluence of about 50 % the next day. On the fourth day, the cells were washed with pre-warmed (37°C) PBS-A (0.2 g/l KCl, 0.2 g/l KH_2PO_4, 8 g/l NaCl, 2.2 g/l Na_2HPO_4 $7H_2O$, pH 7.4). The cells must not dry out and thus, the following solutions were aspirated and at the same time, the new solution was added. The cells were fixed to the cover-slips by adding pre-warmed fixation solution (37 g/l Paraformaldehyde in PBS-A) and incubating them for 10 min at 37°C. This fixation was stopped, using PBS-G (7.5 g/l glycine in PBS-A), which was incubated for 5 min. The cover-slips were then washed twice with PBS-A. After this step, the handling was done on the non-sterile bench. The cells were permeabilised with a 15-min incubation at room temperature with the permeabilisation buffer (0.2 % Triton X-100 in PBS). After three washing steps with the blocking solution (1 % BSA (Cohn fraction V), 0.05 % Triton-X-100 in PBS), the cells were blocked for 1 h at room temperature with blocking solution. The primary antibody was prepared in blocking solution and also incubated for 1 h on the cover slips. To save antibody, only 30 µl were prepared and the cover-slips were placed upside down onto a strip of parafilm with the drop of antibody solution. After four wash steps with blocking solution, incubation with the secondary antibody for 1 h followed (ALEXA antibodies, diluted 1:400 in blocking solution). The last washing steps with blocking solution and PBS-A (4 x) should wash out all the unbound antibodies. The cover-slips were then mounted with prolong gold containing DAPI onto microscopy slides. Simultaneously, DAPI stained the nuclei. The image acquisition was performed, using the confocal laser scanning microscopy platform Leica TCS SP8 equipped with acousto-optical beam splitter, 405 nm laser (for DAPI) and argon laser (488 nm for α-rat and α-rabbit Alexa 488(Invitrogen)). A multidimensional image with the wavelengths of the used secondary antibody-coupled fluorescent pigments was recorded. Signal intensity was quantified using ImageJ (Wayne Rasband, NIH).

A number of the methods and other content of this chapter are part of the manuscript *Generation and validation of monoclonal antibodies specific to modified nucleotides, Saller, F. et al.,* which was under revision for publication at the time of writing this thesis.

5. APPENDIX

5.1 References

1. Adler, M., Weissmann, B. & Gutman, A. B. Occurence of methylated purine bases in yeast ribonucleic acid. *J. Biol. Chem.* **230**, 717–723 (1957).

2. Littlefield, J. W. & Dunn, D. B. Natural occurrence of thymine and three methylated adenine bases in several ribonucleic acids. *Nature* **181**, 254–255 (1958).

3. Brown, G. M. & Attardi, G. Methylation of nucleic acids in HeLa Cells. *Biochem. biopysical Res. Commun.* **20**, 298–302 (1965).

4. Greenberg, H. & Penman, S. Methylation and Processing of Ribosomal RNA in HeLa Cells. *J.Mol.Biol.* **21**, 527–535 (1966).

5. Davis, F. F. & Allen, F. W. Ribonucleic Acids from yeast which contain a fifth nucleotide. *J. Biol. Chem.* **227**, 907–915 (1956).

6. Desrosiers, R., Friderici, K. & Rottman, F. Identification of Methylated Nucleosides in Messenger RNA from Novikoff Hepatoma Cells. *Proc. Natl. Acad. Sci.* **71**, 3971–3975 (1974).

7. Saletore, Y. *et al.* The birth of the Epitranscriptome : deciphering the function of RNA modifications. *Genome Biol.* **13**, 1–11 (2012).

8. Johnson, T. B. & Coghill, R. D. The discovery of 5-methyl-cytosine in tuberculinic acid, the nucleic acid of the tubercle bacillus. *J. Am. Chem. Soc.* **47**, 2838–2844 (1925).

9. Watson, J. D. & Crick, F. H. C. A structure for Desoxyribose Nucleic Acid. *Nature* **171**, 737–738 (1953).

10. Wilkins, M. H. F., Stokes, A. R. & Wilson, H. R. Molecular Structure of Deoxypentose Nucleic Acids. *Nature* **171**, 738–740 (1953).

11. Franklin, R. E. & Gosling, R. G. Molecular Configuration in Sodium Thymonucleate. *Nature* **171**, 740–741 (1953).

12. Caspersson, T. & Schultz, J. Pentose Nucleotides in the Cytoplasm of Growing Tissues. *Nature* **143**, 602–603 (1939).

13. Wyatt, G. R. Recognition and Estimation of 5-Methylcytosine in Nucleic Acids Eii. *Biochem. J.* **48**, 581–584 (1950).

14. Dunn, D. B. & Smith, J. D. Occurence of a new base in the deoxyribonucleic acid of a strain of Bacterium Coli. *Nature* **175**, 336–337 (1955).

15. Cohn, W. E. 5-Ribosyl uracil, a carbon-carbon ribofuranosyl nucleoside in ribonucleic acids. *Prelim. notes* **32**, 569–571 (1959).

16. Cohn, W. E. Pseudouridine, a Carbon-Carbon Linked Ribonucleoside in Ribonucleic Acids : Isolation, Structure and Chemical Characteristics. *J. Biol. Chem.* **235**, 1488–1498 (1960).

17. Littlefield, J. W. & Dunn, D. B. Natural occurence of thymine and three methylated adenine bases in several ribonucleic acids. *Nature* **181**, 254–255 (1958).

18. Dunn, D. B. Additional components in ribonucleic acid of rat-liver fractions. *Biochim Biophys Acta* **34**, 286–288 (1959).

19. Hurwitz, J., Gold, M. & Anders, M. The Enzymatic and Methylation of Ribonucleic Acid and Deoxyribonucleic Acid. *J. Biol. Chem.* **239**, 3462–3473 (1964).

20. Bergquist, P. L. & Matthews, R. E. F. Occurrence and Distribution of Methylated Purines in the Ribonucleic Acids of Subcellular Fractions. *Biochem. J.* **85**, 305–313 (1962).

21. Boccaletto, P. *et al.* MODOMICS : a database of RNA modification pathways . 2017 update. *Nucleic Acids Res.* **46**, 1–5 (2017).

22. Holley, R. W. *et al.* Structure of Ribonucleic Acid. *Science (80-.).* **147**, 1462–1465 (1965).

23. Holley, R. W., Everett, G. A., Madison, J. T. & Zamir, A. Nucleotide Sequences in the Yeast Alanine Transfer Ribonucleic Acid. *J. Biol. Chem.* **240**, 2122–2128 (1965).

24. Madison, J. T., Everett, G. A. & H., K. Nucleotide Sequence of a Yeast Tyrosine Transfer RNA. *Science (80-.).* **153**, 531–534 (1966).

25. RajBhandary, U. L. *et al.* The primary structure of yeast phenylalanine transfer RNA. *Proc. Natl. Acad. Sci.* **57**, 751–758

(1967).

26. Goodman, H. M., Abelson, J., Landy, A., Brenner, S. & Smith, J. D. Amber Suppression : a Nucleotide Change in the Anticodon of a Tyrosine Transfer RNA. *Nature* **217**, 1019–1024 (1968).

27. Dube, S. K., Marcker, K. A., Clark, B. F. C. & Cory, S. Nucleotide Sequence of N-Formyl-methionyl-transfer RNA. *Nature* **218**, 232–233 (1968).

28. Takemura, S., Murakami, M. & Miyazaki, M. The Primary Structure of Isoleucine Transfer Ribonucleic Acid from Torulopsis utilis. *J. Biochem.* **65**, 553–566 (1969).

29. Starr, J. L. & Fefferman, R. The Occurrence of Methylated Bases in Ribosomal Ribonucleic Acid of Escherichia coli K12 W-6. *J. Biol. Chem.* **239**, 3457–3461 (1964).

30. Penman, S., Smith, I. & Holtzman, E. Ribosomal RNA Synthesis and Processing in a Particulate Site in the HeLa Cell Nucleus. *Science (80-.).* **154**, 786–789 (1966).

31. Penman, S. RNA Metabolism in the HeLa Cell Nucleus. *J. Mol. Biol.* **17**, 117–130 (1966).

32. Iwanami, Y. & Brown, G. Methylated Bases of Ribosomal ribonucleic acid from HeLa Cells. *Arch. Biochem. Biophys.* **126**, 8–15 (1967).

33. Srinivasan, P. R. & Borek, E. The Methylation of nucleic acids. *Annu. Rev. Biochem.* **35**, 275–298 (1966).

34. Starr, J. L. & Sells, B. H. Methylated Ribonucleic Acids. *Physiol. Rev.* **49**, 623–667 (1969).

35. Perry, R. P. & Kelley, D. E. Existence of Methylated Messenger RNA in Mouse L Cells. *Cell* **I**, 37–42 (1974).

36. Dubin, D. T. & Taylor, R. H. The methylation state of poly A-containing- messenger RNA from cultured hamster cells. *Nucleic Acids Res.* **2**, 1653–1668 (1975).

37. Furuichi, Y. *et al.* Methylated, Blocked 5' Termini in HeLa Cell mRNA. *Proc. Natl. Acad. Sci. USA* **72**, 1904–1908 (1975).

38. Adams, J. M. & Cory, S. Modified nucleosides and bizarre 5 ' -termini in mouse myeloma mRNA. *Nature* **255**, 28–33 (1975).

39. Kane, S. E. & Beemon, K. Precise Localization of m6A in Rous Sarcoma Virus RNA Reveals Clustering of Methylation Sites : Implications for RNA Processing. *Mol. Cell. Biol.* **5**, 2298–2306 (1985).

40. Horowitz, S., Horowitz, A., Nilsen, T. W., Munns, T. W. & Rottman, F. M. Mapping of N6-methyladenosine residues in bovine prolactin mRNA. *Proc. Natl. Acad. Sci.* **81**, 5667–5671 (1984).

41. Schibler, U., Kelley, D. E. & Perry, R. P. Comparison of methylated sequences in messenger RNA and heterogeneous nuclear RNA from mouse L cells. *J. Mol. Biol.* **115**, 695–714 (1977).

42. Wei, C. & Moss, B. Nucleotide Sequences at the N6-Methyladenosine Sites of HeLa Cell Messenger Ribonucleic Acid. *Biochemistry* **16**, 1672–1676 (1977).

43. Nichols, J. L. & Welder, L. Nucleotides adjacent to N6-methyladenosine in maize poly(A)-containing RNA. *Plant Sci. Lett.* **21**, 75–81 (1981).

44. Selinger, D. W. *et al.* RNA expression analysis using a 30 base pair resolution Escherichia coli genome array. *Nat. Biotechnol.* **18**, 1262–1268 (2000).

45. Tjaden, B. *et al.* Transcriptome analysis of Escherichia coli using high-density oligonucleotide probe arrays. *Nucleic Acids Res.* **30**, 3732–3738 (2002).

46. Bertone, P. *et al.* Global Identification of Human Transcribed Sequences with Genome Tiling Arrays. *Science (80-.).* **306**, 2242–2246 (2004).

47. Mortazavi, A., Williams, B. A., Mccue, K., Schaeffer, L. & Wold, B. Mapping and quantifying mammalian transcriptomes by RNA-Seq. *Nat. Methods* **5**, 1–8 (2008).

48. Nagalakshmi, U. *et al.* The Transcriptional Landscape of the Yeast Genome Defined by RNA Sequencing. *Science (80-.).* **320**, 1344–1349 (2008).

49. Wilhelm, B. T. *et al.* Dynamic repertoire of a eukaryotic transcriptome surveyed at single-nucleotide resolution. *Nat. Lett.* **453**, 1239–1245 (2008).

50. Morin, R. D. *et al.* Profiling the HeLa S3 transcriptome using randomly primed cDNA and massively parallel short-read sequencing. *Biotechniques* **45**, 81–94 (2008).

51. Lister, R. *et al.* Highly Integrated Single-Base Resolution Maps of the Epigenome in Arabidopsis. *Cell* **133**, 523–536 (2008).

52. Dominissini, D. *et al.* Topology of the human and mouse m6A RNA methylomes revealed by m6A-seq. *Nature* **485**,

201–206 (2012).

53. Meyer, K. D. *et al.* Comprehensive analysis of mRNA methylation reveals enrichment in 3′ UTRs and near stop codons. *Cell* **149**, 1635–1646 (2012).

54. Squires, J. E. *et al.* Widespread occurrence of 5-methylcytosine in human coding and non-coding RNA. *Nucleic Acids Res.* **40**, 5023–5033 (2012).

55. Carlile, T. M. *et al.* Pseudouridine profiling reveals regulated mRNA pseudouridylation in yeast and human cells. *Nature* **515**, 143–146 (2014).

56. Edelheit, S., Schwartz, S., Mumbach, M. R., Wurtzel, O. & Sorek, R. Transcriptome-Wide Mapping of 5-methylcytidine RNA Modifications in Bacteria, Archaea, and Yeast Reveals m5C within Archaeal mRNAs. *PLoS Genet.* **9**, 1–14 (2013).

57. Schwartz, S. *et al.* Transcriptome-wide Mapping Reveals Widespread Dynamic-Regulated Pseudouridylation of ncRNA and mRNA. *Cell* **159**, 148–162 (2014).

58. Lovejoy, A. F., Riordan, D. P. & Brown, P. O. Transcriptome-Wide Mapping of Pseudouridines : Pseudouridine Synthases Modify Specific mRNAs in. *PLoS One* **9**, 1–15 (2014).

59. Machnicka, M. a. *et al.* http://modomics.genesilico.pl/. *MODOMICS: a database of RNA modification pathways. 2017 update* (2017).

60. Agris, P., Crain, P. F., Rozenski, J., Fabris, D. & Vendeix, F. A. P. http://mods.rna.albany.edu/home. *Supported by the SUNY Albany Research IT Group*

61. Motorin, Y. & Helm, M. RNA nucleotide methylation. *WIREs RNA* **2**, 611–631 (2011).

62. Motorin, Y. & Grosjean, H. Transfer RNA Modification. *Annu. Rev. Biochem.* **56**, 263–287 (2005).

63. Chen, Y., Sierzputowska-Gracz, H., Guenther, R., Everett, K. & Agris, P. F. 5-Methylcytidine is required for cooperative binding of Mg2+ and a conformational transition at the anticodon stem-loop of yeast phenylalanine tRNA. *Biochemistry* **32**, 10249–53 (1993).

64. Väre, V. Y. P., Eruysal, E. R., Narendran, A., Sarachan, K. L. & Agris, P. F. Chemical and Conformational Diversity of Modified Nucleosides Affects tRNA Structure and Function. *Biomolecules* **7**, 1–32 (2017).

65. Giegé, R. & Eriani, G. Transfer RNA Recognition and Aminoacylation by Synthetases. in *eLS* 1–18 (2014). doi:10.1002/9780470015902.a0000531.pub3

66. Muramatsu, T. & Nishikawatll, K. Codon and amino-acid specificities of a transfer RNA are both converted by a single post-transcriptional modification. *Nature* **336**, 179–181 (1988).

67. Perret, V. *et al.* Relaxation of a transfer RNA specificity by removal of modified nucleotides. *Nature* **344**, 787–789 (1990).

68. Favre, A. & Hajnsdorf, E. Photoregulation of E. Coli Growth and the near Ultraviolet Photochemistry of tRNA. in *Molecular Models of Photoresponsiveness* 75–92 (1983).

69. Manickam, N., Joshi, K., Bhatt, M. J. & Farabaugh, P. J. Effects of tRNA modification on translational accuracy depend on intrinsic codon – anticodon strength. *Nucleic Acids Res.* **44**, 1871–1881 (2016).

70. Kiesewetter, S., Ott, G. & Sprinzl, M. The role of modified purine 64 in initiator / elongator discrimination of tRNA et from yeast and wheat germ. *Nucleic Acids Res.* **18**, 4677–4682 (1990).

71. Pereira, M. *et al.* Impact of tRNA Modifications and tRNA-Modifying Enzymes on Proteostasis and Human Disease. *Int. J. Mol. Sci.* **19**, 1–18 (2018).

72. Bednarova, A., Hanna, M., Durham, I., Vancleave, T. & Bedná, A. Lost in Translation : Defects in Transfer RNA Modifications and Neurological Disorders. *Front. Mol. Neurosci.* **10**, 1–8 (2017).

73. Koh, C. S. & Sarin, L. P. Transfer RNA modification and infection – Implications for pathogenicity and host responses. *BBA - Gene Regul. Mech.* **1861**, 419–432 (2018).

74. Taoka, M. *et al.* Landscape of the complete RNA chemical modifications in the human 80S ribosome. *Nucleic Acids Res.* **46**, 9289–9298 (2018).

75. Sloan, K. E. *et al.* Tuning the ribosome : The influence of rRNA modification on eukaryotic ribosome biogenesis and function. *RNA Biol.* **14**, 1138–1152 (2017).

76. Birkedal, U. *et al.* Profiling of Ribose Methylations in RNA by High-Throughput Sequencing. *Angew. Chemie* **54**, 451–455 (2015).

77. Lestrade, L. & Weber, M. J. snoRNA-LBME-db , a comprehensive database of human H / ACA and C / D box snoRNAs.

Nucleic Acids Res. **34**, 158–162 (2006).

78. Piekna-przybylska, D., Decatur, W. A. & Fournier, M. J. The 3D rRNA modification maps database : with interactive tools for ribosome analysis. *Nucleic Acids Res.* **36**, 178–183 (2008).

79. Ma, H. *et al.* N6-Methyladenosine methyltransferase ZCCHC4 mediates ribosomal RNA methylation. *Nat. Chem. Biol.* **15**, 88–94 (2019).

80. Cantara, W. a. *et al.* The RNA modification database, RNAMDB: 2011 update. *Nucleic Acids Res.* **39**, 195–201 (2011).

81. Polikanov, Y. S., Melnikov, S. V, Söll, D. & Steitz, T. A. Structural insights into the role of rRNA modifications in protein synthesis and ribosome assembly. *Nat. Struct. Mol. Biol.* **22**, 342–345 (2015).

82. Höbartner, C. & Micura, R. Bistable Secondary Structures of Small RNAs and Their Structural Probing by Comparative Imino Proton NMR Spectroscopy. *JMB* **325**, 421–431 (2003).

83. Höbartner, C., Ebert, M., Jaun, B. & Micura, R. RNA Two-State Conformation Equilibria and the Effect of Nucleobase Methylation **. *Angew Chem Int Ed Engl* **41**, 605–609 (2002).

84. Blanchard, S. C. & Puglisi, J. D. Solution structure of the A loop of 23S ribosomal RNA. *PNAS* **98**, 3720–3725 (2001).

85. Micura, R. *et al.* Methylation of the nucleobases in RNA oligonucleotides mediates duplex – hairpin conversion. *Nucleic Acids Res.* **29**, 3997–4005 (2001).

86. Heus, H. A., Formenoy, L. J. & Knippenberg, P. H. V. A. N. Conformational and thermodynamic effects of naturally occurring base methylations in a ribosomal RNA hairpin of Bacillus stearothermophilus. *Eur. J. Biochem.* **188**, 275–281 (1990).

87. Agris, P. F., Sierzputowska-gracz, H. & Smith, C. Transfer RNA Contains Sites of Localized Positive Charge : Carbon NMR Studies of [13C] Methyl-Enriched Escherichia coli and Yeast tRNAPhe. *Biochemistry* **25**, 5126–5131 (1986).

88. Decatur, W. A. & Fournier, M. J. rRNA modifications and ribosome function. *Trends Biochem. Sci.* **27**, 344–351 (2002).

89. Ben-Shem, A. *et al.* The Structure of the Eukaryotic Ribosome at 3.0 Å Resolution. *Science (80-.).* **334**, 1524–1530 (2011).

90. Baudin-Baillieu, A. *et al.* Nucleotide modifications in three functionally important regions of the Saccharomyces cerevisiae ribosome affect translation accuracy. *Nucleic Acids Res.* **37**, 7665–7677 (2009).

91. Liang, X., Liu, Q. & Fournier, M. J. Loss of rRNA modifications in the decoding center of the ribosome impairs translation and strongly delays pre-rRNA processing. *RNA* **15**, 1716–1728 (2009).

92. Kanazawa, H., Baba, F., Koganei, M. & Kondo, J. A structural basis for the antibiotic resistance conferred by an N1-methylation of A1408 in 16S Rrna. *Nucleic Acids Res.* **45**, 12529–12535 (2017).

93. Stojkovic, V., Noda-garcia, L., Tawfik, D. S. & Galonic Fujimori, D. Antibiotic resistance evolved via inactivation of a ribosomal RNA methylating enzyme. *Nucleic Acids Res.* **44**, 8897–8907 (2016).

94. Vester, B. & Long, K. S. Antibiotic Resistance in Bacteria Caused by Modified Nucleosides in 23S Ribosomal RNA. in *DNA and RNA Modification Enzymes: Structure, Mechanism, Function and Evolution* 532–549 (2009).

95. Conn, G. L., Savic, M. & Macmaster, R. Antibiotic resis- tance in bacteria through modification of nucleosides in 16S ribosomal RNA. in *DNA and RNA Modification Enzymes: Structure, Mechanism, Function and Evolution* 524–536 (2009).

96. Douthwaite, S., Fourmy, D. & Yoshizawa, S. Nucleotide methylations in rRNA that confer resistance to ribosome-targeting antibiotics. in *Fine-Tuning of RNA Functions by Modification and Editing* 287–309 (2005). doi:10.1007/b105586

97. Gaynor, M. & Mankin, A. S. Macrolide Antibiotics : Binding Site , Mechanism of Action , Resistance. *Front. Med. Chem.* **2**, 21–35 (2005).

98. Warda, A. S. *et al.* Human METTL16 is a N6-methyladenosine (m6A) methyltransferase that targets pre-mRNAs and various non-coding RNAs. *EMBO Rep.* 1–11 (2017). doi:10.15252/embr.201744940

99. Pendleton, K. E. *et al.* The U6 snRNA m6A Methyltransferase METTL16 Regulates SAM Synthetase Intron Retention. *Cell* **169**, 824–835 (2017).

100. Massenet, S. & Branlant, C. A limited number of pseudouridine residues in the human atac spliceosomal UsnRNAs as compared to human major spliceosomal UsnRNAs. *RNA* **5**, 1495–1503 (1999).

101. Karijolich, J. & Yu, Y. Spliceosomal snRNA modifications and their function. *RNA Biol.* **7**, 192–204 (2010).

102. Dönmez, G., Hartmuth, K. & Lührmann, R. Modified nucleotides at the 5' end of human U2 snRNA are required for

spliceosomal E-complex formation. *RNA* **10**, 1925–1933 (2004).

103. Alarcón, C. R., Lee, H., Goodarzi, H., Halberg, N. & Tavazoie, S. F. N 6 -methyladenosine marks primary microRNAs for processing. *Nature* **519**, 482–485 (2015).

104. Xhemalce, B., Robson, S. C. & Kouzarides, T. Human RNA Methyltransferase BCDIN3D Regulates MicroRNA Processing. *Cell* **151**, 278–288 (2012).

105. Ren, G. *et al.* Methylation protects microRNAs from an AGO1- associated activity that uridylates 5 ′ RNA fragments generated by AGO1 cleavage. *PNAS* **111**, 6365–6370 (2014).

106. Ekdahl, Y., Farahani, H. S., Behm, M., Lagergren, J. & Öhman, M. A-to-I editing of microRNAs in the mammalian brain increases during development. *Genome Res.* **22**, 1477–1487 (2012).

107. Kawahara, Y. *et al.* Frequency and fate of microRNA editing in human brain. *Nucleic Acids Res.* **36**, 5270–5280 (2008).

108. Kawahara, Y., Zinshteyn, B. & Nishikura, K. Redirection of Silencing Targets by Adenosine-to-Inosine Editing of miRNAs. *Science (80-.).* **315**, 1137–1140 (2007).

109. Nishikura, K. A-to-I editing of coding and non-coding RNAs by ADARs. *Nat Rev Mol Cell Biol* **17**, 83–96 (2016).

110. Kim, Y., Heo, I. & Kim, V. N. Review Modifications of Small RNAs and Their Associated Proteins. *Cell* **143**, 703–709 (2010).

111. Li, L. *et al.* The landscape of miRNA editing in animals and its impact on miRNA biogenesis and targeting. *Genome Res.* 132–143 (2017). doi:10.1101/gr.224386.117.2

112. Gallie, D. R. The cap and poly(A) tail function synergistically to regulate mRNA translational efficiency. *Genes Dev.* **5**, 2108–2116 (1991).

113. Cowling, V. H. Regulation of mRNA cap methylation. *Biochem. J.* **425**, 295–302 (2010).

114. Shimotohno, K., Kodama, Y., Hashimoto, J. & Miura, K.-I. Importance of 5'-terminal blocking structure to stabilize mRNA in eukaryotic protein synthesis. *Proc. Natl. Acad. Sci. USA* **74**, 2734–2738 (1977).

115. Furuichi, Y., Lafiandra, A. & Shatkin, A. J. 5′ -Terminal structure and mRNA stability. *Nature* **266**, 235–239 (1977).

116. Song, M. G., Li, Y. & Kiledjian, M. Multiple mRNA Decapping Enzymes in Mammalian Cells. *Mol Cell* **40**, 423–432 (2010).

117. Werner, M. *et al.* 2 0 - O -ribose methylation of cap2 in human : function and evolution in a horizontally mobile family. *Nucleic Acids Res.* **39**, 4756–4768 (2011).

118. Akichika, S. *et al.* Cap-specific terminal N 6 -methylation of RNA by an RNA polymerase II–associated methyltransferase. *Science (80-.).* **363**, 1–12 (2018).

119. Bélanger, F., Stepinski, J., Darzynkiewicz, E. & Pelletier, J. Characterization of hMTr1, a Human Cap1 2'-O-Ribose Methyltransferase. *J. Biol. Chem.* **285**, 33037–33044 (2010).

120. Jiao, X. *et al.* 5′ End Nicotinamide Adenine Dinucleotide Cap in Human Cells Promotes RNA Decay through DXO-Mediated deNADding. *Cell* **168**, 1015–1027 (2017).

121. Bird, J. G. *et al.* The mechanism of RNA 5′ capping with NAD+, NADH and desphospho-CoA. *Nature* **535**, 444–447 (2016).

122. Cahova, H., Winz, M.-L., Höfer, K., Nübel, G. & Jäschke, A. NAD captureSeq indicates NAD as a bacterial cap for a subset of regulatory RNAs. *Nature* **519**, 374–377 (2015).

123. Walters, R. W. *et al.* Identification of NAD + capped mRNAs in Saccharomyces cerevisiae. *PNAS* **114**, 480–485 (2016).

124. Chen, Y. G., Kowtoniuk, W. E., Agarwal, I., Shen, Y. & Liu, D. R. LC/MS analysis of cellular RNA reveals NAD-linked RNA. *Nat Chem Biol* **5**, 879–881 (2009).

125. Grasso, L. *et al.* mRNA Cap Methylation in Pluripotency and Differentiation. *Cell Rep.* **16**, 1352–1365 (2016).

126. Wang, J. *et al.* Quantifying the RNA cap epitranscriptome reveals novel caps in cellular and viral RNA. *Nucleic Acids Res.* 1–16 (2019). doi:10.1093/nar/gkz751

127. Roundtree, I. A., Evans, M. E., Pan, T. & He, C. Review Dynamic RNA Modifications in Gene Expression Regulation. *Cell* **169**, 1187–1200 (2017).

128. Nachtergaele, S. & He, C. Chemical Modifications in the Life of an mRNA Transcript. *Annu. Rev. Genet.* **54**, 1–24 (2018).

129. Zhao, B. S., Nachtergaele, S., Roundtree, I. A. & He, C. Our views of dynamic N 6 -methyladenosine RNA methylation. *RNA* **24**, 268–272 (2018).

130. Lence, T. *et al.* m 6 A modulates neuronal functions and sex determination in Drosophila. *Nat. Publ. Gr.* **540**, 242–247

(2016).

131.   Xiao, W. *et al.* Nuclear m6A Reader YTHDC1 Regulates mRNA Splicing. *Mol. Cell* **61**, 507–519 (2016).

132.   Roundtree, I. A. *et al.* YTHDC1 mediates nuclear export of N 6 - methyladenosine methylated mRNAs. *Elife* 1–28 (2017).

133.   Wang, X. *et al.* N6-methyladenosine-dependent regulation of messenger RNA stability. *Nature* **505**, 117–20 (2014).

134.   Du, H. *et al.* YTHDF2 destabilizes m 6 A-containing RNA through direct recruitment of the CCR4-NOT deadenylase complex. *Nat. Commun.* **7**, 1–11 (2016).

135.   Wang, X. *et al.* N6-methyladenosine Modulates Messenger RNA Translation Efficiency. *Cell* **161**, 1388–1399 (2016).

136.   Geula, S. *et al.* m6A mRNA methylation facilitates resolution of naïve pluripotency toward differentiation. *Stem Cells* **347**, 1002–1006 (2015).

137.   Wang, Y. *et al.* N6-methyladenosine modification destabilizes developmental regulators in embryonic stem cells. *Nat. Cell Biol.* **16**, 191–198 (2014).

138.   Wu, R. *et al.* m 6 A methylation controls pluripotency of porcine induced pluripotent stem cells by targeting SOCS3 / JAK2 / STAT3 pathway in a YTHDF1 / YTHDF2-orchestrated manner. *Cell Death Dis.* **10**, 1–15 (2019).

139.   Chen, T. *et al.* M 6 A RNA methylation is regulated by microRNAs and promotes reprogramming to pluripotency. *Cell Stem Cell* **16**, 289–301 (2015).

140.   Jia, G. *et al.* N6-Methyladenosine in nuclear RNA is a major substrate of the obesity-associated FTO. *Nat. Chem. Biol.* **7**, 885–887 (2011).

141.   Zheng, G. *et al.* ALKBH5 Is a Mammalian RNA Demethylase that Impacts RNA Metabolism and Mouse Fertility. *Mol. Cell* **49**, 18–29 (2013).

142.   Tang, C. *et al.* ALKBH5-dependent m6A demethylation controls splicing and stability of long 3′-UTR mRNAs in male germ cells. *PNAS* 325–333 (2017). doi:10.1073/pnas.1717794115

143.   Mauer, J. *et al.* Reversible methylation of m6Am in the 5′ cap controls mRNA stability. *Nature* **541**, 371–375 (2017).

144.   Meyer, K. D. & Jaffrey, S. R. Rethinking m A Readers , Writers , and Erasers. *Annu. Rev. Cell Dev. Biol.* **33**, 1–24 (2017).

145.   Mauer, J. & Jaffrey, S. R. FTO, m6Am, and the hypothesis of reversible epitranscriptomic mRNA modifications. *FEBS Lett.* **592**, 2012–2022 (2018).

146.   Meyer, K. D. *et al.* 5′ UTR m6A Promotes Cap-Independent Translation. *Cell* **163**, 1–12 (2015).

147.   Yang, X. *et al.* 5-methylcytosine promotes mRNA export — NSUN2 as the methyltransferase and ALYREF as an m 5 C reader. *Cell Res.* **27**, 606–625 (2017).

148.   Schwartz, S. m1A within cytoplasmic mRNAs at single nucleotide resolution : a reconciled transcriptome-wide map. *RNA* **24**, 1427–1436 (2018).

149.   Safra, M. *et al.* The m1A landscape on cytosolic and mitochondrial mRNA at single-base resolution. *Nature* **551**, 251–255 (2017).

150.   Xiong, X., Li, X., Wang, K. U. N. & Yi, C. Perspectives on topology of the human m 1 A methylome at single nucleotide resolution. *RNA Biol.* 1437–1442 (2018). doi:10.1261/rna.067694.118.5

151.   Li, X. *et al.* Base-Resolution Mapping Reveals Distinct m1A Methylome in Nuclear- and Mitochondrial-Encoded Transcripts. *Mol. Cell* **68**, 1–13 (2017).

152.   Li, X. *et al.* Chemical pulldown reveals dynamic pseudouridylation of the mammalian transcriptome. *Nat. Chem. Biol.* **11**, 592–597 (2015).

153.   Gilbert, W. V, Bell, T. A. & Schaening, C. Messenger RNA modifications – Form, distribution, and function. *Science (80-.).* **352**, 1408–1412 (2016).

154.   Fernandez, I. S. *et al.* Unusual base pairing during the decoding of a stop codon by the ribosome. *Nature* **500**, 107–111 (2013).

155.   Karijolich, J. & Yu, Y. Converting nonsense codons into sense codons by targeted pseudouridylation. *Nature* **474**, 395–398 (2011).

156.   Hoernes, T. P. *et al.* Nucleotide modifications within bacterial messenger RNAs regulate their translation and are able to rewire the genetic code. *Nucleic Acids Res.* **44**, 852–862 (2016).

157.   Bokar, J. A., Rath-Shambaugh, M. E., Ludwiczak, R., Narayan, P. & Rottman, F. Characterization and partial purification of mRNA N6-adenosine methyltransferase from HeLa cell nuclei: Internal mRNA methylation requires a multisubunit

complex. *J. Biol. Chem.* **269**, 17697–17704 (1994).

158. Bokar, J. A., Shambaugh, M. E., Polayes, D., Matera, A. G. & Rottman, F. M. Purification and cDNA cloning of the AdoMet-binding subunit of the human mRNA (N6-adenosine)-methyltransferase. *RNA* **3**, 1233–47 (1997).

159. Wang, Y. *et al.* N6-methyladenosine modification destabilizes developmental regulators in embryonic stem cells. *Nat. Cell Biol.* **16**, 191–8 (2014).

160. Liu, J. *et al.* A METTL3-METTL14 complex mediates mammalian nuclear RNA N6-adenosine methylation. *Nat. Chem. Biol.* **10**, (2014).

161. Schwartz, S. *et al.* Perturbation of m6A writers reveals two distinct classes of mRNA methylation at internal and 5' sites. *Cell Rep.* **8**, 284–296 (2014).

162. Ping, X. L. *et al.* Mammalian WTAP is a regulatory subunit of the RNA N6-methyladenosine methyltransferase. *Cell Res.* **24**, 177–189 (2014).

163. Agarwala, S. D., Blitzblau, H. G., Hochwagen, A. & Fink, G. R. RNA Methylation by the MIS Complex Regulates a Cell Fate Decision in Yeast. *PLoS Genet.* **8**, 1–13 (2012).

164. Ortega, A. *et al.* Biochemical Function of Female-Lethal (2) D / Wilms ' Tumor Suppressor-1-associated Proteins in Alternative Pre-mRNA Splicing. *J. Biol. Chem.* **278**, 3040–3047 (2003).

165. Liu, J. *et al.* VIRMA mediates preferential m6A mRNA methylation in 3'UTR and near stop codon and associates with alternative polyadenylation. *Cell Discov.* **4**, 1–17 (2018).

166. Patil, D. P. *et al.* m 6 A RNA methylation promotes XIST - mediated transcriptional repression. *Nature* **537**, 369–373 (2016).

167. Wen, J. *et al.* Zc3h13 Regulates Nuclear RNA m 6 A Methylation and Mouse Embryonic Stem Cell Self-Renewal. *Mol. Cell* **69**, 1028-1038.e6 (2018).

168. Knuckles, P. *et al.* Zc3h13 / Flacc is required for adenosine methylation by bridging the mRNA- binding factor Rbm15 / Spenito to the m 6 A machinery component Wtap / Fl (2) d. *Genes Dev.* **32**, 415–429 (2018).

169. Guo, J., Tang, H.-W., Li, J., Perrimon, N. & Yan, D. Xio is a component of the Drosophila sex determination pathway and RNA N6-methyladenosine methyltransferase complex. *Proc. Natl. Acad. Sci.* 1–6 (2018). doi:10.1073/pnas.1720945115

170. Wang, X. *et al.* Structural basis of N6-adenosine methylation by the METTL3–METTL14 complex. *Nature* 1–15 (2016). doi:10.1038/nature18298

171. Wang, P., Doxtader, K. A. & Nam, Y. Structural Basis for Cooperative Function of Mettl3 and Mettl14 Methyltransferases. *Mol. Cell* **63**, 1–12 (2016).

172. Choe, J. *et al.* mRNA circularization by METTL3-eIF3h enhances translation and promotes oncogenesis. *Nature* **561**, 556–560 (2019).

173. Schöller, E. *et al.* Interactions, localization and phosphorylation of the m6A generating METTL3- METTL14-WTAP complex. *RNA* **24**, 499–512 (2018).

174. Huang, H. *et al.* Histone H3 trimethylation at lysine 36 guides m6A RNA modification co-transcriptionally. *Nature* **567**, 414–419 (2019).

175. Horiuchi, K. *et al.* Identification of Wilms' Tumor 1-associating Protein Complex and Its Role in Alternative Splicing and the Cell Cycle. *J. Biol. Chem.* **288**, 33292–33302 (2013).

176. Bujnicki, J. M., Feder, M., Ayres, C. L. & Redman, K. L. Sequence-structure-function studies of tRNA:m5C methyltransferase Trm4p and its relationship to DNA:m5C and RNA:m5U methyltransferases. *Nucleic Acids Res.* **32**, 2453–2463 (2004).

177. Trixl, L. & Lusser, A. The dynamic RNA modification 5-methylcytosine and its emerging role as an epitranscriptomic mark. *WIREs RNA* 1–17 (2018). doi:10.1002/wrna.1510

178. Sharma, S., Yang, J., Watzinger, P., Kötter, P. & Entian, K. Yeast Nop2 and Rcm1 methylate C2870 and C2278 of the 25S rRNA, respectively. *Nucleic Acids Res.* **41**, 9062–9076 (2013).

179. Gigova, A., Duggimpudi, S., Pollex, T., Schaefer, M. & Kos, M. A cluster of methylations in the domain IV of 25S rRNA is required for ribosome stability. *RNA* **20**, 1632–1644 (2014).

180. Cámara, Y. *et al.* MTERF4 Regulates Translation by Targeting the Methyltransferase NSUN4 to the Mammalian Mitochondrial Ribosome. *Cell Metab.* **13**, 527–539 (2011).

181. Metodiev, M. D. *et al.* NSUN4 Is a Dual Function Mitochondrial Protein Required for Both Methylation of 12S rRNA and Coordination of Mitoribosomal Assembly. *PLoS Genet.* **10**, 1–11 (2014).

182. Dong, A. *et al.* Structure of human DNMT2 , an enigmatic DNA methyltransferase homolog that displays denaturant-resistant binding to DNA. *Nucleic Acids Res.* **29**, 439–448 (2001).

183. Wilkinson, C. R. M., Bartlett, R., Nurse, P. & Bird, A. P. The fission yeast gene pmt1 encodes a DNA methyltransferase homologue. *Nucleic Acids Res.* **23**, 203–210 (1995).

184. Goll, M. G. *et al.* Methylation of tRNA Asp by the DNA Methyltransferase Homolog Dnmt2. *Science (80-.).* **311**, 395–399 (2006).

185. Tuorto, F. *et al.* RNA cytosine methylation by Dnmt2 and NSun2 promotes tRNA stability and protein synthesis. *Nat. Struct. Mol. Biol.* **19**, 900–905 (2012).

186. Schaefer, M. *et al.* RNA methylation by Dnmt2 protects transfer RNAs against stress-induced cleavage. *Genes Dev.* **24**, 1590–1595 (2010).

187. Haag, S. *et al.* NSUN 3 and ABH 1 modify the wobble position of mt-tRNA Met to expand codon recognition in mitochondrial translation. *EMBO J.* **35**, 2104–2119 (2016).

188. Van Haute, L. *et al.* Deficient methylation and formylation of mt-tRNAMet wobble cytosine in a patient carrying mutations in NSUN3. *Nat. Commun.* **7**, 1–10 (2016).

189. Trixl, L. *et al.* RNA cytosine methyltransferase Nsun3 regulates embryonic stem cell differentiation by promoting mitochondrial activity. *Cell. Mol. Life Sci.* **75**, 1483–1497 (2018).

190. Haag, S. *et al.* NSUN6 is a human RNA methyltransferase that catalyzes formation of m 5 C72 in specific tRNAs. *RNA* **21**, 1532–1543 (2015).

191. Blanco, S. *et al.* Aberrant methylation of tRNAs links cellular stress to neuro-developmental disorders. *EMBO J.* **33**, 2020–2039 (2014).

192. Brzezicha, B. *et al.* Identification of human tRNA:m5C methyltransferase catalysing intron-dependent m5C formation in the first position of the anticodon of the pre-tRNA Leu (CAA). *Nucleic Acids Res.* **34**, 6034–6043 (2006).

193. Hussain, S. *et al.* NSun2-mediated cytosine-5 methylation of vault noncoding RNA determines its processing into regulatory small RNAs. *Cell Rep.* **4**, 255–261 (2013).

194. Khoddami, V., Yerra, A. & Cairns, B. R. Experimental Approaches for Target Profiling of RNA Cytosine Methyltransferases. in *Methody in Enzymology* **560**, 273–296 (Elsevier Inc., 2015).

195. Li, Q. *et al.* NSUN2-Mediated m5C Methylation and METTL3/METTL14-Mediated m6A Methylation Cooperatively Enhance p21 Translation. *J. Cell. Biochem.* **118**, 2587–2598 (2017).

196. Tang, H. *et al.* NSun2 delays replicative senescence by repressing p27 (KIP1) translation and elevating CDK1 translation. *Aging (Albany. NY).* **7**, 1143–1155 (2015).

197. Xing, J. *et al.* NSun2 Promotes Cell Growth via Elevating Cyclin-Dependent Kinase 1 Translation. *Mol. Cell. Biol.* **35**, 4043–4052 (2015).

198. Aguilo, F. *et al.* Deposition of 5-Methylcytosine on Enhancer RNAs Enables the Coactivator Function of PGC-1 a. *Cell Rep.* **14**, 479–492 (2016).

199. Ito, S. *et al.* Tet proteins can convert 5-methylcytosine to 5-formylcytosine and 5-carboxylcytosine. *Science (80-.).* **333**, 1300–1303 (2011).

200. Fu, L. *et al.* Tet-Mediated Formation of 5 - Hydroxymethylcytosine in RNA. *JACS* **136**, 11582–11585 (2014).

201. Rintala-Dempsey, A. C. & Kothe, U. Eukaryotic stand-alone pseudouridine synthases – RNA modifying enzymes and emerging regulators of gene expression? *RNA Biol.* **24**, 1185–1196 (2017).

202. Becker, H. F., Motorin, Y., Planta, R. J. & Grosjean, H. The yeast gene YNL292w encodes a pseudouridine synthase (Pus4) catalyzing the formation of Ψ 55 in both mitochondrial and cytoplasmic tRNAs. *Nucleic Acids Res.* **25**, 4493–4499 (1997).

203. Behm-Ansmant, I. *et al.* The Saccharomyces cerevisiae U2 snRNA:pseudouridine-synthase Pus7p is a novel multisite–multisubstrate RNA:Psi-synthase also acting on tRNAs. *RNA* **9**, 1371–1382 (2003).

204. Ansmant, I. *et al.* Identification of the Saccharomyces cerevisiae RNA : pseudouridine synthase responsible for formation of Ψ 2819 in 21S mitochondrial ribosomal RNA. *Nucleic Acids Res.* **28**, 1941–1946 (2000).

205. Watkins, N. J. *et al.* Cbf5p, a potential pseudouridine synthase, and Nhp2p, a putative RNA-binding protein, are

present together with Gar1p in all H BOX/ACA-motif snoRNPs and constitute a common bipartite structure. *RNA* **4**, 1549–1568 (1998).

206. Hamma, T., Reichow, S. L., Varani, G. & Amaré, A. R. F. The Cbf5 – Nop10 complex is a molecular bracket that organizes box H / ACA RNPs. *Nat. Struct. Mol. Biol.* **12**, 1101–1107 (2005).

207. Rashid, R. *et al.* Crystal Structure of a Cbf5-Nop10-Gar1 Complex and Implications in RNA-Guided Pseudouridylation and Dyskeratosis Congenita. *Mol. Cell* **21**, 249–260 (2006).

208. Li, L. & Ye, K. Crystal structure of an H / ACA box ribonucleoprotein particle. *Nature* **443**, 302–307 (2006).

209. Li, S. *et al.* Reconstitution and structural analysis of the yeast box H / ACA RNA-guided pseudouridine synthase. *Genes Dev.* **25**, 2409–2421 (2011).

210. Girard, J. *et al.* GAR1 is an essential small nucleolar RNP protein required for pre-rRNA processing in yeast. *EMBO J.* **11**, 673–682 (1992).

211. Kiss, T. Small Nucleolar RNAs : An Abundant Group of Noncoding RNAs with diverse cellular functions. *Cell* **109**, 145–148 (2002).

212. Ganot, P., Caizergues-ferrer, M. & Kiss, T. The family of box ACA small nucleolar RNAs is defined by an evolutionarily conserved secondary structure and ubiquitous sequence elements essential for RNA accumulation. *Genes Dev.* **11**, 941–956 (1997).

213. Balakin, A. G., Smith, L. & Fournier, M. J. The RNA World of the Nucleolus : Two Major Families of Small RNAs Defined by Different Box Elements with Related Functions. *Cell* **86**, 823–834 (1996).

214. Ni, J., Tien, A. L. & Fournier, M. J. Small Nucleolar RNAs Direct Site-Specific Synthesis of Pseudouridine in Ribosomal RNA. *Cell* **89**, 565–573 (1997).

215. Ganot, P., Bortolin, M. & Sabatier, P. Site-Specific Pseudouridine Formation in Preribosomal RNA Is Guided by Small Nucleolar RNAs. *Cell* **89**, 799–809 (1997).

216. Kawarada, L. *et al.* ALKBH1 is an RNA dioxygenase responsible for cytoplasmic and mitochondrial tRNA modifications. *Nucleic Acids Res.* **45**, 7401–7415 (2017).

217. Chen, Z. *et al.* Transfer RNA demethylase ALKBH3 promotes cancer progression via induction of tRNA-derived small RNAs. *Nucleic Acids Res.* 1–13 (2018). doi:10.1093/nar/gky1250

218. Yang, Y., Hsu, P. J., Chen, Y. & Yang, Y. Dynamic transcriptomic m 6 A decoration : writers , erasers , readers and functions in RNA metabolism. *Cell Res.* **28**, 616–624 (2018).

219. Zhang, Z. *et al.* The YTH domain is a novel RNA binding domain. *J. Biol. Chem.* **285**, 14701–14710 (2010).

220. Theler, D., Dominguez, C., Blatter, M., Boudet, J. & Allain, F. H.-T. Solution structure of the YTH domain in complex with N6-methyladenosine RNA: a reader of methylated RNA. *Nucleic Acids Res.* **42**, 13911–13919 (2014).

221. Stoilov, P., Rafalska, I. & Stamm, S. YTH: A new domain in nuclear proteins. *Trends Biochem. Sci.* **27**, 495–497 (2002).

222. Liao, S., Sun, H. & Xu, C. YTH Domain: A Family of N6-methyladenosine (m6A) Readers. in *Genomics, Proteomics and Bioinformatics* **16**, 99–107 (The Authors, 2018).

223. Hazra, D., Chapat, C. & Graille, M. m6A mRNA Destiny: Chained to the rhYTHm by the YTH-Containing Proteins. *Genes (Basel).* **10**, 1–15 (2019).

224. Kasowitz, S. D. *et al.* Nuclear m6A reader YTHDC1 regulates alternative polyadenylation and splicing during mouse oocyte development. *PLoS Genet.* 1–28 (2018).

225. Wojtas, M. N. *et al.* Regulation of m6A Transcripts by the 3 ' / 5 ' RNA Helicase YTHDC2 Is Essential for a Successful Meiotic Program in the Mammalian Germline. *Mol. Cell* **68**, 374–387 (2017).

226. Jain, D. *et al.* ketu mutant mice uncover an essential meiotic function for the ancient RNA helicase YTHDC2. *Elife* **7**, 1–41 (2018).

227. Tanabe, A. *et al.* RNA helicase YTHDC2 promotes cancer metastasis via the enhancement of the efficiency by which HIF-1α mRNA is translated. *Cancer Lett.* 1–9 (2016). doi:10.1016/j.canlet.2016.02.022

228. Tanabe, A., Konno, J. & Sahara, H. Transcriptional machinery of TNF- α -inducible YTH domain containing 2. *Gene* **535**, 24–32 (2014).

229. Kretschmer, J. *et al.* The m 6 A reader protein YTHDC2 interacts with the small ribosomal subunit and the 5 ′ – 3 ′ exoribonuclease XRN1. *RNA* **24**, 1339–1350 (2018).

230. Hsu, P. J. *et al.* Ythdc2 is an N 6 -methyladenosine binding protein that regulates mammalian spermatogenesis. *Cell*

Res. **27**, 1115–1127 (2017).

231. Abby, E. *et al.* Implementation of meiosis prophase I programme requires a conserved retinoid-independent stabilizer of meiotic transcripts. *Nat. Commun.* 1–16 (2016). doi:10.1038/ncomms10324

232. Soh, Y. Q. S. *et al.* Meioc maintains an extended meiotic prophase I in mice. *PLoS Genet.* 1–33 (2017).

233. Kang, H. *et al.* A novel protein , Pho92 , has a conserved YTH domain and regulates phosphate metabolism by decreasing the mRNA stability of PHO4 in Saccharomyces cerevisiae. *Biochem. J.* **457**, 391–400 (2014).

234. Park, O. H. *et al.* Endoribonucleolytic cleavage of m6A-containing RNAs by RNase P/MRP complex. *Mol. Cell* **74**, 1–14 (2019).

235. Li, A. *et al.* Cytoplasmic m 6 A reader YTHDF3 promotes mRNA translation. *Cell Res.* **27**, 444–447 (2017).

236. Shi, H. *et al.* YTHDF3 facilitates translation and decay of N6-methyladenosine-modified RNA. *Cell Res.* **27**, 315–328 (2017).

237. Anders, M. *et al.* Dynamic m 6 A methylation facilitates mRNA triaging to stress granules. *Life Sci. Alliance* **1**, 1–12 (2018).

238. Tirumuru, N., Zhao, B. S., Lu, W. & Lu, Z. N 6 -methyladenosine of HIV-1 RNA regulates viral infection and HIV-1 Gag protein expression. *Elife* 1–20 (2016). doi:10.7554/eLife.15528

239. Kennedy, E. M. *et al.* Post-transcriptional m6A editing of HIV-1 mRNAs enhances viral gene expression. *Cell Host Microbe* **19**, 675–685 (2016).

240. Lichinchi, G. *et al.* Dynamics of Human and Viral RNA Methylation during ZIKA Virus Infection. *Cell Host Microbe* **20**, 666–673 (2016).

241. Gokhale, N. S. *et al.* N6 -Methyladenosine in Flaviviridae Viral RNA Genomes Regulates Infection. *Cell Host Microbe* 654–665 (2016). doi:10.1016/j.chom.2016.09.015

242. Krug, R. M., Morgan, M. A. & Shatkin, A. J. Influenza Viral mRNA Contains Internal N6- Methyladenosine and 5 ′ - Terminal 7-Methylguanosine in Cap Structures. *J. Virol.* **20**, 45–53 (1976).

243. Edupuganti, R. R. *et al.* N6-methyladenosine (m6A) recruits and repels proteins to regulate mRNA homeostasis. *Nat. Struct. Mol. Biol.* **24**, 870–878 (2017).

244. Liu, N. *et al.* N6-methyladenosine alters RNA structure to regulate binding of a low-complexity protein. *Nucleic Acids Res.* **45**, 6051–6063 (2017).

245. Alarcón, C. R. *et al.* HNRNPA2B1 Is a Mediator of m 6 A-Dependent Nuclear RNA Processing Events. *Cell* **162**, 1299–1308 (2015).

246. Liu, N. *et al.* N6-methyladenosine-dependent RNA structural switches regulate RNA-protein interactions. *Nature* **518**, 560–564 (2015).

247. Huang, H. *et al.* Recognition of RNA N6-methyladenosine by IGF2BP proteins enhances mRNA stability and translation. *Nat. Cell Biol.* **20**, 182–295 (2018).

248. Pfaff, C. *et al.* ALY RNA-Binding Proteins Are Required for Nucleocytosolic mRNA Transport and Modulate Plant Growth and Development. *Plant Physiol.* **177**, 226–240 (2018).

249. Chen, X., Zhang, J. & Zhu, J. The role of m 6 A RNA methylation in human cancer. *Mol. Cancer* **18**, 1–9 (2019).

250. Yang, Y. *et al.* RNA 5-Methylcytosine Facilitates the Maternal-to- Zygotic Transition by Preventing Maternal mRNA Decay. *Mol. Cell* **75**, 1–15 (2019).

251. Chen, X. *et al.* 5-methylcytosine promotes pathogenesis of bladder cancer through stabilizing mRNAs. *Nat. Cell Biol.* **21**, 978–990 (2019).

252. Lao, N. & Barron, N. Cross-talk between m6A and m1A regulators, YTHDF2 and ALKBH3 fine-tunes mRNA expression. *bioRxiv* **589747**, 1–20 (2019).

253. Legrand, C. *et al.* Statistically robust methylation calling for whole- transcriptome bisulfite sequencing reveals distinct methylation patterns for mouse RNAs. *Genome Res.* **27**, 1589–1596 (2017).

254. Ke, S. *et al.* m 6 A mRNA modifications are deposited in nascent pre-mRNA and are not required for splicing but do specify cytoplasmic turnover. *Genes Dev.* **31**, 990–1006 (2017).

255. Rosa-mercado, N. A., Withers, J. B. & Steitz, J. A. Settling the m6A debate: methylation of mature mRNA is not dynamic but accelerates turnover. *Genes Dev.* **31**, 957–958 (2017).

256. Wei, J. *et al.* Differential m6A, m6Am, and m1A Demethylation Mediated by FTO in the Cell Nucleus and Cytoplasm.

Mol. Cell **71**, 973–985 (2018).

257. Bachvaroff, R. & McMaster, P. R. B. Separation of microsomal RNA into five bands during agar electrophoresis. *Science (80-.).* **143**, 1177–1179 (1964).

258. Holland, L. J. & Wangh, L. J. Efficient recovery of functionally intact mRNA from agarose gels via transfer to an ion-exchange membrane. *Nucleic Acids Res.* **11**, 3283–3300 (1983).

259. Pomerantz, S. C., Kowalak, J. A. & McCloskey, J. A. Determination of Oligonucleotide Composition from Mass Spectrometrically Measured Molecular Weight. *Am. Soc. Mass Spectrom.* **4**, 204–209 (1993).

260. Limbach, P. A., Crain, P. F. & Mccloskey, J. A. Molecular Mass Measurement of Intact Ribonucleic Acids Via Electrospray Ionization Quadrupole Mass Spectrometry. *Am. Soc. Mass Spectrom.* **6**, 27–39 (1995).

261. Limbach, P. A., Crain, P. F. & McCloskey, J. A. Summary: the modified nucleosides of RNA. *Nucleic Acids Res.* **22**, 2183–2196 (1994).

262. Alon, S. *et al.* Systematic identification of edited microRNAs in the human brain. *Genome Res.* **22**, 1533–1540 (2012).

263. Dominissini, D., Moshitch-moshkovitz, S., Amariglio, N. & Rechavi, G. Adenosine-to-inosine RNA editing meets cancer. *Carcinogenesis* **32**, 1569–1577 (2011).

264. Tserovski, L. *et al.* High-throughput sequencing for 1-methyladenosine (m 1 A) mapping in RNA. *Methods* **107**, 110–121 (2016).

265. Hauenschild, R. *et al.* The reverse transcription signature of N-1-methyladenosine in RNA-Seq is sequence. **43**, 9950–9964 (2015).

266. Wilusz, J. E. Removing roadblocks to deep sequencing of modified RNAs. *Nat. Methods* **12**, 821–822 (2015).

267. Kietrys, A. M., Velema, W. A. & Kool, E. T. Fingerprints of Modi fi ed RNA Bases from Deep Sequencing Profiles. *J. Am. Chem. Soc.* **139**, 17074–17081 (2017).

268. Potapov, V. *et al.* Base modifications affecting RNA polymerase and reverse transcriptase fidelity. *Nucleic Acids Res.* **46**, 5753–5763 (2018).

269. Macon, J. B. & Wolfenden, R. 1-Methyladenosine. Dimroth Rearrangement and Reversible Reduction. *Biochemistry* **7**, 3453–3458 (1968).

270. Dominissini, D. *et al.* The dynamic N1-methyladenosine methylome in eukaryotic messenger RNA. *Nature* **530**, 441–446 (2016).

271. Motorin, Y., Muller, S., Behm-Ansmant, I. & Branlant, C. Identification of Modified Residues in RNAs by Reverse Transcription-Based Methods. in *Methods in Enzymology* **425**, 21–53 (2007).

272. Helm, M. & Motorin, Y. Detecting RNA modifications in the epitranscriptome: predict and validate. *Nat. Publ. Gr.* **18**, 275–291 (2017).

273. Bakin, A. & Ofengand, J. Four Newly Located Pseudouridylate Residues in Escherichia coli 23s Ribosomal RNA Are All at the Peptidyltransferase Center : Analysis by the Application of a New Sequencing Technique. *Biochemistry* **32**, 9754–9762 (1993).

274. Schaefer, M., Pollex, T., Hanna, K. & Lyko, F. RNA cytosine methylation analysis by bisulfite sequencing. *Nucleic Acids Res.* **37**, 1–10 (2009).

275. Suzuki, T., Ueda, H., Okada, S. & Sakurai, M. Transcriptome-wide identification of adenosine-to- inosine editing using the ICE-seq method. *Nat. Protoc.* **10**, 715–732 (2015).

276. Hussain, S., Aleksic, J., Blanco, S., Dietmann, S. & Frye, M. Characterizing 5-methylcytosine in the mammalian epitranscriptome. *Genome Biol.* **14**, 1–10 (2013).

277. Hartstock, K., Nilges, B., Ovcharenko, A., Puellen, N. & Leidel, S. Enzymatic or in vivo installation of propargyl groups in combination with click chemistry enables enrichment and detection of methyltransferase target sites in RNA. *Angew. Chemie* **57**, 6342–6346 (2018).

278. Linder, B. *et al.* Single-nucleotide-resolution mapping of m6A and m6Am throughout the transcriptome. *Nat. Methods* **12**, 767–772 (2015).

279. Chen, K. *et al.* High-Resolution N6Methyladenosine (m6A) Map Using Photo-CrosslinkingAssisted m6A Sequencing. *Angew Chem Int Ed Engl* **54**, 1587–1590 (2015).

280. Jenner, E. Further Observations on the Variolae Vaccinae, or Cow-pox. *Med. Phys. J.* **1**, 313–318 (1799).

281. Jenner, E. On the Origin of the Vaccine Inoculation. *Med Phys J.* **5**, 505–508 (1801).

106

282. Behring, E. A. & Kitasato, S. Ueber das Zustandekommen der Diphterie-Immunität und der Tetanus-Immunität bei Thieren. *Dtsch. Med. Wochenschrift* **49**, 1–6 (1890).

283. Gronski, P., Seiler, F. P. & Schwick, H. G. Discovery of antitoxins and development of antibody preparations for clinical uses from 1890 to 1990. *Mol. Immunol.* **28**, 1321–1332 (1991).

284. Behring, E. The Nobel Price. https://www.nobelprize.org/

285. Male, D., Brostoff, J., Roth, D. B. & Roitt, I. *Immunology - Eighth edition*. (2012).

286. Leo, O., Cunningham, A. & Stern, P. L. Vaccine immunology. in *Perspectives in Vaccinology* **1**, 25–59 (Elsevier B.V., 2011).

287. Morrison, S. & Neuberger, M. S. The structure of a typical antibody molecule. in *Immunobiology: The Immune System in Health and Disease. 5th edition* 93–123 (2001).

288. Saeed, A. F. U. H., Wang, R., Ling, S. & Wang, S. Antibody engineering for pursuing a healthier future. *Front. Microbiol.* **8**, 1–28 (2017).

289. Köhler, G. & Milstein, C. Continuous cultures of fused cells secreting antibody of predefined specificity. *Nature* **265**, 495–497 (1975).

290. Zhang, C. Hybridoma Technology for the Generation of Monoclonal Antibodies. in *Methods in Molecular Biology: Antibody methods and protocols* **901**, 117–135 (2012).

291. Erlanger, B. F. & Beiser, S. M. Antibodies Specific for Ribonucleosides and Ribonucleotides and their Reaction with DNA. *Proc. Natl. Acad. Sci. U. S. A.* **52**, 68–74 (1964).

292. Plescia, O. J. & Braun, W. Nucleic Acids as Antigens. *Adv Immunol* 231–252 (1967).

293. Feederle, R. & Schepers, A. Antibodies specific for nucleic acid modifications. *RNA Biol.* **14**, 1089–1098 (2017).

294. Poirier, M. C. Antibodies to Carcinogen-DNA Adducts. *JNCl* **67**, 515–519 (1981).

295. Poirier, M. C. Antisera specific for carcinogen-DNA adducts and carcinogen-modified DNA: Applications for detection of xenobiotics in biological samples. *Mutat. Res.* **288**, 31–38 (1993).

296. Müller, R. & Rajewsky, M. F. Antibodies Specific for DNA Components Structurally Modified by Chemical Carcinogens. *J. Cancer Res. Clin. Oncol.* **102**, 99–113 (1981).

297. Munns, T. W., Liszewski, M. K. & Sims, H. F. Characterization of Antibodies Specific for N6-Methyladenosine and for 7-Methylguanosine. *Biochemistry* **16**, 2163–2168 (1977).

298. Sawicki, D. L., Erlanger, B. F. & Beiser, S. M. Immunochemical Detection of Minor Bases in Nucleic Acids. *Science (80-.).* **174**, 70–72 (1971).

299. Milstone, D. S., Vold, B. S., Glitz, D. G. & Shutt, N. Antibodies to N64A2-isopentenyl) adenosine and its nucleotide. *Nucleic Acids Res.* **5**, 3439–3455 (1978).

300. Vold, B. S., Longmire, M. E. & Keith, D. E. Thiolation and 2-Methylthio- Modification of Bacillus subtilis Transfer Ribonucleic Acids. *J. Bacteriol.* **148**, 869–876 (1981).

301. Zhou, C. *et al.* Genome-Wide Maps of m6A circRNAs Identify Widespread and Cell-Type-Specific Methylation Patterns that Are Distinct from mRNAs. *Cell Rep.* **20**, 2262–2276 (2017).

302. Meyer, K. D. & Jaffrey, S. R. The dynamic epitranscriptome: N6-methyladenosine and gene expression control. *Nat. Rev. Mol. Cell Biol.* **15**, 313–326 (2014).

303. Molinie, B. *et al.* m6A-LAIC-seq reveals the census and complexity of the m6A epitranscriptome. *Nat. Methods* **13**, 692–698 (2016).

304. Mishima, E. *et al.* Immuno-northern blotting: Detection of RNA modifications by using antibodies against modified nucleosides. *PLoS One* **10**, 1–17 (2015).

305. Itoh, K., Mizugaki, M. & Ishida, N. Preparation of a monoclonal antibody specific for 1-methyladenosine and its application for the detection of elevated levels of 1-methyladenosine in urines from cancer patients. *Jpn. J. Cancer Res.* **79**, 1130–1138 (1988).

306. Amort, T. *et al.* Distinct 5-methylcytosine profiles in poly(A) RNA from mouse embryonic stem cells and brain. *Genome Biol.* **18**, 1–16 (2017).

307. Cui, X. *et al.* 5-Methylcytosine RNA Methylation in Arabidopsis Thaliana. *Mol. Plant* **10**, 1387–1399 (2017).

308. Ghanbarian, H., Wagner, N., Polo, B. & Baudouy, D. Dnmt2 / Trdmt1 as Mediator of RNA Polymerase II Transcriptional Activity in Cardiac Growth. *PLoS One* **11**, 1–13 (2016).

309. Itoh, K., Mizugaki, M. & Ishida, N. Detection of elevated amounts of urinary pseudouridine in cancer patients by use of a monoclonal antibody. *Clin. Chim. Acta* **181**, 305–315 (1989).

310. Reynauda, C. *et al.* Monitoring of urinary excretion of modified nucleosides in cancer patients using a set of six monoclonal antibodies. *Cancer Lett.* 255–262 (1991).

311. Zeng, Y. *et al.* Refined RIP-seq protocol for epitranscriptome analysis with low input materials. *PLoS Biol.* **16**, 1–20 (2018).

312. Rubin, G. M. The Nucleotide Sequence of Saccharomyces cerevisiae 5.8 S ribosomal Ribonucleic Acid. *J. Biol. Chem.* **248**, 3860–3875 (1973).

313. Iwanami, Y. & Brown, G. M. Methylated bases of ribosomal ribonucleic acid from HeLa cells. *Arch. Biochem. Biophys.* **126**, 8–15 (1968).

314. Klagsbrun, M. An evolutionary study of the methylation of transfer and ribosomal ribonucleic acid in prokaryote and eukaryote organisms. *J. Biol. Chem.* **248**, 2612–2620 (1973).

315. Boccaletto, P. *et al.* MODOMICS: A database of RNA modification pathways. 2017 update. *Nucleic Acids Res.* **46**, 303–307 (2018).

316. Bisswanger, H. Multiple Equilibria. in *Enzyme Kinetics: Principles and Kinetics* 7–58 (2008). doi:10.1002/9783527622023.ch1

317. Hollemans, H. J. G. & Bertina, R. M. Scatchard plot and heterogeneity in binding affinity of labeled and unlabeled ligand. *Clin. Chem.* **21**, 1769–1773 (1975).

318. Scatchard, G. The Attractions of Proteins for Small Molecules and Ions. *Ann. N. Y. Acad. Sci.* **51**, 660–672 (1949).

319. Seber, G. A. F. & Wild, C. J. *Nonlinear Regression*. (John Wiley & Sons, Inc., 1989). doi:10.1002/0471725315

320. Dominissini, D. *et al.* Topology of the human and mouse m6A RNA methylomes revealed by m6A-seq. *Nature* **485**, 201–206 (2012).

321. Treiber, T. *et al.* A Compendium of RNA-Binding Proteins that Regulate MicroRNA Biogenesis. *Mol. Cell* **66**, 270–284 (2017).

322. He, C. Recognition of RNA N 6-methyladenosine by IGF2BP Proteins Enhances mRNA Stability and Translation contributed reagents/analytic tools and/or grant support; HHS Public Access. *Nat Cell Biol* **20**, 285–295 (2018).

323. Patil, D. P., Pickering, B. F. & Jaffrey, S. R. Reading m6A in the Transcriptome: m6A-Binding Proteins. *Trends Cell Biol.* **28**, 113–127 (2018).

324. Sun, C. *et al.* Crystal structure of the YTH domain of YTHDF2 reveals mechanism for recognition of N6-methyladenosine. *Cell Res.* **24**, 1493–1496 (2014).

325. Alarcón, C. R. *et al.* HNRNPA2B1 Is a Mediator of m6A-Dependent Nuclear RNA Processing Events. *Cell* **162**, 1299–1308 (2015).

326. Xiong, X., Li, X. & Yi, C. N1-methyladenosine methylome in messenger RNA and non-coding RNA. *Curr. Opin. Chem. Biol.* **45**, 179–186 (2018).

327. Feederle, R. & Schepers, A. Antibodies specific for nucleic acid modifications. *RNA Biol.* **14**, 1089–1098 (2017).

328. Cathala, G. *et al.* A Method for Isolation of Intact , Translationally Active Ribonucleic Acid. *DNA* **2**, 329–335 (1983).

329. J.J. Barlow, A. P. M. and R. W. A Simple Method For The Quantitative Isolation Of Undegraded High Molecular Weight Ribcnucleic Acid. *Biochem. Biophys. Res. Commun.* **13**, 61–66 (1963).

330. Bartoli, K. M., Schaening, C., Carlile, T. & Gilbert, W. V. Conserved Methyltransferase Spb1 Targets mRNAs for Regulated Modification with 2′-O-Methyl Ribose. *bioRxiv* 271916 (2018). doi:10.1101/271916

331. Motorin, Y. & Marchand, V. Detection and Analysis of RNA Ribose 2′-O-Methylations: Challenges and Solutions. *Genes (Basel).* **9**, 642 (2018).

332. Munns, T. W., Liszewski, M. K. & Sims, H. F. Characterization of Antibodies Specific for N6-Methyladenosine and for 7-Methylguanosine. *Biochemistry* **16**, 2163–2168 (1977).

333. Ho, J. J., Cattoglio, C., McSwiggen, D. T., Tjian, R. & Fong, Y. W. Regulation of DNA demethylation by the XPC DNA repair complex in somatic and pluripotent stem cells. *Genes Dev.* **31**, 830–844 (2017).

334. Grozhik, A. V, Linder, B., Olarerin-George, A. O. & Jaffrey, S. R. Mapping m6A at individual-nucleotide resolution using crosslinking and immunoprecipitation (miCLIP). *Methods Mol Biol* **1562**, 55–78 (2017).

335. Hawley, B. R. & Jaffrey, S. R. Transcriptome-Wide Mapping of m 6 A and m 6 Am at Single-Nucleotide Resolution Using

miCLIP. *Curr. Protoc. Mol. Biol.* **126**, 1–22 (2019).

336. Clery, A. & Allain, F. H. T. From Structure to Function of RNA Binding Domains. in *RNA Binding Proteins* 137–158 (2014).

337. Stöhr, N. *et al.* Control of c-myc mRNA stability by IGF2BP1-associated cytoplasmic RNPs. *RNA* **15**, 104–115 (2009).

338. Prokipcakss, R. D., Herrick, D. J. & Jeffrey, R. Purification and Properties of a Protein That Binds to the C-terminal Coding Region of Human c-myc mRNA. *J. Biol. Chem.* **269**, 9261–9269 (1994).

339. Chionh, Y. H. *et al.* Three distinct 3-methylcytidine (m 3 C) methyltransferases modify tRNA and mRNA in mice and humans . *J. Biol. Chem.* **292**, 14695–14703 (2017).

340. Shi, Z. *et al.* Mettl17, a regulator of mitochondrial ribosomal RNA modifications , is required for the translation of mitochondrial coding genes. *FASEB J.* **33**, 1–11 (2019).

341. Zorbas, C. *et al.* The human 18S rRNA base methyltransferases DIMT1L and WBSCR22-TRMT112 but not rRNA modification are required for ribosome biogenesis. *Mol. Biol. Cell* **26**, 2080–2095 (2015).

342. Dominissini, D., Moshitch-Moshkovitz, S., Salmon-Divon, M., Amariglio, N. & Rechavi, G. Transcriptome-wide mapping of N6-methyladenosine by m 6A-seq based on immunocapturing and massively parallel sequencing. *Nat. Protoc.* **8**, 176–189 (2013).

343. Pfaffl, M. W. A new mathematical model for relative quantification in real-time RT-PCR. *Nucleic Acids Res.* **29**, 2002–2007 (2001).

344. Pall, G. S., Codony-servat, C., Byrne, J., Ritchie, L. & Hamilton, A. Carbodiimide-mediated cross-linking of RNA to nylon membranes improves the detection of siRNA , miRNA and piRNA by northern blot. *Nucleic Acids Res.* **35**, 1–9 (2007).

345. Motulsky, H. & Christopoulos, A. Fitting Models to Biological Data using Linear and Nonlinear Regression. A practical guide to curve fitting. in *Graph Pad Software* 97–103 (2003). doi:10.1002/pst.167

346. Treiber, T. *et al.* A Compendium of RNA-Binding Proteins that Regulate MicroRNA Biogenesis. *Mol. Cell* **66**, 270–284 (2017).

347. Treiber, T., Treiber, N. & Meister, G. Identification of microRNA Precursor-Associated Proteins. *Methods Mol. Biol.* **1823**, 103–114 (2018).

5.2 Supplemental Material

5.2.1 Complete list of antibodies

Table 16: Antibody clones against RNA base modifications, generated in the course of this work. The respective base modification, species, in which it was generated, the clone number and subtype of each antibody clone is listed below. The in the right part, the performance in the particular tests (dotblot, immunoprecipitation, competition assay, *ivt*-TLC experiment) of each clone is depicted. The most right column shows, if a clone was established (+) or not (-).

Modification	Source organism	Clone	Subtype	Dotblot	IP	Comp.	*ivt*-TLC	Established
m5U	rat	15D4		+	-	~	-	+
m5U	rat	19D1		-	-	-	n.a.	-
m5U	rat	22B2		-	-	-	n.a.	-
m5U	mouse	25F5		~	-	+	n.a.	-
m5U	mouse	28 E6		+	~	+	-	+
m5U	rat	24B3	2a	~	+	-	n.a.	-
m5U	rat	3F8	2a	~	+	~	n.a.	-
m5U	rat	24G8	2a	~	+	+	~	-
m5U	rat	22H4	2b	-	-	-	n.a.	-

m5U	rat	2D2	2c	+	+	~	n.a.	-
m26A	rat	1B3		+	-	+	n.a.	-
m26A	rat	1B9		+	-	-	n.a.	-
m26A	rat	1C8		+	-	-	n.a.	-
m26A	rat	1F6		~	-	-	n.a.	+
m26A	rat	1H7		~	+	+	n.a.	+
m26A	rat	2C4		+	-	-	n.a.	-
m26A	rat	58H10		+	+	+	n.a.	+
m26A	rat	60G3		+	+	+	n.a.	+
Ψ	mouse	25C6	2b	+	-	+	-	+
Ψ	mouse	26H5	2b	+	+	+	-	+
Ψ	mouse	26A7	2a	+	~	-	n.a.	-
Ψ	mouse	35C6	2a	-	-	-	n.a.	-
Ψ	mouse	27C8	2b	-	~	+	~	+
Ψ	mouse	32 E 9	2a	+	-	-	n.a.	-
m5C	rat	10F8	G1	-	-	-	n.a.	-
m5C	mouse	26B7	2a, G1	+	-	-	n.a.	-
m5C	mouse	31B10	G1	+	+	~	~	+
m5C	mouse	31D1	G1	+	-	-	n.a.	-
m5C	mouse	31E 12	2a	+	-	-	n.a.	-
m5C	mouse	32E 2	2a	+	+	+	+	+
m5C	mouse	25F6	G1	-	-	-	n.a.	-
m5C	mouse	28F6	2b	+	+	~	+	+
m5C	mouse	25H1	G1	+	-	-	n.a.	-
m5C	mouse	29H9	2b, G1	+	-	-	n.a.	-
m3U	mouse	25A1	G1	~	-	-	n.a.	-
m3U	mouse	28A7	2b	-	-	-	n.a.	-
m3U	mouse	27C8	G1	~	-	-	n.a.	-
m3U	mouse	26D11	2b	-	-	-	n.a.	-
m3U	mouse	28D11	G3, 2b	+	+	+	n.a.	+
m3U	mouse	32F5	G1	+	+	~	n.a.	+
m3U	mouse	25G8	2a	~	-	-	n.a.	-
m3U	mouse	29H8	G1	~	-	-	n.a.	-
m3U	rat	4A7	2a	~	-	-	n.a.	-
m3U	rat	6A2	2a	~	+	+	n.a.	+
m3U	rat	1B6	2a	+	+	+	n.a.	-
m3U	rat	13B8	2a	+	-	-	n.a.	-
m3U	rat	23B1	G1, 2c	+	+	+	n.a.	-
m3U	rat	3C7	2a	-	-	-	n.a.	-
m3U	rat	10C2	2a	+	+	~	n.a.	+
m3U	rat	9D7	2a	+	-	-	n.a.	-
m3U	rat	1F8	G1	+	+	+	n.a.	-
m3U	rat	10F10	G1	-	-	-	n.a.	-
m3U	rat	13F4	2c	-	-	-	n.a.	-
m3U	rat	23F8	2a	+	-	-	n.a.	-

m3U	rat	38D11	2b	+		+	n.a.	+
m6A	rat	14D11	2b	-	-	-	n.a.	-
m6A	rat	1H9	2a + 2c	-	-	-	n.a.	-
m6A	rat	23D10	2b	-	-	-	n.a.	-
m6A	rat	2F2	G1	-	-	-	n.a.	-
m6A	rat	14H7	G1	-	-	-	n.a.	-
m6A	rat	16D11	2b	-	-	-	n.a.	-
m6A	rat	1A10	G1 + 2a	-	-	-	n.a.	-
m6A	rat	15D6	2b	-	-	-	n.a.	-
m6A	rat	15C12	G1 + 2a	-	-	-	n.a.	-
m6A	rat	13G9	G1	-	-	-	n.a.	-
m6A	rat	16D3	2a	-	-	-	n.a.	-
m6A	rat	16B7	2b	-	-	-	n.a.	-
m6A	rat	11E 1	2a + 2c	-	-	-	n.a.	-
m6A	rat	15B8	2b	-	-	-	n.a.	-
m6A	rat	8C11	G1	-	-	-	n.a.	-
m6A	rat	21A11	G1	-	-	-	n.a.	-
m6A	rat	11G9	G1	-	-	-	n.a.	-
m6A	rat	2E 9	G1	-	-	-	n.a.	-
m6A	rat	18E 12	G1	-	-	-	n.a.	-
m6A	rat	23B12	2a + 2c	-	-	-	n.a.	-
m6A	rat	12F4	2a	-	-	-	n.a.	-
m6A	rat	11A5	2a	-	-	-	n.a.	-
m6A	rat	11B7	G1 + 2a	+	-	-	n.a.	-
m6A	rat	11C3	2a	+	-	-	n.a.	-
m6A	rat	5C5	2a	+	+	-	n.a.	-
m6A	rat	13G10	2a	+	+	-	n.a.	-
m6A	rat	11D11	G1	+	+	+	+	+
m6A	rat	11B9	2a	+	+	-	n.a.	-
m6A	rat	13G2	2a	+	+	+	+	+
m6A	rat	13C5	2a	+	+	-	n.a.	-
m6A	rat	13D2	2a	+	+	-	n.a.	-
m6A	rat	13F3	2a	-	-	-	n.a.	-
m6A	rat	13F12	2a	-	-	-	n.a.	-
m6A	rat	5E 2	2a	-	-	-	n.a.	-
m6A	rat	5D7	2a	+	+	-	n.a.	-
m6A	rat	4H6	2a	-	-	-	n.a.	-
m6A	rat	2A6	2b	-	-	-	n.a.	-
m6A	rat	5A10	2a	-	-	-	n.a.	-
m6A	rat	5F10	2a	+		-	n.a.	-
m6A	rat	5A1	2a	-	-	-	n.a.	-
m6A	rat	4C10	2b	-	-	-	n.a.	-
m6A	rat	7E 4	2a	-	-	-	n.a.	-
m6A	rat	5H1	2a	-	-	-	n.a.	-
m6A	rat	4D9	2a	-	-	-	n.a.	-
m6A	rat	6A10	2a	-	-	-	n.a.	-

m6A	rat	8E 10	2a	+	-	-	n.a.	-
m6A	rat	6H9	2a	-	-	-	n.a.	-
m6A	rat	9C9	2a	+	-	-	n.a.	-
m6A	rat	2A1	G1	+	-	-	n.a.	-
m6A	rat	8G9	2b	-	-	-	n.a.	-
m6A	rat	6E 7	2a	+	-	-	n.a.	-
m6A	rat	9B7	G1 + 2a	+	+	+	+	+
m6A	rat	7E 10	2a	-	-	-	n.a.	-
m6A	rat	7D9	2a	-	-	-	n.a.	-
m6A	rat	6B10	2b	-	-	-	n.a.	-
m6A	rat	10C11	2a	-	-	-	n.a.	-
m6A	rat	10A7	2a	+	+	-	n.a.	-
m6A	rat	9E 6	2a	-	-	-	n.a.	-
m6A	rat	8F5	2a	+	-	-	n.a.	-
m6A	rat	11B4	2a	+	+	-	n.a.	-
m6A	rat	9D4	2a	+	-	-	n.a.	-
m6A	rat	9A5	2a	-	-	-	n.a.	-
m6A	rat	12A5	G1	-	-	-	n.a.	-
m6A	rat	19B7	G1	+	+	+	+	+
m3C	rat	13A7	2b	~	-	-	n.a.	-
m3C	rat	5H2	2b	+	~	-	n.a.	-
m3C	rat	5H9	2b	+	-	-	n.a.	-
m3C	rat	15H5	2a	+	+	+	n.a.	+
m3C	rat	13E 2	2a	+	+	~	n.a.	+
m3C	rat	21F3	2a	~	-	-	n.a.	-
m3C	rat	22D9	2c	~	-	-	n.a.	-
m3C	rat	21B5	2b	~	-	-	n.a.	-
m3C	rat	14A11	2c	~	-	-	n.a.	-
m3C	rat	23F10	2b	+	~	-	n.a.	-
m3C	rat	13A5	2b	+	-	-	n.a.	-
m3C	rat	16A10	2b	~	-	-	n.a.	-
m3C	rat	21F12	2b	~	-	-	n.a.	-
m3C	rat	16H1	2b	+	~	-	n.a.	-
m3C	rat	6F2	2b	~	-	-	n.a.	-
m3C	rat	6E 11	2b	~	-	-	n.a.	-
m3C	rat	4D6	2c	~	-	-	n.a.	-
m3C	rat	5D5	2b	+	+	~	n.a.	+
m3C	rat	7F1	2c	+	+	~	n.a.	-
m3C	rat	7B5	2c	~	-	-	n.a.	-
m3C	rat	5C11	2c	+	+	-	n.a.	-
m3C	rat	1B11	2c	+	+	+	n.a.	+
m3C	rat	1A6	2b/c	~	-	-	n.a.	-
m3C	rat	4D8	2c	~	-	-	n.a.	-
m3C	rat	3C1	2b2c	+	+	-	n.a.	-
m3C	rat	5F5	2c	+	-	-	n.a.	-
m3C	rat	1B7	2c	+	+	+	n.a.	+

m3C	rat	1E 5	2c	~	-	-	n.a.	-
m3C	rat	4B2	2a	~	-	-	n.a.	-
m3C	rat	1C3	2b	~	-	-	n.a.	-
m3C	rat	18A3	2c	+	+	~	n.a.	-
m3C	rat	7F8	2c	+	~	-	n.a.	-
m3C	rat	6C1	2c	+	~	-	n.a.	-
m1G	rat	24F8	2b	-	-	-	n.a.	-
m1G	rat	6A3	2b	~	-	-	n.a.	-
m1G	rat	22H3	2b	-	-	-	n.a.	-
m1G	rat	10G4	2c	~	-	-	n.a.	-
m1G	rat	13C11	2a	+	-	-	n.a.	-
m1G	rat	13G4	2b	-	-	-	n.a.	-
m1G	rat	15B9	2c	~	-	-	n.a.	-
m1G	rat	7F3	2b	+	-	-	n.a.	-
m1G	rat	24B3	2b&c	+	-	-	n.a.	-
m1G	rat	16H6	2a&b	~	-	-	n.a.	-
m1G	rat	14F11	2b	+	~	-	n.a.	-
m1G	rat	15D7	2a	~	-	-	n.a.	-
m1G	rat	20A1	2c	~	-	-	n.a.	-
m1G	rat	7B3	2b	-	-	-	n.a.	-
m1G	rat	19C9	2c	~	-	-	n.a.	-
m1G	rat	17F7	2c	+	-	-	n.a.	-
m1G	rat	20D4	2c	-	-	-	n.a.	-
m1G	rat	5H7	2b	-	-	-	n.a.	-
m1G	rat	6E 3	2b	+	+	+	n.a.	+
m1G	rat	18H9	2a	-	-	-	n.a.	-
m1G	rat	20G6	2c	~	-	-	n.a.	-
m1G	rat	19H4	2b	+	+	+	n.a.	+
m1G	rat	19E 2	2c	~	-	-	n.a.	-
m1G	rat	4G10	2a	+	+	+	n.a.	+
m1G	rat	19C11	2a	+	-	-	n.a.	-
m1G	rat	18H5	2a	-	-	-	n.a.	-
m1G	rat	20F2	2c	~	-	-	n.a.	-
m1A	rat	5E 3	2b	+	+	+	n.a.	+
m1A	rat	14B10	2b	+	+	+	n.a.	+
m1A	rat	23F11	2b	~	-	-	n.a.	-
m1A	rat	5H11	2a	~	-	-	n.a.	-
m1A	rat	6A7	2b	~	-	-	n.a.	-
m1A	rat	21G5	2b	~	-	-	n.a.	-
m1A	rat	5F4	2b	~	-	-	n.a.	-
m1A	rat	21F3	2a	~	-	-	n.a.	-
m1A	rat	6E 1	2b	~	-	-	n.a.	-
m1A	rat	20C1	2a	~	-	-	n.a.	-
m1A	rat	8D8	2b	~	-	-	n.a.	-
m1A	rat	10G1	2b	~	-	-	n.a.	-
m1A	rat	17A10	2b	~	-	-	n.a.	-

m1A	rat	3C11	2b	~	-	-	n.a.	-
m1A	rat	21C4	2b	~	-	-	n.a.	-
m1A	rat	13A6	2b	~	-	-	n.a.	-
m1A	rat	14A8	2b	~	-	-	n.a.	-
m1A	rat	3G3	2b	~	-	-	n.a.	-
m1A	rat	15D2	2b	~	-	-	n.a.	-
m1A	rat	23F12	2b	~	-	-	n.a.	-
m1A	rat	16F1	2b	~	-	-	n.a.	-
m1A	rat	17D11	2b	~	-	-	n.a.	-
m1A	rat	13G7	2b	~	-	-	n.a.	-
m1A	rat	14G9	2b	~	-	-	n.a.	-
m1A	rat	18F9	2b	~	-	-	n.a.	-
m1A	rat	16A7	2b	~	-	-	n.a.	-
m1A	rat	13B7	2b	~	-	-	n.a.	-
m1A	rat	14C1	2b	~	-	-	n.a.	-
m1A	rat	17C1	2b	+	~	~	n.a.	-
m1A	rat	5G5	2b	~	-	-	n.a.	-
m1A	rat	13A9	2b	~	-	-	n.a.	-
m1A	rat	18H2	2b	~	-	-	n.a.	-
m1A	rat	19B4	2b	+	+	+	n.a.	+
m1A	rat	13F10	2b	~	-	-	n.a.	-

5.2.2   Binding models and Scatchard plots for K_D determination
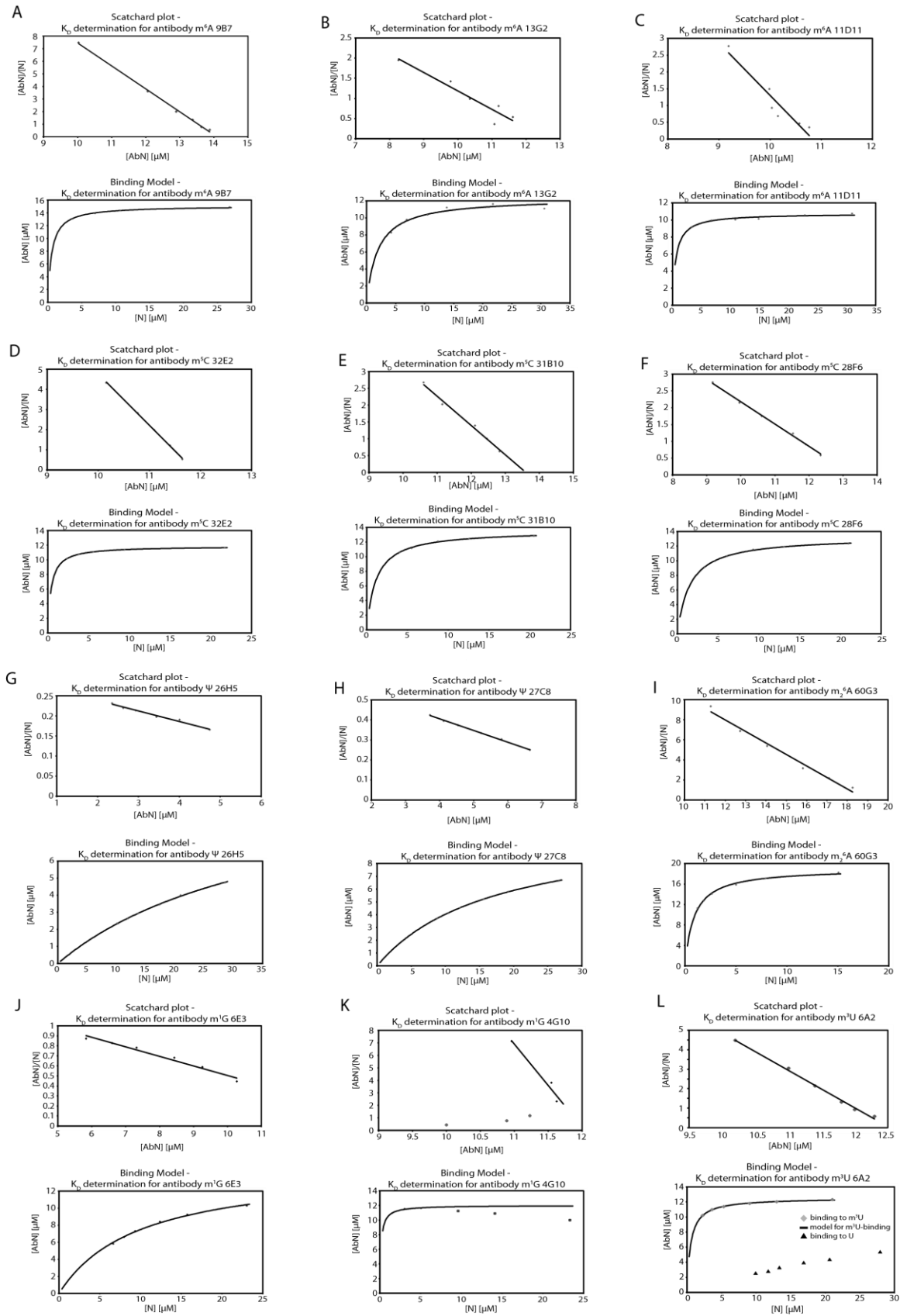
Figure 43: Complete list of Scatchard plots and binding models for the determination of the K_D-values of the antibodies. (A) – (C) shows the data for all the m⁶A antibodies 9B7, 13G2 and 11D11. (D) – (F) depicts scatchard plots and binding models for m⁵C antibody clones 32E2, 31B10 and 28F6. (G) and (H) show the data for the Ψ-

antibodies 26H5 and 27C8. (I) Data for the m_2^6A clone 60G3. (J) and (K) depict K_D-determination data for m^1G antibody clones 6E3 and 4G10. The antibody clone m^1G 4G10 shows unspecific binding to G at higher concentration, which is depicted with red squares. In (L), the data for the m^3U antibody is shown. The binding model includes binding data of the antibody to m^3U (squares) and to unmodified U (triangles).

5.2.3 Relevant pulldown data

5.2.3.1 1-Methyladenosine pulldown data

Table 17: Candidates for the m^1A pulldown. The proteins, listed here are potential m^1A binding proteins. On the left side, they are ranked by the height of the score, the right side shows the ranking by peptide amounts in the samples. The preclear, score results for the RNA base modifications m^1A, m^6A and m_2^6A and the compared peptide occurrences are shown.

			sorted by peptide score										sorted by peptide amount						
			score				peptides						score				peptides		
protein	Pc	*m1A*	m6A	m26A	A	m1A	m6A	m26A		protein	Pc	m1A	m6A	m26A	A	*m1A*	m6A	m26A
TBA4A		921				1	-1	-1		PLAK	124	152		25	42	4	-5	-4
H2B1M		711			575	1	-2	-2		UN45A		71,3				3	-3	-3
FXR1	212	398	364	300	197	0	0	-1		RBM40		60,7	45,3	49		3	-3	-4
FXR2	166	358	337	333	210	-1	1	-2		ZC3H8		43			30	3	-5	-3
VSIG8		352				1	-1	-1		SYTC2		239	157	175		2	-2	-2
YTDC2	161	340	280	233	96,2	-1	1	-1		TPM2		123				2	-2	-2
SYTC2		239	157	175		2	-2	-2		TBL2	72	86	50	50	32	2	-2	-3
MCA3		230	203	185	76,6	1	-1	-1		EXOS8	64,7	76,4	66,7	38	62	2	-2	-4
FUBP3	96	220	189	204	154	0	0	-2		RCC1		75,7	59	35		2	-2	-2
DICER		197	175	89	46	1	-2	-1		GSTP1		55				2	-2	-2
1433G		157				1	-1	-1		L2HDH		52,7	38	25	38	2	-2	-2
PLAK	124	152		25	42	4	-5	-4		THUM1		52	48	27		2	-2	-2
NACAM		135				1	-1	-1		TBA4A		921				1	-1	-1
TGM3		127	35		97	1	-1	-2		H2B1M		711			575	1	-2	-2
TNIK		125		110		1	-2	-1		VSIG8		352				1	-1	-1
NUCB1		124				1	-1	-1		MCA3		230	203	185	76,6	1	-1	-1
TPM2		123				2	-2	-2		DICER		197	175	89	46	1	-2	-1
RADI		122				1	-1	-1		1433G		157				1	-1	-1
EZRI		121				1	-1	-1		NACAM		135				1	-1	-1
DIM1	67,7	117	93	95	77,6	-2	2	-2		TGM3		127	35		97	1	-1	-2
LAP2A		115				1	-1	-1		TNIK		125		110		1	-2	-1
PINX1	74,5	101	80,7	55,6	63,7	1	-2	-1		NUCB1		124				1	-1	-1
S10A3		90				1	-1	-1		RADI		122				1	-1	-1
LYG2		88				1	-1	-1		EZRI		121				1	-1	-1
MYO15		88				1	-1	-1		LAP2A		115				1	-1	-1
PHF5A	27	87,7	56,5	46,5		1	-1	-1		PINX1	74,5	101	80,7	55,6	63,7	1	-2	-1
TBL2	72	86	50	50	32	2	-2	-3		S10A3		90				1	-1	-1
RT18B	74,3	84,2	68,8	69,6	62	1	-1	-1		LYG2		88				1	-1	-1
INCE		83				1	-1	-1		MYO15		88				1	-1	-1

protein	Pc	m1A	m6A	m26A	A	m1A	m6A	m26A
SPF27	63	82,4	74,6	69,3	42,7	1	-1	-1
RN3P2	73,3	82	60,3	52	34	-2	0	0
RBBP6		82				1	-1	-1
EXOS8	64,7	76,4	66,7	38	62	2	-2	-4
RCC1		75,7	59	35		2	-2	-2
UN45A		71,3				3	-3	-3
AMYP		68				1	-1	-1
DMBT1		67				1	-1	-1
G45IP		67	28	33		1	-1	-2
WDR55		65				1	-1	-1
RALA	57	64,3	32	40	37	1	-2	-2
DI3L2		62	40	27		1	-1	-1
BT1A1		62				1	-1	-1
PADI4		61				1	-1	-1
RBM40		60,7	45,3	49		3	-3	-4
UCHL5		60				1	-1	-1
FEN1	39	59,5	29			1	-1	-2
MET17		59	33,5	50		1	-1	-2
PEF1		59				1	-1	-1
THOC7		57				1	-1	-1
CASC3		57				1	-1	-1
GSTP1		55				2	-2	-2
PEX19		54				1	-1	-1
L2HDH		52,7	38	25	38	2	-2	-2
THUM1		52	48	27		2	-2	-2
ZC3H8		43	38	35		1	-1	-2
NMNA1		43		30		3	-5	-3
ZCHC8		36,5	31	29		0	0	-1
ALKB5		36				1	-1	-1

protein	Pc	m1A	m6A	m26A	A	m1A	m6A	m26A
PHF5A	27	87,7	56,5	46,5		1	-1	-1
RT18B	74,3	84,2	68,8	69,6	62	1	-1	-1
INCE		83				1	-1	-1
SPF27	63	82,4	74,6	69,3	42,7	1	-1	-1
RN3P2		82				1	-1	-1
AMYP		68				1	-1	-1
DMBT1		67				1	-1	-1
G45IP		67	28	33		1	-1	-2
WDR55		65				1	-1	-1
RALA	57	64,3	32	40	37	1	-2	-2
DI3L2		62	40	27		1	-1	-1
BT1A1		62				1	-1	-1
PADI4		61				1	-1	-1
UCHL5		60				1	-1	-1
FEN1	39	59,5	29			1	-1	-2
MET17		59	33,5	50		1	-1	-2
PEF1		59				1	-1	-1
THOC7		57				1	-1	-1
CASC3		57				1	-1	-1
PEX19		54				1	-1	-1
NMNA1		43	38	35		1	-1	-2
ALKB5		36				1	-1	-1
FXR1	212	398	364	300	197	0	0	-1
FUBP3	96	220	189	204	154	0	0	-2
ZCHC8		36,5	31	29		0	0	-1
FXR2	166	358	337	333	210	-1	1	-2
YTDC2	161	340	280	233	96,2	-1	1	-1
DIM1	67,7	117	93	95	77,6	-2	2	-2
RBBP6	73,3	82	60,3	52	34	-2	0	0

5.2.3.2 N6-Methyladenosine pulldown data

Table 18: Pulldown results for the m6A experiments. The table is built up like Table 16. Potential m6A binding proteins are listed below.

	sorted by peptide score										sorted by peptide amount							
			score				peptides						score				peptides	
protein	Pc	m1A	*m6A*	m26A	A	m1A	m6A	m26A		protein	Pc	m1A	m6A	m26A	A	m1A	*m6A*	m26A
TBB6	690	727	846,3	628,5	695	-2	2	-2		SRRT		55,5	77,4	48		-3	3	-3
TADBP	157	145,3	253,3	212,4	121,6	0	0	0		YTHD2			59,7			-3	3	-3
FMR1	137,3	186,7	196,7	166,9	137,2	-1	-2	1		AGO2		32	45,1	38,3		-5	3	-3
XPO1	76	145,6	157,2	67,25	68,67	-1	1	-2		TBB6	690	727	846	629	695	-2	2	-2
UBA1	53,5	119,2	153,1	106	78,17	-2	1	-2		MSH2	32	77,7	100	34	76	-2	2	-3
H2B2D		101	150,7		104,5	-1	1	-3		ICAM1			59,5			-2	2	-2
NSUN2	40	100,8	141,2	107	75,67	-2	-1	-2		CCDC8	29	32	57,3	36		-2	2	-2

DDX20	85	104,6	123	91,4	27	-1	1	-1
CPSF6		80	123	91,75	70,5	0	0	0
CAPR1	49	87,2	115,5	72	70	-1	1	-1
SF01		58	114,7	36		-1	1	-2
PI51A	89,33	82,4	112,2	72,8	58	-1	1	-1
SF3B6	101	95,17	107,8	65,38	65	-3	1	-1
HBA			102			-1	1	-1
MSH2	32	77,67	100,4	34	76	-2	2	-3
MECP2			94			-1	1	-1
ATD3B			94			-1	1	-1
ERLN1			92			-1	1	-1
TF2H2			90			-1	1	-1
ZC11A		61,33	84,5	70,5		-1	1	-2
EI2BB		58	82	40,5		-1	1	-1
CD11A			81			-1	1	-1
EIF3G		44,67	78,75	34,67	36	-1	1	-1
CPNE9			78			-1	1	-1
SRRT		55,5	77,4	48		-3	3	-3
PSIP1			71,25	40,33	27	-4	1	-1
TF2H4	37	33	65,33	54		-1	1	-2
FLNA			64			-1	1	-1
GBB1			64			-1	1	-1
MIC60	41	27	62	27		-1	1	-1
MRCKB			62			-1	1	-1
UBP10		47,5	60	39,5		-1	1	-1
YTHD2			59,67			-3	3	-3
ICAM1			59,5			-2	2	-2
IGJ			59			-1	1	-1
CCDC8	29	32	57,25	36		-2	2	-2
DCAF7			55			-1	1	-1
DDB1		32	54,33	29		-1	1	-2
RPP38	27	33,33	53,5	37		-1	1	-2
VIR		32	52,5			-1	1	-2
S30BP		27	50,5			-1	1	-2
YTDC1	29	34,5	46,67	44		-1	1	-1
AGO2		32	45,14	38,25		-5	3	-3
TRM2A			36,67		31	-3	2	-3
NSUN5			36			-1	1	-1

TRM2A			36,7		31	-3	2	-3
XPO1	76	146	157	67,3	68,7	-1	1	-2
UBA1	53,5	119	153	106	78,2	-2	1	-2
H2B2D		101	151		105	-1	1	-3
DDX20	85	105	123	91,4	27	-1	1	-1
CAPR1	49	87,2	116	72	70	-1	1	-1
SF01		58	115	36		-1	1	-2
PI51A	89,33	82,4	112	72,8	58	-1	1	-1
SF3B6	101	95,2	108	65,4	65	-3	1	-1
HBA			102			-1	1	-1
MECP2			94			-1	1	-1
ATD3B			94			-1	1	-1
ERLN1			92			-1	1	-1
TF2H2			90			-1	1	-1
ZC11A		61,3	84,5	70,5		-1	1	-2
EI2BB		58	82	40,5		-1	1	-1
CD11A			81			-1	1	-1
EIF3G		44,7	78,8	34,7	36	-1	1	-1
CPNE9			78			-1	1	-1
PSIP1			71,3	40,3	27	-4	1	-1
TF2H4	37	33	65,3	54		-1	1	-2
FLNA			64			-1	1	-1
GBB1			64			-1	1	-1
MIC60	41	27	62	27		-1	1	-1
MRCKB			62			-1	1	-1
UBP10		47,5	60	39,5		-1	1	-1
IGJ			59			-1	1	-1
DCAF7			55			-1	1	-1
DDB1		32	54,3	29		-1	1	-2
RPP38	27	33,3	53,5	37		-1	1	-2
VIR		32	52,5			-1	1	-2
S30BP		27	50,5			-1	1	-2
YTDC1	29	34,5	46,7	44		-1	1	-1
NSUN5			36			-1	1	-1
TADBP	157	145	253	212	122	0	0	0
CPSF6		80	123	91,8	70,5	0	0	0
NSUN2	40	101	141	107	75,7	-2	-1	-2
FMR1	137,3	187	197	167	137	-1	-2	1

5.2.3.3 N6-N6-Dimethyladenosine pulldown data

Table 19: Proteins with potential affinity to m2^6A Analogous to Tables 15 and 16, the proteins, listed here, are potential m2^6A reader proteins. They are ranked by score (left) and peptide amount (right).

sorted by peptide score

protein	Pc	m1A	m6A	_m26A_	A	m1A	m6A	m26A
H2B1O				850		-1	-1	1
H2B2F				826		-1	-1	1
IF2B3	339	433	457	482	421	0	0	0
PLOD1		265	191	333	57	-2	-1	1
FUBP2		199	212	280	188	-3	-3	-4
TUT4		118	62	196	50	-2	-3	2
YLPM1				144		-2	-2	2
VIGLN	36	76,5	118	129,2	50	-3	-1	1
RBM15	68	102	111	124	113	0	0	0
SF3B4	70	77,5	105	124		1	-1	-3
H32				115		-1	-1	1
NOLC1	48,3	67,7	87	112	92,8	-1	-1	1
RL36L				111		-1	-1	1
LAT1				106		-1	-1	1
AMPN			34	103		-2	-1	1
SMC2		53,6	56	101	26	-1	-1	1
PRS6A				94		-1	-1	1
PDIP3		28	74,5	90,3		-1	-1	1
MD12L				90		-1	-1	1
CS047				88		-1	-1	1
PLOD3		39	38	85,5		-1	-1	1
PLEC		36	39	85		-1	-1	1
PP1B				82,2	68,7	-5	-5	1
RIF1				69		-1	-1	1
NDUS3		35		63	39	-1	-2	1
IKIP				60		-1	-1	1
STT3A		27		60	31	-1	-2	1
PLIN3				58,5		-2	-2	2
TMA16		40	40	55,3	40,5	-2	-1	1
AL1A2				55		-1	-1	1
CDK5		36	33	54,5		-2	-3	2
FANCI				54		-1	-1	1
RM04	28	29	42	53,7		-3	-1	1
GMPPA			43	52,5	32	-2	-1	1
PON2				52		-1	-1	1
NDUS1				51,5	35	-2	-2	1
PPHLN			38	48,3		-3	-2	2

sorted by peptide amount

protein	Pc	m1A	m6A	m26A	A	m1A	m6A	_m26A_
TUT4		118	62	196,8	50	-2	-3	2
YLPM1				144,5		-2	-2	2
PLIN3				58,5		-2	-2	2
CDK5		36	33	54,5		-2	-3	2
PPHLN			38	48,33		-3	-2	2
RPC1				46,5		-2	-2	2
GALK1			36	46		-3	-2	2
METL8				34,5		-2	-2	2
H2B1O				850		-1	-1	1
H2B2F				826		-1	-1	1
PLOD1		265,1	191,9	333,9	57	-2	-1	1
VIGLN	36	76,5	118	129,2	50	-3	-1	1
H32				115		-1	-1	1
NOLC1	48,3	67,7	87	112,3	92,83	-1	-1	1
RL36L				111		-1	-1	1
LAT1				106		-1	-1	1
AMPN			34	103		-2	-1	1
SMC2		53,6	56	101,3	26	-1	-1	1
PRS6A				94		-1	-1	1
PDIP3		28	74,5	90,33		-1	-1	1
MD12L				90		-1	-1	1
CS047				88		-1	-1	1
PLOD3		39	38	85,5		-1	-1	1
PLEC		36	39	85		-1	-1	1
PP1B				82,2	68,75	-5	-5	1
RIF1				69		-1	-1	1
NDUS3		35		63	39	-1	-2	1
IKIP				60		-1	-1	1
STT3A		27		60	31	-1	-2	1
TMA16		40	40	55,33	40,5	-2	-1	1
AL1A2				55		-1	-1	1
FANCI				54		-1	-1	1
RM04	28	29	42	53,75		-3	-1	1
GMPPA			43	52,5	32	-2	-1	1
PON2				52		-1	-1	1
NDUS1				51,5	35	-2	-2	1
DHX40				47		-1	-1	1

DHX40		47		-1	-1	1		
RPC1		46,5		-2	-2	2		
GALK1	36	46		-3	-2	2		
SUN2		46		-1	-1	1		
METL8		34,5		-2	-2	2		

SUN2				46		-1	-1	1
IF2B3	339	433	457,1	482,1	421,1	0	0	0
RBM15	68	102,4	111,9	124,7	113,2	0	0	0
SF3B4	70	77,5	105	124,3		1	-1	-3
FUBP2		199	212,6	280,8	188,1	-3	-3	-4

5.3 Tables

5.4 Figures